

Understanding lightning : experiments on meter long discharges and their x-rays

Citation for published version (APA):

Kochkin, P. (2014). *Understanding lightning : experiments on meter long discharges and their x-rays*. [Phd Thesis 1 (Research TU/e / Graduation TU/e), Electrical Engineering]. Technische Universiteit Eindhoven. <https://doi.org/10.6100/IR783261>

DOI:

[10.6100/IR783261](https://doi.org/10.6100/IR783261)

Document status and date:

Published: 01/01/2014

Document Version:

Publisher's PDF, also known as Version of Record (includes final page, issue and volume numbers)

Please check the document version of this publication:

- A submitted manuscript is the version of the article upon submission and before peer-review. There can be important differences between the submitted version and the official published version of record. People interested in the research are advised to contact the author for the final version of the publication, or visit the DOI to the publisher's website.
- The final author version and the galley proof are versions of the publication after peer review.
- The final published version features the final layout of the paper including the volume, issue and page numbers.

[Link to publication](#)

General rights

Copyright and moral rights for the publications made accessible in the public portal are retained by the authors and/or other copyright owners and it is a condition of accessing publications that users recognise and abide by the legal requirements associated with these rights.

- Users may download and print one copy of any publication from the public portal for the purpose of private study or research.
- You may not further distribute the material or use it for any profit-making activity or commercial gain
- You may freely distribute the URL identifying the publication in the public portal.

If the publication is distributed under the terms of Article 25fa of the Dutch Copyright Act, indicated by the "Taverne" license above, please follow below link for the End User Agreement:

www.tue.nl/taverne

Take down policy

If you believe that this document breaches copyright please contact us at:

openaccess@tue.nl

providing details and we will investigate your claim.

Understanding Lightning: experiments on meter long discharges and their x-rays

PROEFSCHRIFT

ter verkrijging van de graad van doctor aan de
Technische Universiteit Eindhoven, op gezag van de
rector magnificus prof.dr.ir. C.J. van Duijn, voor een
commissie aangewezen door het College voor
Promoties, in het openbaar te verdedigen
op dinsdag 02 december 2014 om 16.00 uur

door

Pavlo Kochkin

geboren te Krim, Oekraïne

Dit proefschrift is goedgekeurd door de promotoren en de samenstelling van de promotiecommissie is als volgt:

voorzitter:	prof.dr.ir. A.C.P.M. Backx
1 ^e promotor:	prof.ir. W.L. Kling
copromotor:	dr. A.P.J. van Deursen
leden:	prof.dr. U.M. Ebert (CWI)
	prof.dr. N. Østgaard (University of Bergen)
	prof.dr.ir. G.M.W. Kroesen
	dr. T. Neubert (Technical University of Denmark)
adviseur:	ir. A. de Boer (NLR Amsterdam)

Dit onderzoek werd gesteund door project 10757 van Technologiestichting STW dat deel uitmaakt van de Nederland Organisatie voor Wetenschappelijk Onderzoek (NWO). STW heeft bijgedragen in de drukkosten van het proefschrift.



Nederlandse Organisatie voor Wetenschappelijk Onderzoek

ISBN:

Copyright ©2014 by P. Kochkin

All right reserved. No part of the material protected by this copyright notice may be reproduced or utilized in any form or by any means, electronic or mechanical, including photocopying, recording or by any information storage and retrieval system, without the prior permission of the author.

Cover design: P. Kochkin

Typeset by the author with the latex Documentation System

Printed in The Netherlands by: Ipskamp Drukkers Print Service

To my family.

CONTENTS

Summary	iii
1 Introduction	1
1.1 High-energy atmospheric physics	1
1.1.1 Runaway electron and RREA	2
1.1.2 Relativistic feedback	2
1.1.3 Thermal runaway	3
1.2 Observations	3
1.2.1 Terrestrial Gamma-Ray Flashes	3
1.2.2 Transient Luminous Events	4
1.2.3 Lightning and its x-ray emission	5
1.2.4 Long laboratory sparks	7
1.3 Thesis structure	8
2 X-rays from meter-scale positive discharges in air	11
2.1 Introduction	11
2.2 Experimental setup	12
2.3 Results	14
2.3.1 Discharge development process	15
2.3.2 X-ray timing	20
2.3.3 Probability of X-ray registration	21
2.3.4 Cathode shape	22
2.3.5 The region of X-ray emission	23
2.3.6 Energy spectra and attenuation curves	25
2.4 Discussion and conclusions	27
3 Development of meter-scale negative discharge in air	29
3.1 Introduction	29
3.2 Experimental setup	30
3.3 Results	32
3.3.1 Sequence of time-integrated images	33
3.3.2 Pre-breakdown in time-resolved image sequence	38
3.3.3 Detailed discharge structures near the high-voltage electrode	43
3.3.4 Leader phase	45
3.3.5 Similarities between phenomena in the laboratory and in nature	48
3.4 Discussion and conclusions	49
4 X-ray bursts from negative discharge	51
4.1 Introduction	51
4.2 Experimental setup	52
4.3 Results	54
4.3.1 Discharge development	54
4.3.2 Influence of the gap length on the electrical characteristics and on the X-ray time	55

4.3.3	X-ray measurements	57
4.3.4	X-ray registration rate	58
4.3.5	Ns-fast photography of the cathode area at x-ray time	60
4.3.6	Energy spectra and attenuation curves	64
4.4	Discussion	65
4.5	Conclusions	67
5	Monte Carlo simulation of x-ray emission	71
5.1	Introduction	71
5.2	Experimental setup	72
5.3	Experimental data	73
5.3.1	Registration rate	73
5.3.2	Spectrum and attenuation curves	77
5.4	Model	78
5.4.1	Model validation	78
5.5	Results	80
5.5.1	Spectrum	81
5.6	Discussion and conclusions	82
6	In-flight measurements of high energy radiation from thunderclouds and lightning	83
6.1	Introduction	83
6.2	The ILDAS system	84
6.3	Two selected lightning strikes	86
6.4	Continuous data file	88
6.5	Discussion	88
7	Conclusions and outlook	95
7.1	Conclusions	95
7.2	Outlook	96
7.3	Fundamental research on HV discharge initiation versus lightning research	96
	Bibliography	99
	List of Publications	109
	Acknowledgements	113
	Curriculum Vitae	115

SUMMARY

It had been known for several decades that lightning is not an isolated phenomenon but rather a part of a complex global system of earth-atmosphere-space interactions. Lightning can be triggered by cosmic rays and it can emit an enormous flux of high-energetic photons and particles back to the space. Lightning causes marvelous upper atmosphere electrical discharges that attain the ionosphere at 100 km altitude and stretch dozens of kilometers wide. Since two centuries mankind influences the atmosphere more and more actively, but we still only know little about the impact. The STW Dutch Technology Foundation started a project in 2010 aimed to deepen our understanding of lightning and its related phenomena, as a topic of the broader program 'Building on Transient Plasmas'. The project was split into two studies, an experimental and a theoretical part. In this thesis I describe the experimental part. The accompanying theoretical study is the subject of the PhD study by Christopher Köhn at the CWI in Amsterdam.

Among many lightning mysteries two concern the gamma and x-ray radiation. First, high-energetic bursts of gammas were detected by NASA's satellite BATSE in 1991. These were associated with lightning activity inside a thundercloud and, surprisingly, they always precede a lightning strike. These bursts are called Terrestrial Gamma-Ray Flashes or TGFs for short. Secondly, it is well known that a negative lightning leader propagates in steps. Recently it has been found that each step is accompanied by an intensive x-ray burst with photon energies up to several hundred keV. It is still unclear whether and how the two phenomena are related. But in 2005 measurements have been reported that meter-sized laboratory sparks can also emit x-rays. Our laboratory (still) has a 2 MV Marx generator that generates a voltage pulse of 1.5/50 microsecond rise/fall time when not loaded. The voltage is applied to a spark gap of about one meter. The spark is preceded by a large number of streamers: relatively cold ionized channels that grow from the high-voltage electrode. The head of a channel propagates at a velocity of about 1 millimeter per nanosecond. Strong electric fields occur at the head. The electric field and photons that are generated cause new ionization in front of the head. It takes about 1 microsecond for a conductive channel to bridge the one meter gap between the

electrodes. Then Ohmic dissipation heats the air and the so-called leader is formed, which after sufficient heating transforms into a spark that short-circuits the gap. X-rays occur mostly in the streamer phase.

The previous thesis at TU/e by C.V. Nguyen gave preliminary information on the x-ray source and energy spectrum. This work builds on that research and extends the analysis by more measurements and by statistical analysis, in combination with nanosecond fast photography of the spark formation. This work focusses on the x-ray generation, the determination of the x-ray source and the phenomena responsible for the x-ray generation. In a medium consisting mainly of light atoms such as air, the only process that can lead to x-rays is bremsstrahlung: the deflection of high-energy electrons by a nitrogen or oxygen nucleus. The electrons obtain their kinetic energy from the applied electric field. When the average loss of energy in collisions becomes smaller with increasing energy, the electrons may become run-away and attain relativistic energies. For run-away the electric field strength must be greater than so-called break-even field E_b which is 218 kV/m in air at a density corresponding to 1 atmosphere and room temperature. The observed x-rays then act as a probe for the high-energy tail of the electron energy distribution. We measured the x-ray intensity and the spectrum by attenuation with lead attenuators of varying thickness. In addition, we studied the overall development of the meter-long discharge in details on a millimeter scale by nanosecond fast photography. When we combined the measured electrical parameters of the discharge with the photography, the encounter of positive and negative streamers emerged as most likely phenomenon that generates the x-rays. At x-ray time, positive and negative streamers approach each other and the electric field between their heads exceeds E_b during a very short time just before the merging. From the photography we concluded that this time span is one up to at most a few nanoseconds. At x-ray time, the discharge near the negative electrode consists of a chaotic bundle of streamers of both polarities. Although we cannot directly link a single encounter with a single x-ray burst, we showed experimentally that many encounters between positive and negative streamers happen at the most intense x-ray time. We also increased the number of encounters with a specially designed 'fakirs bed' negative electrode and found that the number of streamers and x-rays increased dramatically. The encounter is also a good candidate because of its relatively short duration. Obviously, short bursts of x-ray photons (1 ns duration) can be generated only by comparatively fast process. Moreover, similar encounters should happen in natural lightning just before the leader step. And since the leader step is also accompanied by a short x-ray burst we have all reasons to believe that streamers encounters are also responsible for lightning x-rays.

To our great surprise, in the experiments on negative discharges we photographed structures that strikingly resemble one of those marvelous upper atmosphere electrical discharges called 'Sprites'. This discovery needs further investigation and might boost our understanding of the Global Electric Circuit and the earth-atmosphere-space interactions. Recently, next to x-rays also neutrons have been detected in meter-long discharges in air. One may ask what other high-energy phenomenon will be discovered in similar discharges.

Apart of this, we measured energetic radiation from lightning and thunderclouds during actual flights with large aircrafts such as an A350. In the certification procedure

aircraft builders carry out so-called icing test flights, where the zero degree Celsius altitude is deliberately sought by the aircraft and crossed in or under thundercloud. Airbus used these flights to also test ILDAS, a system aimed to determine lightning severity/intensity and attachment points during flight from high speed data on the electric and magnetic field at the aircraft surface. We used this unique opportunity to enhance the ILDAS systems with two x-ray detectors coupled to high speed data recorders in an attempt to determine the x-rays produced by lightning in-situ, with synchronous determination of the lightning current and electric fields. Such new data highly interest geophysicists studying lightning physics. In addition, the data may provide clues to the x-ray dose for personnel and equipment during flights. The icing campaign ran in April 2014; in eight flights we collected data of 62 lightning strikes on an Airbus flight test aircraft. In this manuscript we briefly describe the system and show some selected results of the campaign.

CHAPTER 1

INTRODUCTION

The major part of the thesis, Section 2 up to 5, is dedicated to long laboratory sparks and experiments on them. In Sect. 6 I present first results on real lightning strikes on an aircraft during flight. But in Introduction Section I briefly touch phenomena I frequently faced during the research. By this work we significantly contributed to their understanding.

1.1 High-energy atmospheric physics

Recently a new branch of physics dynamically developed - High-Energy Atmospheric Physics [Dwy12b]. It is built upon classical physics of the atmosphere, lightning and space, upon electromagnetism, and upon the physics of plasmas and elementary particles, in close cooperation with radio-science, solar physics research, aviation safety and Global Electrical Circuit theory. A large assortment of measuring and observation technologies revealed a number of unknown processes in our atmosphere that are as yet beyond our understanding: Terrestrial Gamma-Ray Flashes and Electron Beams (TGFs and TEBs); a class of Transient Luminous Events (TLEs) including sprites, halos and jets; long gamma-ray glows and neutron radiation from thunderclouds. The first attempt to explain sprites numerically was done in 2009 [Luq09]. Besides these, many questions remain open from physics of lightning. Unbelievably, but we know little about lightning despite the fact humanity encounters it every day. We learned how to protect ourselves and our equipment against it, but we are still puzzled by lightning initiation, propagation and attachment processes. The high-energy atmospheric physics is dedicated to investigate several of these phenomena.

1.1.1 Runaway electron and RREA

In 1925 the Scottish physicist and Nobel laureate Charles Thomson Rees Wilson proposed a runaway electron mechanism [Wil25]. He demonstrated how a fast electron can accumulate vast energies from electric field in air. In sufficiently strong static electric fields the electron can obtain more energy from the field than it loses on collision and ionization processes. In such a way its kinetic energy increases continuously and finally becomes run-away. To this end the electric field strength must be higher than so-called break-even field E_b which is 218 kV/m at sea level atmospheric conditions.

As was discovered later, an important feature of Wilsons run-away electron is its ability to create an electron avalanche. When a seed high-energy electron runs through a high-field region it creates new free electrons that, in turn, can become run-away, and the process repeats. This phenomenon is called the Relativistic Runaway Electron Avalanche (RREA) [Gur92]. Dwyer investigated the avalanche development and showed that threshold electric field for the avalanche is about 30% higher than E_b [Dwy03a]. This is about the maximum field that has been ever measured inside thunderclouds. Such electron avalanches increase the air conductivity and are good candidates for triggering the lightning discharge through the cloud. But the theory did not explain how the initial seed electron acquired its high energy.

One possible source cosmic rays have been suggested. Cosmic rays are very energetic particles that mainly originate outside the Solar System. The energy spectrum follows approximately an $E^{-2.7}$ distribution, and extends up to 10^{20} eV per nucleus [Car12]. Composed primarily of protons and atomic nuclei they create vast particle showers colliding with air molecules in atmosphere. Most showers reach Earth surface. At thundercloud altitude the shower mainly consist of high-energy electrons and positrons. Those can be the seed particles to initiate RREAs. Another possible source of the seed electrons is the large field enhancement somewhere inside the thundercloud, perhaps at the sharp edge of an ice crystal or other hydrometeor. The field in this region can be sufficiently large to accelerate low-energetic electrons via the thermal runaway mechanism [Gur61] to relativistic energies. Then the electron undergoes avalanche multiplication and creates RREAs.

1.1.2 Relativistic feedback

The relativistic feedback mechanism was extensively developed by Professor Joseph Dwyer from Florida Institute of Technology and accessibly explained in his review [Dwy12b]. When electrons with relativistic energies run through matter they emit x- and gamma rays via Bremsstrahlung. If RREAs exist in thunderclouds these would cause hard radiation. And indeed such radiation has been measured in space, in airplanes and on ground. At least two types of gamma emission from thunderclouds are known by now: long gamma-ray glows and TGFs. The glow lasts for minutes while TGFs can be tens of microseconds fast. Both possess a spectrum predicted by RREA mechanism but both are surprisingly brighter than expected. To solve the brightness problem a new mechanism was proposed by Dwyer - relativistic feedback [Dwy03a]. When the RREA develops in a high electric field of a thundercloud it emits gammas, x-rays and positrons. There is a

finite chance that these secondary particles are emitted in the direction opposite to the avalanche development. When positron or gamma particle moves back into the high field region they can collide with air molecules and produce new high-energy electron, which, in turn, can create a new RREA. The process repeats. The main characteristic of the feedback mechanism is its feedback factor λ . It reflects relative amount of runaway electrons after one cycle. The factor λ depends on the electric field strength and the configuration. Already in relatively small electric fields the number of new runaway electrons decreases or remains constant after each cycle. This might explain the long duration gamma glow from thundercloud. But when the field is strong enough, the amount of runaway electrons and associated RREAs will increase exponentially until the field collapses creating enormous and fast gamma burst like TGF. The beauty of the relativistic feedback is its simplicity. It is developed upon classic RREA and can explain both phenomena. The central idea resembles the feedback mechanism that occurs in low-energetic Townsend discharges, but now adapted to higher energies. Further development of the relativistic feedback mechanism spawned a new phenomenon dark lightning - a wonderful atmospheric feature that has not yet been observed and exists only in theory for the moment.

1.1.3 Thermal runaway

It is known that lightning itself emits bursts of hard radiation [Moo01, Dwy03b] which requires high-energy electrons. The lightning channel might be accompanied by sufficiently large electric fields that free electrons in the thermal energy distribution can be accelerated to relativistic energies. For example, the lightning leader tip or streamers in front of the leader are good candidates to generate such extreme fields. These thermal runaway electrons can be the seed electrons and undergo avalanche multiplication. In this case, the TGFs might be triggered by intense lightning discharges and long gamma ray glow can be explained by continuous discharge activity inside a thundercloud. Undoubtedly, the following authors and work should be cited in this context - [Gur61, Mos06, Li09, Cel11, Gur07, Cha08, Cha10]. Production of very high potential differences by intracloud lightning discharges was investigated in connection with TGFs [Mal13]. Electron acceleration in streamer region of lightning was studied in [Cha14]. The importance of electron-electron Bremsstrahlung was discussed in [Koe14b].

1.2 Observations

Similar to the other side of the moon, for eons we could only see the bottom of a thundercloud. Progress in aero-space technology not only allowed us to look at the moons other side, but also to investigate our atmosphere in more detail.

1.2.1 Terrestrial Gamma-Ray Flashes

A particular case of serendipity is the discovery of TGFs. In 1963 United States developed a group of 12 satellites named Vela in order to detect covert nuclear weapon tests that

might be performed by Soviet Union. In 1967 the satellites detected an intensive flash of gamma radiation with a signature unlike any known nuclear weapon [Kle73]. Most likely it did not come from the USSR but from outer space. The flashes were named Gamma-Ray Bursts (GRBs). It turned out that these were of cosmic origin, billions of light years away from Earth. Given that distance, the energy should be incredibly large. A typical burst releases as much energy in a few seconds as the Sun does in its entire 10-billion-year life [Wika]. Later in 1991, a special instrument BATSE was placed on-board of a NASA's spacecraft "Compton Gamma Ray Observatory" (CGBO) to look way from the Earth and investigate the cosmic Gamma-Ray Bursts. One day in 1991 the satellite reported a burst that clearly did not come from outer space but from its back from Earth. Such bursts we now call Terrestrial Gamma-Ray Flashes or TGFs for short [Fis94]. First they were associated with thunderstorms and few years later with a lightning strike [Ina96]. It is a hot discussion nowadays about a TGF origin: are these generated by conventional lightning discharge or are these the product of mysterious phenomenon called "dark lightning"? Nevertheless TGFs are the most energetic electromagnetic events in our atmosphere and deserve more scientific attention. The main physical properties like spectrum, brightness, duration and even radio emission can be described by relativistic feedback mechanism [Dwy03a]. Although recent space observations of extremely high-energy photons (up to 100 MeV) by the AGILE satellite [Mar11b] challenge this theory. The thermal runaway mechanism [Gur61] correctly describes the leader x-rays, but it still needs to be accurately extended to TGFs. TGFs are associated with negative upward-directed intracloud lightning [Cum11]. As we know from many observations, negative lightning propagates in steps, which, in turn, can generate x-ray bursts [Dwy05a]. Some TGFs also show burst-like features. One may think that leader x-rays plus avalanche multiplication is a good candidate to explain TGFs.

1.2.2 Transient Luminous Events

Up to the nineties a class of marvelous discharges was hidden from our objectives: sprites, blue jets, gigantic jets, starters, elves and halos. Their collective name is Transient Luminous Events (TLEs). Elves and sprites are the most common among them (1.1). Already in the 1920s, the Scottish physicist C. T. R. Wilson also predicted that electrical breakdown may occur above large thunderclouds. Even though such high altitude electrical discharges were observed by aircraft pilots for decades, the first videotaped evidence was provided only in 1989. Sprites propagate downwards from ionosphere stretching over several tens of kilometers. All TLEs are now known to be lightning related. For example, sprites are apparently triggered by a strong positive lightning. Even the TGFs were first associated with TLEs after the discovery [Bel95, RD96, Leh96, Gur96], but later it was shown that the TGF source altitude is lower and that TGFs are rather associated with an intracloud processes [Sta06].

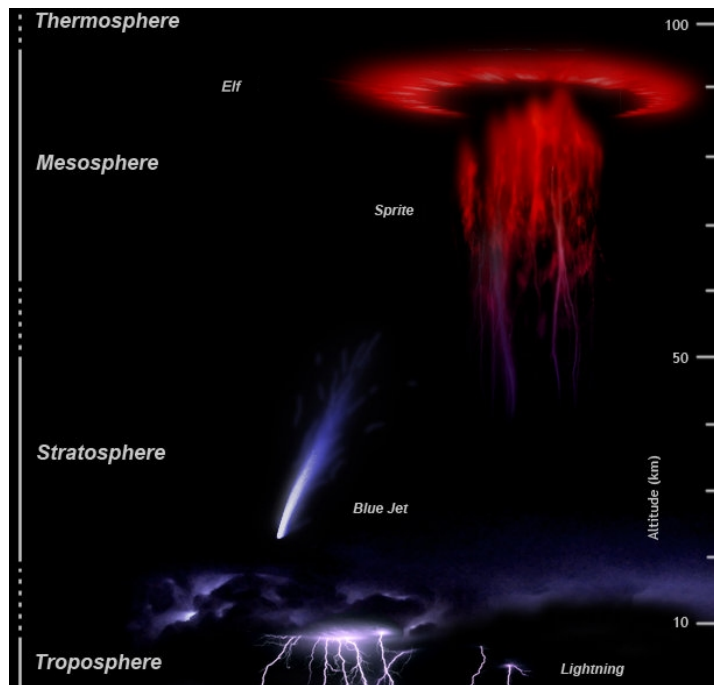


Figure 1.1: Upper-atmospheric lightning and electrical-discharge phenomena [Wike].

1.2.3 Lightning and its x-ray emission

There are roughly 50 lightning strikes per second worldwide, or a total of nearly 1.5 billion flashes per year. But the discharges are not evenly distributed around the planet and are season dependent. Approximately 70% of lightning occurs in the tropics where the majority of thunderstorms develop. The north and south poles have almost no lightning over the year. Ocean areas also have fewer discharges than continental. Places with the highest lighting activity are located in Venezuela, Florida (US), Democratic Republic of the Congo and Singapore (1.2).

Lightning was a real headache in the past when wood was the most popular construction material. As buildings became taller lightning became more of a threat. Until the lightning rod was invented by Benjamin Franklin in North America in 1749 and in Europe by Czech priest Prokop Divis in 1754. The story of lightning investigation begins in those times. We know nowadays pretty well how to protect our buildings against lightning, but new challenges arose in modern society. Avionics, telecommunication, transmission lines pose new questions to lightning protection systems. The group currently named Electrical Energy Systems EES - earlier acronyms were EPS, EHC, and EHO - has a long record of research directed towards effective counter measures against electromagnetic interference including those caused by lightning [Van98, Grc05]; the research lead to several PhD theses [Hou90, Hel95, Hor98, Kap05, Bar11]. Some of the techniques developed have been published through international standardization

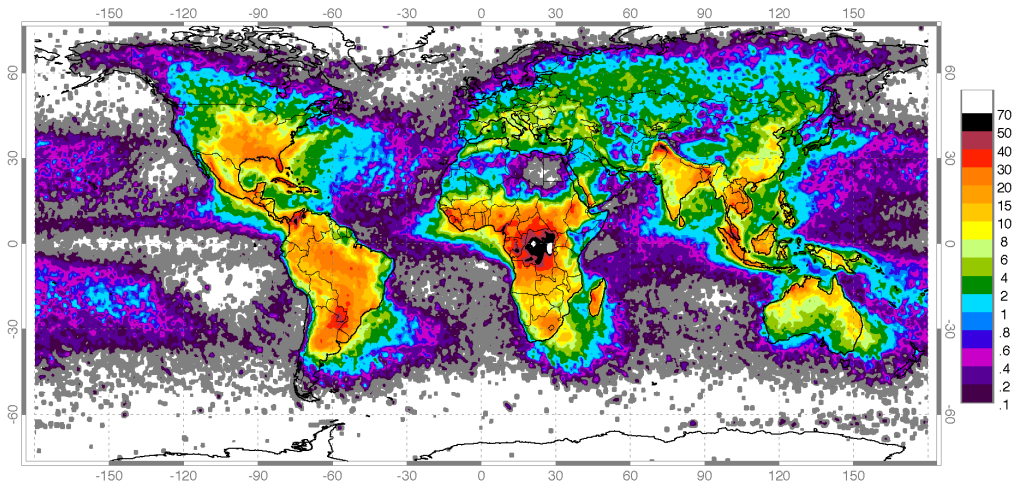


Figure 1.2: Global lightning distribution map in strikes/ km^2/yr [Wikb].

organizations such as IEC [IEC97]. The experiments mentioned in this work required sensitive high-speed electronics to function flawlessly close to the high voltage spark. The work could only be performed because of the thorough understanding of electromagnetic compatibility (EMC) available in EES.

Twentyfive years ago the first TLE has been documented and twenty years back the TGFs were discovered. These are of the most actively discussed lightning-related topics in atmospheric electricity today. The reader may be surprised but, besides TLEs and TGFs, among top ten questions in lightning research ([Dwy14] three concern *how* lightning initiates, propagates and attaches to a tall object. But this does not mean we know nothing about lightning; we just can ask the question "How?" infinitely.

In our subjective view, one of the most intriguing lightning features is the ability to generate bursts of hard radiation. The lightning channel is extremely hot: 30,000 K, or 5 times hotter than the suns surface. When a lightning channel approaches the ground its tip emits x-rays in hundreds keV energy range [Dwy11, Dwy03b, Dwy04b, Moo01], which is two orders of magnitude higher than what can be expected from the hot lightning channel and thermal bremsstrahlung process. So, some interesting physics happens there that is the topic of this thesis. What we can say with a certain level of confidence, that the bursts of hard radiation are related to a stepped leader.

What is interesting is that long laboratory sparks also produces x-ray bursts in similar circumstances. Although the actual scaling from a meter-length spark to kilometer-length lightning is still under discussion, we have a good opportunity to unveil the mystery behind the lightning hard radiation.

1.2.4 Long laboratory sparks

Pioneering work on negative long laboratory spark and its comparison with lightning has been done in 1962 [Stef62]. Using optical intensifier together with streak photography technique authors showed many details of pre-breakdown phenomena for the first time. Later, this work was followed by Les Renardieres group in France in more fundamental investigation [Les77, Les81]. New details have been added by experiments on long negative discharges by Reess in 1995 [Ree95]. And finally, numerical models for both positive and negative discharges that allowed to calculate relevant discharge parameters (positions, velocities, current, charge, etc.) as a function of space and time taking as an input the electrode geometry and the voltage waveshape have been presented in [Gal02].

This investigation started at Eindhoven University of Technology in 2008 after the x-ray radiation from long laboratory sparks has been reported in [Dwy05b]. Vuong Nguyen assembled the high-voltage setup based upon 2 MV Marx generator and confirmed the existence of the radiation. He also added accurate measurements of the discharge electrical parameters such as high-voltage and currents through both electrodes [Ngu08, Ngu10]. This formed the basis of his PhD thesis [Ngu12]. All lab measurements presented in this manuscript have been conducted using and extending the setup assembled by Vuong.

During four years we recorded about 5000 discharges of positive and negative polarity also in collaboration with other research groups. The high-speed intensified CCD camera has been added to visualise the discharge development process. This allowed us to document the phenomenon in details never available before. In particular, we showed how a space stem/leader originates and develops which is the key element to leader stepping mechanism puzzle. Such substantial amount of experiments allowed us to collect statistic on x-rays, their spectrum, timing, intensity, place of origin. This data will serve as an input for existing and future theoretical models.

The main contributions of this work can be summarized as follows:

- X-ray emission from long laboratory sparks has been measured from different positions around the spark gap. No indication of anisotropy has been found.
- Spectrum and attenuation curves have been measured at different detector positions.
- Pre-breakdown phenomena have been investigated with unprecedented time and space resolution.
- The x-ray source was found to be located at the cathode vicinity.
- The process responsible for the x-ray production was proposed. The most probable source of high-energy electrons is an encounter of two opposite polarity streamers. The electrons then produce x-rays via Bremsstrahlung. The same process is apparently responsible for the x-rays from lightning leader.
- A mathematical model of the x-ray generation has been proposed. We quantitatively described x-ray production by long laboratory spark and practically showed how to increase their amount by changing electrode shape.
- Hard radiation from real lightning has been measured *in situ* for the first time during icing tests flights with an A350 aircraft through thunderstorms.

1.3 Thesis structure

The next five Chapters of the thesis consist of publications that appeared in Journal of Physics D, or as manuscripts that have been submitted. Only the text has been reformatted. Therefore, some information, in particular the description of the instruments, occurs in duplicate to make the papers self-contained.

The second Chapter of the thesis is dedicated to long laboratory *positive* discharge and its x-ray emission. Previously Nguyen [Ngu12] showed that no x-rays appear before the cathode current starts to flow. By using lead collimators around the x-ray detectors we confirmed that most of x-rays come from the cathode area. Then we investigated the discharge development process by time resolved ns-fast images and showed that the negative streamers from the cathode played the major role in x-ray generation mechanism. Finally, I designed an alternative cathode electrode to increase the amount of negative streamers resulting in a 10 times increased x-ray production. The measured energy spectra and attenuation curves of the radiation were consistent with an exponential distribution with about 0.2 MeV characteristic energy. The positive discharge development process is always rather smooth and continuous. Each feature observed by the camera could be correlated with measured electrical signals from voltage and current sensors.

The third Chapter describes a *negative discharge development* process. We photograph the process in time-resolved and time-integrated images with accurate linkage to the measured electrical data. We show that, in contrast with positive discharge, the negative one develops in steps. Apart of it, we document structures called "pilot system" with unprecedented time and space resolution. A pilot system is a bipolar structure that originates near the cathode and can develop into a space leader in longer gaps. We precise the mechanism of their development and notice their striking similarity to TLEs sprites. Pilot systems apparently also occur in natural lightning.

In Chapter 4 we investigate the x-ray emission from long *negative* discharges. We used lead collimators as for positive discharges, to show that the cathode area is the most intense x-ray region. We also demonstrate that the pilot systems play an important role in the x-ray production. Most of x-rays appear when the pilots attach to the main leader or cathode. Eventually, we conclude that an encounter between positive and negative streamers is the most likely candidate for the x-ray source. Such encounters have been observed in discharges of both polarities and fit other parameters as timing, duration, and electromagnetic high-frequency signature.

By analogy with positive discharge we measure the attenuation curves and the spectra of the incoming x-rays. They are all in a good agreement with positive discharges, previous measurements and our general understanding of the processes between electrodes.

Chapter 5 is dedicated to modeling. We pursue two goals: 1) to test our theories and 2) to find some basic properties of the x-ray source. To do this we built a mathematical model and ran a Monte Carlo simulation. Using GEANT4 toolkit we obtain very good agreement between our understanding and what is measured and observed in the laboratory.

Chapter 6 describes an exciting experiment. In the test-campaigns to demonstrate the reliability of aircrafts, icing flights are required. In our case, an Airbus A350 flew at

the zero degree Celsius level in thunderstorms on several days between December 2013 and May 2014. These flights also served to test the ILDAS system, an In-flight Lightning Strike Damage Assessment Systems where the aircraft is equipped with several sensors for the electric and magnetic field to determined attachment and severity of lightning strikes [ILD]. The group EES at TU/e developed the sensors and first data acquisition stages [Ste08, Deu11b, Deu11a], the National Aerospace Laboratory (NLR, Amsterdam) the recording and on-board data storage system [Zwe09]. As contribution to the STW BTP project, NLR extended the ILDAS system to also store two X-ray signals in perfect synchronization with the lightning data. In other words, we turned the aircraft into a sophisticated x-ray detector and embedded it right into a lightning channel. This was never done before. During six days of flying campaign 62 lightning strikes to the aircraft were detected. In Chapter 6 we give an overview of the campaign, the ILDAS system, the sensors and some measured data. Full evaluation of the 160 GB of data obtained in the campaign is deferred to a later period.

In Chapter 7 we summarize the conclusions and give an outlook on and recommendations for future works.

CHAPTER 2

X-RAYS FROM METER-SCALE POSITIVE DISCHARGES IN AIR

We investigate structure and evolution of long positive spark breakdown; and we study at which stage pulses of hard X-rays are emitted. Positive high-voltage pulses of standardized lightning impulse wave form of about 1 MV were applied to about 1 meter of ambient air. The discharge evolution was imaged with a resolution of tens of nanoseconds with an intensified CCD camera. $\text{LaBr}_3(\text{Ce}^+)$ scintillation detectors recorded the X-rays emitted during the process. The voltage and the currents on both electrodes were measured synchronously. All measurements indicate that first a large and dense corona of positive streamers emerges from the high voltage electrode. When they approach the grounded electrode, negative counter-streamers emerge there, and the emission of hard X-rays coincides with the connection of the positive streamers with the negative counter-streamers. Leaders are seen to form only at later stages.

2.1 Introduction

The generation of X-rays from electrical discharges at near to atmospheric pressure requires that electrons reach very high energies despite their numerous collisions with gas molecules; the X-rays are then generated by Bremsstrahlung. Wilson [Wil25] suggested that favourable conditions for electron run-away to high energies could exist in thunderclouds. After unsuccessful attempts in the 1930ies it took many years before the association of X-rays and thunderstorms could be established. In Chapters 2 and 6 of his book [Bab03] Babich presents an extensive overview of the early and later experiments. McCarthy [McC85] observed X-rays of the order of 10 keV in aircraft flights through thunderstorms in the 1980ies. At surface level, X-rays associated with

the approaching lightning leader have been detected in triggered lightning measurements [Dwy03b, Dwy04b, Dwy11]; their energy is of the order of 250 keV. Terrestrial gamma-ray flashes from thunderstorms with energies of up to 20 MeV [Smi05] or even up to 40 MeV [Mar10] are measured from satellites. X-rays can also occur during the initiation of sparks in the laboratory on a scale of millimetres up to meters, even with standard atmospheric conditions of approximately 1 bar and 20 °C. Unrolling adhesive tapes generates X-rays [Cam08], as do helium filled spark chambers [Fra66], the formation of corona discharges [Ngu10] on a centimetre scale, or meter long discharges [Dwy08, Ngu08, Mar11a, Coo09]. X-rays are a common feature of a high-voltage discharge, regardless of size.

While in short gaps the accelerated electrons actually might emit their Bremsstrahlung during collision with surrounding metal equipment, experiments in sufficiently long air gaps are actually similar to thunderstorm conditions as the Bremsstrahlung photons are generated by collisions with air molecules as well. We will argue that for the experiments reported here the photons are indeed generated in open air.

As shown in recent simulations [Mos06, Li09, Cha10, Cel11], the highly enhanced electric field at the tip of a negative streamer discharge could actually accelerate the electrons into the run-away regime, and the effect is even stronger at the tip of a naked lightning leader with its larger dimensions and higher voltage [Xu12] if such a naked corona-less leader exists. We will show below how the streamers develop in our experiment, and at which stage they actually emit the hard X-rays. The effect is created here not by a single streamer, but by the complete streamer corona.

We study the initiation phase before breakdown. Such studies have been performed earlier by several groups. Here we refer in particular to the early work in France [Ree95] [Les77]. Les Renardieres group investigated static, streak and Schlieren photos of positive discharges. They described first corona formation followed by leader propagation, final jump and return stroke. But they did not measure X-rays emitted from a spark during this processes. We measure the voltage and the current on both electrodes, synchronized with nanosecond fast photography and X-ray detection. Our aim is to find where and when the X-rays are generated.

2.2 Experimental setup

The 2 MV Marx generator at Eindhoven University of Technology delivers an IEC standardized lightning impulse voltage waveform of 1.2/50 μ s rise/fall time when not loaded. The generator is connected to a spark gap with cone-shaped electrodes. The setup is similar to the one described in [Ngu08], with five changes worth mentioning here. First, the discharge channel is vertical rather than horizontal. This provided a more symmetrical environment of the discharge than in [Ngu08]. Second, conductive Velostat plastic covered all sharp protruding objects close to the gap, in order to avoid local streamer formation. Third, current probes were mounted on both electrodes. Fourth, an image intensified CCD camera was used. Finally, two scintillator detectors were placed at varying positions. The goal was to find the angular distribution of the X-ray emission.

The distance between the high-voltage (HV) and grounded (GND) electrodes was 1 meter. It is small enough to perform the optical observations accurately and large

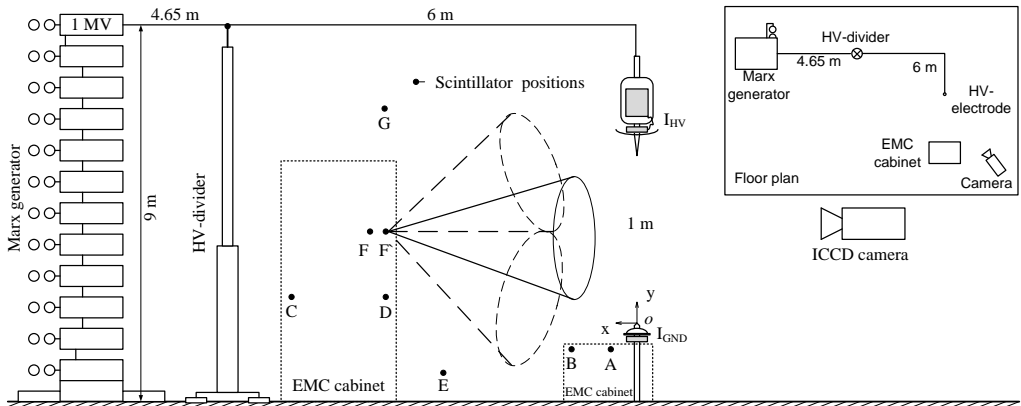


Figure 2.1: Schematic sketch of the spark-gap geometry and positions of X-ray detectors. Each dot labelled from A up to G corresponds to a $\text{LaBr}_3(\text{Ce}^+)$ detector scintillator position; all positions are in a single vertical plane. Cones indicate the field of view of the detector when placed inside the lead collimator discussed in 2.3.5. The ICCD camera is located at 4 m distance from the gap; it is shown in correct relative height, but not in the scaled position. The distance between Marx generator and the spark gap is 8 m. The upper right inset shows the correctly scaled floor plan of the setup.

enough to allow many pre-breakdown features to develop. The applied voltage between electrodes was about 1 MV and did not change within all experimental study.

To obtain time-integrated and time-resolved images of the pre-breakdown phenomena, a ns-fast 4Picos ICCD camera was located at 4 m distance from the gap, perpendicular to discharge-developing axes. The camera was placed inside a small and well-protected cabinet. The cables between the camera cabinet and the large cabinet with registration equipment (figure 2.1) were about 5 m long. All cables were placed inside a stainless steel flexible hose. The hose and its mounting were near to vacuum tight; this ensured adequate electromagnetic compatibility (EMC) and interference-free operation of the camera. The field of view of the camera just covered the full gap, including grounded and high-voltage electrodes. The optical gain by a built-in image intensifier was 10^4 . The camera has a black and white CCD; it was not calibrated. However, the camera parameters and optical system remained the same, except only one parameter: the exposure time.

Two $\text{LaBr}_3(\text{Ce}^+)$ scintillator detectors manufactured by Saint-Gobain were mounted in EMC cabinets and recorded the X-rays. Any interference on their signals due to the discharge initiation can be excluded, since such interference would most likely manifest itself as oscillatory signal, and not mimic a clear scintillator signal. Also, in many discharges only the signal channel noise floor was measured. The scintillators have a fast primary rise/decay time (11/16 ns) and a high light yield of 63 photons/keV, which is 165% of the more common $\text{NaI}(\text{TI})$. The linearity of the detectors has been tested [Ngu12] on ^{241}Am , ^{137}Cs , ^{60}Co and remains perfect up to 2.5 MeV, which is the total absorbed energy from two gamma quanta of the ^{60}Co source in the scintillator. The slight deviation from linearity at higher energies is attributed to saturation of the

photomultiplier. The output of the photomultiplier is recorded directly on the oscilloscope without any waveshaping electronics usually employed in photon counting. This allows to distinguish individual pulses even when pile-up occurs within the decay time of the scintillator. In some series of measurements the detectors were located inside separate EMC-cabinets; one detector was placed in a small cabinet at positions A and B and the other detector was placed in the large cabinet at positions C, D, F, F' as indicated in figure 2.1.

The total aluminium thickness between the scintillator and surrounding area is $550\ \mu\text{m}$. This shielding is almost transparent for photons with an energy above 30 keV (attenuation 15% or less). To determine the origin and the energy composition of the X-ray signals, we used up to 2.5 cm thick lead attenuators and collimators around one detector. The attenuators effectively absorb photons with energies up to 1 MeV (10 times attenuation). Attenuation by 2 m of air between the spark gap and detector is 8% including scattering and photoelectric absorption for 30 keV photons. At 200 keV energy level the air impact is less than 3%. We did not take attenuation by air into account.

Some X-ray signals corresponded to a total absorbed energy of about 3.4 MeV. We determined the attenuation curve by measurements with lead attenuators of different thickness. The slope of the curves contains information about the incident radiation. Additional measurements with the 662 keV gammas of ^{137}Cs confirmed the analysis (see 2.3.6).

The spark gap with two cone-shaped electrodes deviates from the more commonly used point-plane configuration. Two cones provide clear points for the corona discharge to start, and allow more precise measurements of currents due to moving charges. Two Pearson 7427 current probes detected the pre-breakdown currents on both electrodes. In order to protect the probes against a direct discharge we mounted a vaulted aluminium disk between probe and electrode tip. The probe for the HV electrode had an optical transmission system. Suitable attenuators and two antiparallel high speed diodes protected the input of the transmitter. The diodes limited the linear response to 250 A. The GND electrode and the probe were mounted on top of the small EMC cabinet containing the scintillator detector (figure 2.1).

The Marx generator HV divider (80.000:1) was used for voltage measurements. In spite of the large distance between divider and gap, this voltage measurement sufficed to distinguish the different phases of the discharge development. That voltage recording should not be considered as the gap voltage, because of the inductive effects caused by the 8 m long leads between divider top and spark gap HV electrode. Two 4-channel Lecroy oscilloscopes with a maximum sampling rate of 5 Giga-Samples/s collected the data of the X-rays, current and voltage synchronously.

2.3 Results

Several reports on the observation of X-rays with lightning impulse generators have been published [Dwy08, Ngu08, Mar11a]. Up to a few meter distance between detector and discharge is usually maintained because of safety. In this study X-rays are observed in many, but not in all discharges. We studied the formation of X-rays during the

initiation of 951 discharges of positive polarity. The minimal time from one discharge to the next was 10 seconds. In some discharges, we observed up to three easily recognizable individual X-ray peaks with different times and amplitudes. This allowed us to obtain statistical information on the energy spectra and the time distribution averaged over many HV discharges.

2.3.1 Discharge development process

The growth of the discharge is shown in figure 2.2. Every picture corresponds to a single discharge. We applied a special linear colour coding scheme to the CCD output in order to enhance the faint streamers (pictures *a* up to *i*). For low luminosity the coding approaches an emulsion film negative with white as lowest light level. For the very bright leaders, this coding uses colour (pictures *j* up to *o*) up to the white level for maximum brightness. The solid vertical line *z* at $t = 0.36 \mu\text{s}$ in the bottom panel corresponds to the shutter opening time. Dotted vertical lines *a* - *o* correspond to the shutter closing times for the corresponding pictures. Thus, a single picture is time-integrated from the starting time *z* until a camera closing time between 60 (picture *a*) to 1000 (picture *o*) nanoseconds later. Fast moving luminous streamers heads appear as streaks whose lengths correspond to their propagation lengths within the exposure time, similarly as in Figure 1 of [Ebe06]. The electrical signals corresponding to picture *l* are represented at the bottom plot: the voltage waveform *U*, the currents at the high-voltage and at the grounded electrode, and the X-ray signal. On the time axis $t = 0 \mu\text{s}$ corresponds to the start of the voltage waveform. The pictures of the discharge development show a large similarity from discharge to discharge. There is also no significant difference in electrical characteristics. It means that one record represents most of the important steps in the process and can be used to describe the phenomena.

At the beginning, current up to 15 A are measured on the HV electrode during 0.15 to $0.30 \mu\text{s}$, while the voltage starts to exceed 100 kV. The capacitive current due to the increasing voltage is much smaller. Therefore this small current leap must correspond to the first positive corona formation around the sharp tip of the HV electrode. This is probably a highly conductive inception cloud around the tip, similarly to the ones seen at lower voltages in [Bri08a, Bri08b, Nij11b]. It extends radially until the electric field on its surface equals the breakdown field of 30 kV/cm. Image *a* of figure 2.2 shows a cloud of approximately 6 cm radius at some later stage. The required charge is then about $1 \mu\text{C}$, in agreement with the current measurement when integrated up to $0.3 \mu\text{s}$.

After the leap, the first picture *a* represents processes in the gap between 0.351 and $0.420 \mu\text{s}$: the voltage rises approximately linearly in time while the HV current increases rapidly. This high-voltage current jump occurs because of the additional corona formation followed by streamer bursts from the edges of the protection aluminium dish. Below the corona ignition zone there is a diffuse structure originating from the electrode tip (marked *t*). We interpret this as re-excitation of the inception cloud by the current needed for the streamers emanating from the cloud. The current through the grounded electrode remains zero and there is no light emission from that area.

Images *b*, *c*, *d* show that a large number of streamers propagate downward in a rather synchronous manner. Downward streamers from the electrode tip and streamers,

directed sideways from the dish propagate at a speed of $2 \cdot 10^6$ m/s in our experiments. The diameter of a single streamer is of the order of 1 cm measured at FWHM level by technique described in [Nij10]. It is remarkable that HV current gradually decreases then.

Near $t = 0.65 \mu\text{s}$, the downward positive streamers approach the GND electrode and increase the local electric field. At that time for images d and e the distance between the positive streamer tips and the grounded electrode cone is approximately 20 cm. The electric field in this region is now strong enough to initiate the formation of negative streamers out of the grounded electrode. The very first current of the order of 10 Amps is detected on the GND current probe at that moment.

The current through the grounded electrode rises rapidly due to the formation of negative primary upward streamers from the sharp tip. In analogy to the counter-leaders that rise from the ground towards approaching lightning leaders, we will call these negative streamers counter-streamers. All cathode current initiations and steps are accompanied by damped oscillations at frequencies of several hundred MHz, well above the specified bandwidth of the probe 70 MHz.

Immediately after that, at the moment just before f , a positive streamer connects to a negative counter-streamer. At $t = 0.67 \mu\text{s}$ the first channel is formed by the encounter of two streamers - positive from HV and negative from GND electrode. This encounter is again accompanied by high-frequency oscillations at the cathode current signal and more importantly by X-ray emission. This is the beginning of a gradual increase of the HV current. A few more connections between positive and negative streamers will take place later up to moment l when all connection processes end. All of them are accompanied by HF oscillations. We refrain to speculate about the origin of these oscillations until a new current probe with an extended bandwidth is available. It seems safe to presume that many of these encounters are accompanied by X-rays. Some of the X-rays are detected by our detectors as first, second, etc. peaks. As plotted in figure 2.2, we detected X-rays emitted by one on those connection processes.

The HV current measurements after picture i , or current values larger than 250 A should be regarded with caution since the protecting diodes of the optical transmission start to act. The current graph shows the behaviour of the current, whether staying constant or rising, but not the actual values.

At the moment between i and j a hot conductive channel - the leader - arises. We can distinguish the leader from the streamers by its higher luminosity. The leader channel is much brighter than the streamers. Here we should recall that the optical and electrical parameters of the camera remain the same during all pictures from a till o . The leader formation process is the joule heating of one of the conductive streamer channels formed before. The leader tip itself does not emit any new visible streamers during its propagation in our experiments.

On the pictures $j - n$ the development of the positive leader is clearly shown. The leader grows in a highly ionized medium and repeats one of the streamer's paths. The speed of the positive leader is $1.5 \cdot 10^6$ m/s.

Briefly before the exposure time of image l ends, an upward leader rises from the cathode towards the anode. The cathode current I_{GND} increases rapidly. This new

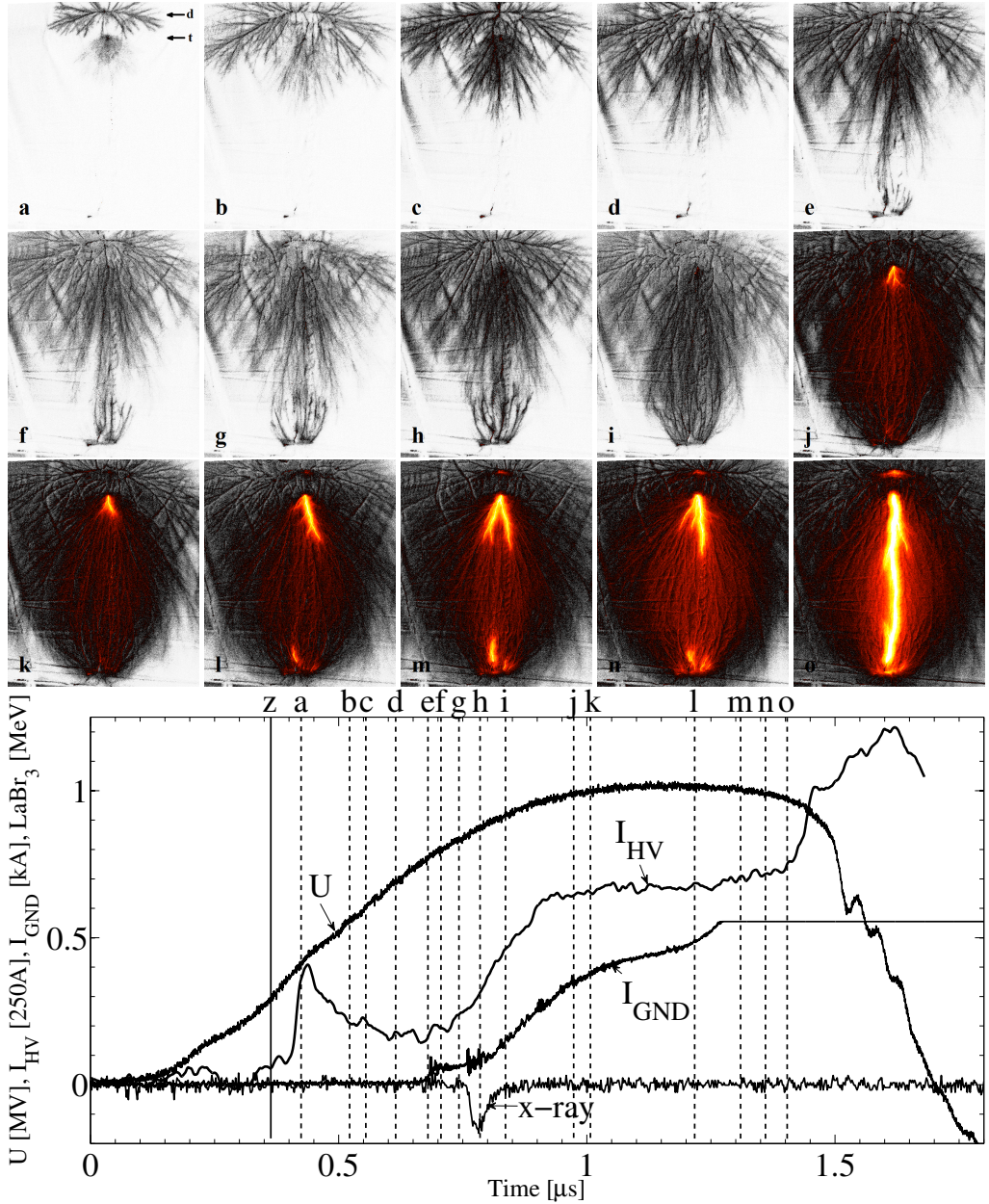


Figure 2.2: Detailed development of one meter length discharge in consecutive time steps. Each picture corresponds to a single discharge. The shutter always opens at $t = 0.36 \mu s$ (solid line z). The exposure time varies from 60 (picture a) to 1000 (picture o) nanoseconds. The jitter with respect to the generator voltage and current is of the order of $0.04 \mu s$. X-rays, voltage, cathode and anode currents are represented in the bottom plot. The data are those of picture l. The moment of X-rays detection coincides with the connection between downward positive streamers and upward negative counter-streamers as shown in pictures e - h.

counter-leader will propagate upward until it connects with the downward leader.

Continuous Ohmic heating of the conductive streamer channels between anode and cathode leads to a well-conducting leader channel at $t = 1.4 \mu\text{s}$. On image o we see the final breakdown that is accompanied by strong current rises and voltage drop. The high-voltage current curve is limited by the diodes on the input to the optical transmission line. The GND current is limited by clipping of the oscilloscope channel amplifier. The total vertical length of the discharge on image o is equal to 1 meter.

The streamer head propagates and thus the streamer channel must have some finite conductivity, in spite of the low light emission of that channel. According to current understanding [Li09, Ebe06, Ebe97] the density of free electrons is about 10^{13} to 10^{14} cm^{-3} in the freshly formed streamer channel depending on the field enhancement at the streamer tip. This electron density determines the conductivity of the channel. The conductivity will vary in space and time, and clear predictions cannot be given. From the experimental side it is difficult to retrieve conductivity values because many parallel streamers contribute to the current. In figure 2.2 we observe a sudden increase in luminosity starting at picture j . One of the streamers channels heats up critically and increases its conductance to further develop into a leader. Because of the size, our leader is not comparable to a fully developed lightning leader.

The horizontal dimension of the cloud formed collectively by the numerous streamers is much larger than was expected before and equals approximately 1.4 m. This means, that all equipment placed at shorter distances will emit or receive streamers at certain times and will affect the measurements [Ngu08]. This is why we changed the setup and applied the Velostat foil, as mentioned in Section 2.2.

Note that the HV electrode carries a current $0.67 \mu\text{s}$ before the GND electrode does. This is due to the Ramo-Shockley effect. During that time, the loop of the current that includes the HV electrode closes via the displacement current to the environment, most notably to the soil and to the conducting safety fence near the spark gap. Only a very small part of the displacement current dD/dt is captured by the grounded electrode.

The images also show broad slanted streaks and horizontal lines that clearly do not originate from the electrodes. These artefacts are caused by reflections of the light from spark gaps in the Marx generator on the plies in the black background foil. It is worth mentioning that our camera detected emissions not only from the gap and the electrodes. The full conductive 9-meter connection line from the top of the divider to the spark gap and the top of the Marx generator emits streamers. Anyway, this illumination is relatively small and does not affect the pictures but it should be taken into account in the interpretation of the relation of current and voltage.

From the apparently constant luminosity throughout the length of streamer, we conclude that the positive streamer heads are "disconnected" from the HV electrode and fly like bullets through the medium, as also seen for streamers at lower voltages. Pictures with shorter exposure time (such as 20 ns in figure 2.3) confirm this. In the pictures shown in figure 2.2 we see the traces of those bullets. It is well known from streamer studies at lower voltages, that only the active ionization zones at the streamer heads emit light. At the streamer head the electric field is so high that electrons gain high energies and efficiently ionize and excite neutral molecules. The de-excitation of a certain

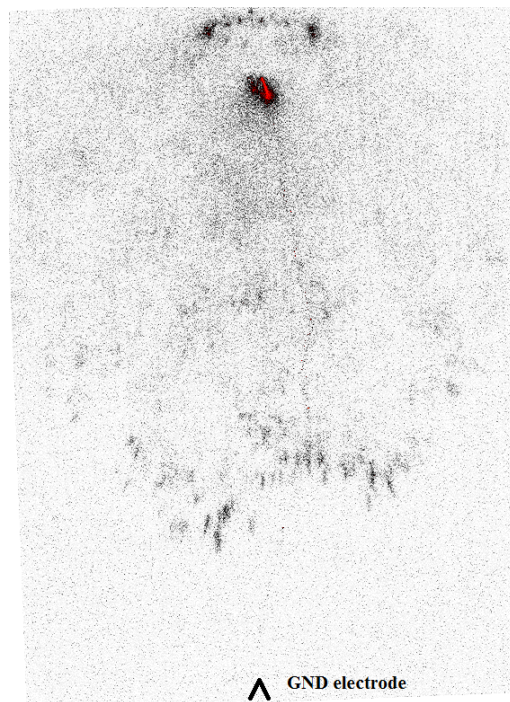


Figure 2.3: Positive streamer heads approach the cathode. A short early positive leader exists before current and counter-streamers appear on the grounded electrode. The gap distance is 1.5 m, and the exposure time is 20 ns.

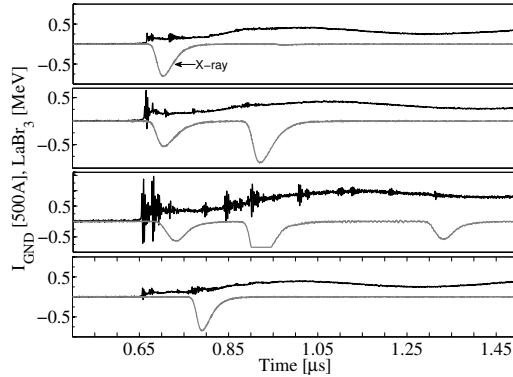


Figure 2.4: Oscillations of the cathode current (black line) and correlated X-rays (grey line). All X-rays were accompanied by high-frequency oscillations of the cathode current that correspond to moments when positive and negative counter-streamers connect.

nitrogen level (within about 1 ns in STP air) creates the light observed by the camera. Therefore the conducting channels stay invisible while the growing streamer tips are seen as "glowing dots". This was first photographed in [Blo97] and is illustrated in Figure 1 of [Ebe06]. The same glowing dots at the tips of growing streamer channels have also been observed in sprite discharges high above thunderstorms at air pressures of about 10 microbar [McH07], and a similar phenomenon also occurs as so-called "plasma bullets" in the complex gas mixture of pulsed atmospheric pressure plasma jets [Sar11, Rob12].

In figure 2.2 the leader develops only after streamers and counter-streamers have connected. There is no leader observed with this 1 m gap before the first conductive channel is formed. But this is only a matter of scale. At larger gap lengths we did observe a positive leader before the positive streamers reached the cathode; this is illustrated in figure 2.3 for a gap of 1.5 m.

In figure 2.3 a faint speckle trace from the anode to cathode can be observed. This is caused by the huge brightness of the main discharge after the camera shutter was closed. The shutter is electronic and very good but not perfect. Some light leaks through the image intensifier even when it is off. But this fact gives us the opportunity to see the final breakdown path even on pre-breakdown pictures. That is why we decided not to suppress it further. For instance, in figure 2.3 it is clear to see that breakdown followed the positive leader path. In figure 2.2 this trace also exists but due to longer exposure time and smaller scale it is almost indistinguishable.

2.3.2 X-ray timing

Some of the discharges had up to three X-rays peaks; see figure 2.4. Triple events were quite rare, of the order of 0.5% occurrence. The discharges with two X-ray events occurred in up to 35% of the discharge.

The first X-ray photons were detected immediately after the first cathode current oscillation. Figure 2.5 shows the distribution of X-ray occurrence times.

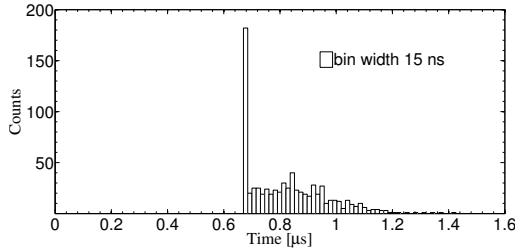


Figure 2.5: *X-rays time distribution. Timescale same as in figure 2.2 and figure 2.4. No X-rays were ever detected before cathode current started.*

The leftmost peak coincides with the onset of the GND current. These immediate X-rays (immediate component) stem from the first early period of active streamer connection. Many upward and downward streamers meet at this time interval. The first encounters occur between positive downward streamers and negative upward counter-streamers emitted from the cone tip of the cathode. As will be shown later, the corresponding X-rays are the most energetic. Negative streamers emitted from the edge of the protection dish are involved in subsequent collisions. Subsequent X-rays still correlate in time with cathode oscillations and are produced in subsequent connection events. The number of these connections is higher than those of the first clashes, but the X-rays registered later have softer spectra. On the other hand, the HF oscillations amplitude is significantly larger during the first connections than during the subsequent ones. That means that the first connection events are more energetic and X-ray productive events than those occurring later.

The total X-ray duration is of the order of 1 μs in our setup. The duration of one X-ray burst is determined by streamer collisions and can be less than the 11 ns of detector resolution.

We finally note that the background of the detector set at a discrimination level of 30 keV is approximately 50 counts per second and was determined by the measuring time needed to register 5000 detector pulses. This includes the contributions from cosmic rays, the laboratory environment and the internal isotope decay. The background remains constant during the day. The chance to observe any background signal that might mimic an X-ray signal from the gap during the X-ray duration time is less than 10^{-4} .

2.3.3 Probability of X-ray registration

We did not register X-rays in all discharges. The registration rate depends on the detector position as well. We determined the X-ray occurrence for different detector positions. Table 2.1 shows the result as the ratio of discharges with X-ray detection over the total number of discharges. To measure the registration rate at the points A and B we have placed a small EMC cabinet under the grounded electrode (as shown in figure 2.1) and this cabinet remained there during all measurements in Series I and II. This cabinet also enhanced the X-ray production by streamers from the four sharp corners, from the surface of the cabinet and from the additional length of shielded cable to the current

Table 2.1: Occurrence of X-ray detection in different positions.

Point	Coordinates x;y (m)	Occurrence out of surges	Occurrence P (%)
A ¹	0.15;-0.13	290/441	66
B ¹	0.35;-0.13	51/120	43
C ¹	2.10; 0.15	54/160	34
D ¹	1.50; 0.15	97/140	69
E ²	1.15;-0.3	10/10	100
F ²	1.50; 0.6	29/30	97
F' up ²	1.50; 0.6	19/50	38
F' mid ²	1.50; 0.6	5/20	25
F' down ²	1.50; 0.6	32/50	64
G ²	1.50; 2.0	48/50	96

¹ Series I. ² Series II.

probe. For instance, at 2.1 meter distance from the gap, the X-ray occurrence was of the order of 7% without the cabinet and 34% with cabinet under otherwise the same conditions and effective registration areas.

The occurrence data for positions A,B,C,D were obtained in one series of experiments. E, F and G were obtained in another series two month later. All numerical values are shown in 2.1.

It is still difficult to find the correlation between registration rate and detector distance due to the significant impact of the registration equipment at distances shorter than 1.5 m from the discharge (see figure 2.2). But the occurrence of registration reduces with larger distance from the gap. In our opinion, the X-ray generation area can be approximated by a point-like source for larger distances. If we consider only geometrical decay (without absorption and scattering), the registration rate will follow an inverse square law for distances larger than 1.5 m, as suggested by the ratio of occurrence for positions D (69%) and C (34%). The run-away electrons from one negative streamer are certainly beamed. But for electron energies below 0.5 MeV, the Bremsstrahlung is rather isotropic (see Figure 3 in [Koe14a]), in contrast to Bremsstrahlung from electrons with relativistic energies.

2.3.4 Cathode shape

Following the thought that mainly the upward negative streamers are responsible for the high-energy electrons that generate the X-rays, the shape of GND electrode should significantly affect the number of negative streamers and thereby the X-ray occurrence. Implicitly we assume that the number of the positive streamers is constant and independent of the shape of the grounded electrode, at least during the first stages of discharge development. To check this, we made an aluminium belt of 55 by 10 cm with 75 sharp dots on its surface (figure 2.6). We bent it according to the positive corona face as shown in picture *d* of figure 2.2 and mounted it on the GND electrode. The small EMC cabinet was replaced by a post of the same height.



Figure 2.6: Our alternative grounded electrode of 55 by 10 cm with 75 sharp points to generate upward negative streamers.

Figure 2.7 shows that the total number of negative streamers is greatly enhanced. The effective connection area and the number of encounters between positive streamers and negative counter-streamers significantly increased while the shape of the positive corona and the streamer density remain the same.

The X-rays were observed from 2.1 m distance by two LaBr_3 detectors. The total effective scintillator area was 23 cm^2 . The X-ray occurrence increased from 7% without the belt up to 70% with the belt. The number of cathode current oscillations also remarkably increased. Without belt we registered triple X-ray signals in 0.5% of the discharges and with belt in 15%. So, a fakirs bed strongly enhances the X-ray production. The small EMC cabinet under the cathode (row C in 2.1) caused a similar increase. This cabinet causes impact on all points in the table. So the all X-ray data during Series I and Series II are intensified by additional negative counter-streamers from the small EMC cabinet.

2.3.5 The region of X-ray emission

In order to determine where the X-rays are generated, we limited the field of view of the detector by lead tubes of 1 and 2.5 cm thickness covering the detector over its full length. This thickness is sufficient as will be shown in 2.3.6 on attenuation curves. A number of 100 surges were enough to determine the probability of seeing X-rays. But we refrained from an analysis of the X-ray energy spectra in these experiments. We pointed the detectors to different parts of the gap: the HV electrode, the GND electrode and the middle (see cones in figure 2.1, point F'). With the detector pointing to the cathode (F' down, 2.1), two times more events were observed than with the detector pointing to the anode (F' up, 2.1). When we directed the detector to the middle position, we found less X-ray events (F' mid, in 2.1) than from the anode and cathode region.

Both first and subsequent X-rays were registered to come from the cathode, anode and central regions. In some cases X-rays from the cathode and from the anode region were detected simultaneously, to within the time resolution of our detectors. It means that the high-energy electrons can emerge from the region between the streamers (see images *e*, *f*, *g* in figure 2.2) but create Bremsstrahlung over the full length of the gap including the anode and the surrounding area. The time that relativistic electrons need to cross the full gap is of the order of 3 nanoseconds or less, which is within the time resolution of the X-ray detectors.



Figure 2.7: Connection between positive downward and negative upward streamers initiated from the sharp belt. Exposure time is 300 ns; the gap length is 1 meter.

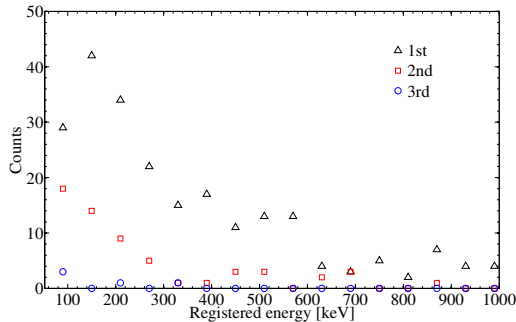


Figure 2.8: Energy spectra of the detected X-ray photons. The three sets of data \triangle , \square and \circ correspond to the first, second and third x-ray burst respectively.

2.3.6 Energy spectra and attenuation curves

We collected data of 441 discharges with the detector at position A (figure 2.1) inside the small EMC cabinet. The number of occurrences as a function of energy is shown in figure 2.8, where each X-ray signal in a discharge is counted individually. The energy scale is divided in bins of 60 keV. Please note that the first X-ray signal can be delayed with respect to the first cathode current. This is because we probably did not register X-rays produced by first streamer encounters. An example is shown in the two lower records of figure 2.4. X-ray in bottom plot is marked as first X-ray. The first occurrence is most often the most energetic. Even a single event with up to 3.4 MeV has been observed. For the sake of clarity we limited the energy scale to 1 MeV, which is also the maximum energy a single electron can acquire with the available voltage. The later X-ray signals are less frequent by a factor of three or more. But the energy of the second signal can still be comparable to or larger than the first; see for example the third record in figure 2.4. As mentioned in 2.3.2, the X-ray signals correlate well in time with the connection moments of positive and negative streamers as shown in the pictures of figure 2.2. In order to determine the actual photon energy of the observed X-rays we carried out a series of experiments with lead attenuators in front of the collimated detector. One detector was again mounted in the small cabinet at position A close to the gap, another in the large cabinet at 1.5 m from the gap. Caps of various thicknesses were used: 1.5, 3.0, 4.5 mm, and 50 to 100 discharges were investigated for every cap thickness. The green (\square) and blue (\circ) data in figure 2.9 show the dependence of X-ray occurrence on the lead thickness.

Figure 2.9 also shows the absorption curve (\triangle) that would be observed assuming that the amplitude of the X-ray signals without absorber would one-to-one correspond to single photon energy. This spectrum integrated absorption curve lies definitely above the experimental data. This indicates that many of the high energy signals are due to pile up: several lesser energy X-ray photons are registered simultaneously within the 11 ns time resolution of the detector. Two additional lines represent the lead absorption for monoenergetic photons of 200 and 300 keV, calculated with data from [Ber98]. The experimental data fit best to the 200 keV line. However, with the wide spectrum of X-rays, one may question whether it is allowed to convert the attenuation curve into an

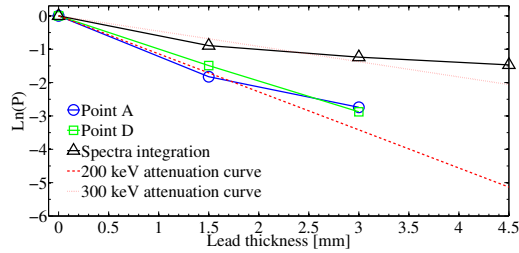


Figure 2.9: X-ray lead attenuation curves at point A close to the grounded electrode and at point D at 1.5 m from the gap (figure 2.1). The integrated spectrum Δ and attenuation lines for 200 and 300 keV from the NIST database are shown as well. The connecting lines between the measurement points are drawn as a guide to the eye.

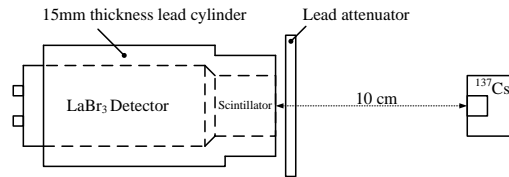


Figure 2.10: Lead attenuation setup of 662 keV photons from ^{137}Cs radioactive source.

equivalent energy.

In order to get some insight into the energy spectrum, we obtained the attenuation curves of 662 keV gammas from a near to monochromatic ^{137}Cs source in a similar setup (figure 2.10), where we focused on the attenuation of all photons arriving at the detector. The question is whether it can be expected that the attenuation curve is a straight line on a semi-logarithmic plot. The experimental linear attenuation coefficient (curve slope) is $\mu = 4.66 \cdot 10^{-2} \text{ cm}^2/\text{g}$. The coefficient μ consist of two parts: τ - the photoelectric component and ε - the Compton effect component. Pair production in the lead can be neglected due to the energy threshold of 1.022 MeV. To draw the attenuation curve (figure 2.11), we counted all photons that penetrated through the lead attenuator. We did not select on energy. Partial absorption by the lead is then not accounted for. This also occurs with the X-rays from the spark, where the photon energy before attenuation is a priori unknown.

According to the NIST database [Ber98], the photoelectric absorption coefficient for 662 keV photons equals $\tau = 4.33 \cdot 10^{-2} \text{ cm}^2/\text{g}$. The small difference between the total attenuation coefficient μ and the photoelectric absorption coefficient from the NIST data implies that the Compton effect inside the lead for this setup is negligible. Most of the Compton-scattered photons penetrate the lead attenuator and hit the scintillator. If this statement is correct for 662 keV energy photons (Compton effect comparable to photoelectric absorption) it is particularly correct for 200 keV energy photons, where the photoelectric component is 10 times larger than the Compton component. Consequently, we should only take the photoelectric part into account for the energy reconstruction from attenuation curves.

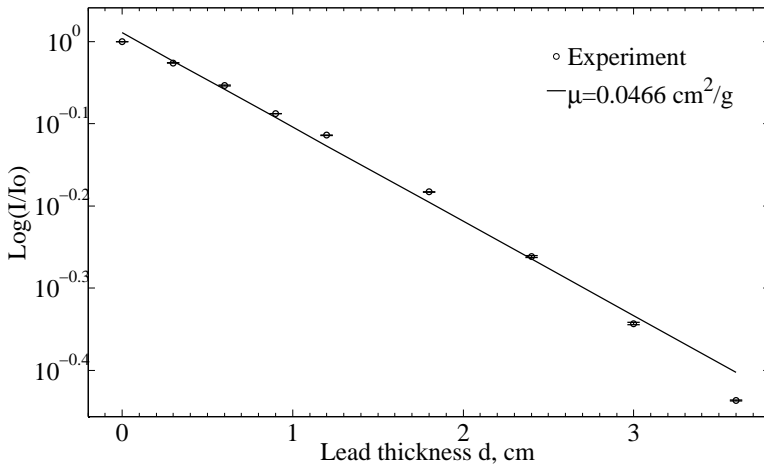


Figure 2.11: Attenuation of 662 keV gammas by lead and comparison with NIST data.

2.4 Discussion and conclusions

Our experimental results clearly demonstrate that the presence of negative streamers is a necessary condition for X-ray generation in meter long positive discharges in the laboratory. There were no X-rays observed before the negative counter-streamers initiated from the grounded electrode. Most of the detected X-rays correlated with high-frequency current oscillations on the current probe of the grounded electrode. By increasing the number of negative streamers with our fakirs bed electrode we dramatically increased the occurrence of X-rays. That negative streamers play a role in X-ray generation is consistent with the theoretical papers quoted in the introduction [Mos06, Li09, Cha10, Cell11] that show how electrons are accelerated out of the streamer tip and away from the electrode. The Bremsstrahlung photons are therefore generated in open air, and not at some metal parts. The X-ray localization confirms this statement.

The current data together with the pictures show that the high-energy electrons necessary for the X-rays correlate in time with the encounter of positive downward and negative upward streamers. It is most probable that the run-away process occurs in the region between positive and negative streamer tips just before the connection because the electric field and total available voltage then and there are higher than anywhere else. It would be a hard but interesting task to assign an individual connection to the run-away process. As mentioned before, run-away process and X-ray generation occur within the 11 ns time resolution of our detectors, but do not need to coincide in space. Streamer encounters generate ns-fast X-ray bursts.

The absorption data are consistent with a predominant photon energy of 200 keV.

There is only a small allusion of non-homogeneity of the X-ray emission present in our data. The spectra in point G (figure 2.1) seem to be more energetic than at other points.

It is unlikely that X-rays were emitted by other parts of the Lightning Surge Generator installation due to absence of negative streamers. No strong orientation dependence of the X-ray emission was found in our experiments, in agreement with [Koe14a].

The pictures discriminate very well between the streamers and the leaders and clearly indicate the moment when the leader starts to develop. Streamers are less bright than leaders. Both appear to have nearly the same velocity ($2 \cdot 10^6$ m/s) and thickness of the order of 1 cm for the streamer channel and for the leader channel core. All thicknesses are measured at FWHM level by the technique described in [Nij10]. Around the leader core there is a region of lower luminosity with a diameter of about 7 cm, that might be identified as leader sheath. A more detailed discussion requires knowledge of the contrast transfer function of the optical chain consisting of lens, image intensifier and CCD. This information is not available yet.

A full breakdown is not a necessary condition to generate X-rays because the X-rays are generated in the streamer phase. Even the leader is not necessary. But it is difficult to avoid full breakdown of the high voltage gap in our setup. The usual way is to short-circuit the generator by a second gap. This gap would then also generate X-rays.

It is interesting to speculate and to extrapolate our results to negative high-voltage discharges. There the space stem that can appear in front of the negative leader can play the role of the positive electrode. The main point from our work is that negative streamers approaching positive ones appear to be a necessary condition for X-rays in our setup, even for positive high-voltage discharges. Though there are certainly features in our setup that are not representative for natural lightning like the gap length and the voltage amplitude and shape, we observe generic phenomena of streamer and leader formation, and our measurements show the dominant role of the negative streamer corona for the production of hard radiation; such negative streamer coronas appear as well at the negative ends of lightning leaders and space stems.

CHAPTER 3

DEVELOPMENT OF METER-SCALE NEGATIVE DISCHARGE IN AIR

We study the development of a negative discharge driven by a Marx generator of about 1 MV in an air gap of 1 up to 1.5 meter, at standard temperature and pressure. We show the evolution of the discharge with nanosecond-fast photography together with the electrical characteristics. The negative discharge develops through four well-distinguished streamer bursts. The streamers have different velocities and life times in different bursts. The last burst triggers a positive inception cloud on the positive grounded electrode and a burst of positive counter-streamers emerges. The pre-discharge then bridges the gap and leaders grow from both electrodes. Finally a spark is formed. Looking closer into the pre-ionized zone near the cathode, we find isolated dots which are potential branching points. These dots act as starting points for positive streamers that move towards the high-voltage electrode. We also find such phenomena as space leaders and leader stepping in our laboratory sparks.

3.1 Introduction

Natural lightning is a very complex phenomenon evolving on multiple temporal and spatial scales. The stepping of lightning leaders, space stems, dart leaders as well as the energetic radiation from thunderstorms such as Terrestrial Gamma-Ray Flashes, electron beams and electron-positron beams are far from being fully understood. Furthermore a wealth of discharge phenomena was discovered above thunderclouds, called Transient Luminous Events (TLE's), including sprite discharges. All these phenomena are currently subject of international research, geophysical conferences, workshops and summer schools. However, natural lightning events are erratic and difficult to access for precise observations.

In previous work [Koc12] we have presented images and analysis of metre length positive discharges, and of their energetic radiation. The same source was a standard lightning impulse generator of 2 MV maximum. Here we focus on the structure and evolution of negative discharges, having in mind that the majority of cloud-to-ground lightning flashes have negative polarity. We find stepping phenomena, space stems and energetic radiation as well, but also discharge features that to our knowledge have not yet been found in lightning. Therefore we believe that our study is of interest for lightning research as well as for lightning protection and high-voltage technology.

Only few studies [Ogi11, Zen13] have been performed recently on metre-scale laboratory discharges in STP air because these require a large experimental facility, modern fast cameras and careful electromagnetic shielding of measuring equipment. A recent overview is given in [Bia11]. The current understanding of long discharges is still mostly based on streak camera observations [Gal02] performed in 1980's. Reess et al. [Ree95] performed an experimental study of negative discharges in a meter-scale gap in 1995 with streak photography. Our voltage amplitude of 1.2 MV and gap length of about 1 m are of the same order. The high-voltage pulse shape differ: 1.2/50 μs versus 0.3/2000 μs in [Ree95]. We use two conical electrodes, instead of a point-plane gap. The conical ground electrode defines a clear starting point for the counter-discharge and allows the current through that electrode to be measured. Two high-resolution, nano-second fast intensified CCD cameras have been used. Their adjustable shutter delay and opening times provide the opportunity to take two subsequent images, which then show the discharge growth, its speed and direction. The synchronised measurement of the electrical parameters gives the stages of the discharge: formation of the inception cloud, streamers bursts, streamer encounters and even leader formation and stepping. With the aid of fast computer storage of data and images, more than 3000 discharges are available for analysis. This large number allows to discern particular and general phenomena.

In this paper we show high-quality images of negative discharges in STP air, combined with the electrical characterization of the discharges. In our setup the streamers emerge in bursts as the voltage rises. We follow the negative discharge development from the first light emission up to the final breakdown, first 3.3.1 in time-integrated images as in [Koc12] or streak photography [Ree95]. The time sequences with two cameras provide more information 3.3.2. We present detailed images of the chaotic phenomena at the high voltage electrode over the fourth streamer burst 3.3.3. Observations on the leader phase 3.3.4 and a brief comparison with phenomena observed in nature 3.3.5 follow.

3.2 Experimental setup

The setup is similar to the one described in [Koc12]; for the sake of completeness it is represented again in figure 3.1. The 2 MV Marx generator delivers a high-voltage (HV) standard lightning pulse with 1.2/50 μs rise/fall time. The upper voltage limit employed was about 1.2 MV. The generator voltage was measured by a capacitive high-voltage divider. The electrodes of the spark gap are cones. The tip distance was varied between 1 m and 1.75 m. Two Pearson 7427 current probes determined the currents through the HV electrode (cathode) and the grounded electrode (anode). An optical transmission system

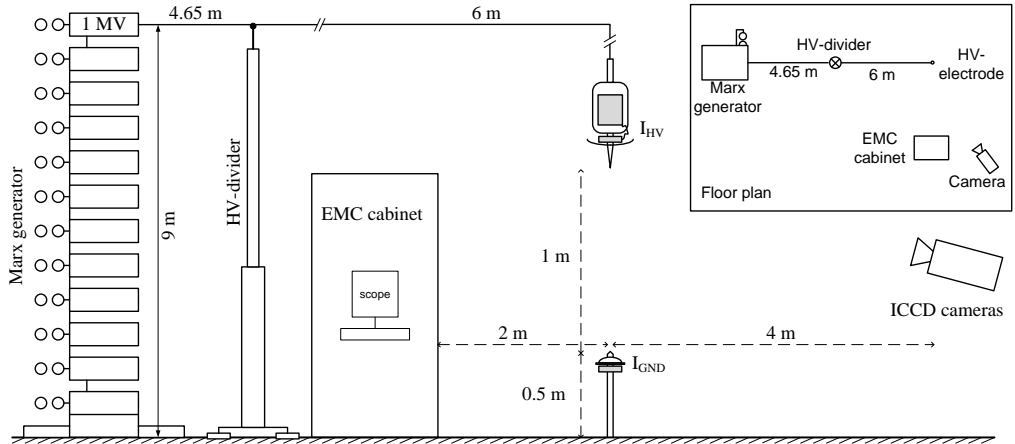


Figure 3.1: Schematic of the experimental setup. Two ICCD cameras are located at 3.5-4.5 m distance from the gap. The distance between Marx generator and the spark gap is 8 m. The upper right inset shows the scaled floor plan of the setup.

inside the HV electrode transported the HV current signal. Suitable attenuators and two antiparallel high-speed diodes protect the input of the transmitter. The diodes limit the linear response to 250 A; above this value the transfer is approximately logarithmic. An RG214 cable connected the current probe for the grounded electrode directly to the measuring system. An aluminum disk mounted near each probe minimised the risk of a direct hit by the full 4 kA spark current.

Two Picos4 Stanford Optical cameras were placed side by side at 4 m distance from the spark gap. The cameras contain charge coupled image sensors preceded by a fast switched image intensifier (ICCD). The image intensifier is a micro-channel plate that allows us to adjust the camera sensitivity by varying the applied voltage. The CCD is read out with 12 bit resolution. The camera optical axis was most often directed towards the spark gap centre. In comparison with our previous study on positive discharges [1], optical shielding of the spark gaps in the Marx generator significantly reduced the laboratory background visibility in the images. Appropriate electromagnetic shielding protected the cameras and their communication cables against electro-magnetic interference. The image intensifier amplification has been set to accommodate the light level and range of a particular experiment. Both cameras were adjusted to the same sensitivity, but no absolute calibration has been carried out. Lenses were either Nikon 35 mm F2.8 fixed focus or Sigma 70-300 mm F/4-5.6 zoom. With the telenses, structures of only half a millimetre in diameter were well resolved near the electrodes. The full optical spectrum was used as emitted by the discharge, as transmitted by the lenses and captured by the ICCD cathode. As mentioned in the Introduction, the cameras were triggered simultaneously and opened their shutters after an adjustable delay, which allowed capturing two subsequent images during one discharge. To smooth the contrast of some images in print, we sometimes applied a gamma correction. The measured light intensity I_m is then scaled between 0 (black) and 1 (white) and is displayed as I_m^γ intensity in the figures. A value of γ less than one increases the relative intensity

of darker pixels. The figure captions mention such a correction when applied. On the cameras leaders appear at least four times brighter than the streamers head traces. The streamer-leader transition is gradual as leaders form out of streamer channels by Ohmic heating of the gas. In this sense, we introduce the term 'pre-leader' for stationary channels that are definitely brighter than the streamer head, but not yet at full leader intensity. But even with the high camera speed, stationary dim phenomena can look bright. Additionally the measured intensity depends on the orientation and direction of movement with respect to the camera axis.

The electrical signal acquisition system consisted of two LeCroy oscilloscopes with 1 GHz bandwidth. The negative edge of the signal from the HV divider triggered the oscilloscopes. One oscilloscope then also triggered both cameras. The differences in the delays caused by the instruments and cables were corrected for to within 1 nanosecond accuracy.

Some remarks on the measured voltage follow: ideally the gap voltage is measured as line integral of the electric field over a straight path between the electrodes. But any object there would interfere with the discharge formation. We use the voltage obtained from the 9 m tall high voltage divider instead, which differs from the gap voltage because of the inductance L in the large loop formed by the divider, wiring and gap. From the measured resonance frequency of 1.7 MHz at gap breakdown and the known 600 pF HV divider capacitance we obtain $L = 15\mu\text{H}$. Values for the current derivative dI/dt at the high voltage electrode of the order of 1 A/ns will be shown below. To this adds the current contribution from discharges at the wiring towards the electrode. The inductive voltage difference between divider and gap is thus 15 kV or more. Faster current variations also occurred occasionally at the electrode, and then the 20 pF capacitance of the high voltage electrode and nearby wiring act as supply. For these reasons we preferred to use the electrode currents as critical parameter in the analysis. The rather high impedance of the surge generator as current source and the microsecond variation of the voltage made the various stages in the discharge formation discernable.

3.3 Results

We studied the different phases of negative discharge development in detail. First one has the inception cloud, a faint ionized region that develops around the sharp edges and tips of the electrodes. Because of the low light level compared to later phases, we set the camera sensitivity to a high level and zoomed in on the electrodes. With rising voltage and electric field at the cloud surface, streamers emerge from the cloud. In 3.3.1 we show the time integrated images taken with increasing exposure times on a single camera. These images can be compared with those presented earlier for positive discharges in [Koc12]. Short exposure images taken with two cameras in sequence are presented in 3.3.2. When the streamers bridge the gap, those between the electrodes become bright because of increased current and Ohmic heating while streamers in other directions extinguish. The fine structure of the later phases near the HV electrode is discussed in 3.3.3. 3.3.4 presents the formation of leaders in our metre-sized gap, which are attached

to the electrodes. For gaps of about one meter or less, the final stage is a spark between the electrodes. The spark properties are outside the scope of this paper. The spark does not occur at 1.75 m electrode distance within the time allowed by the surge generator fall time of 50 μs . In 3.3.5 we show the striking similarity in appearance between some discharges in our set-up and tens of kilometer sized sprite discharges [Cum06, Ebe10] at high altitude and strongly varying low gas pressure.

3.3.1 Sequence of time-integrated images

Figure 3.2 presents the negative discharge development in a series of time-integrated images, taken with a single camera, where the camera shutter always opens at the same moment in the voltage waveform, but the exposure time increases from panel to panel. The high-voltage (top) and grounded electrode (bottom) are indicated in the images. The distance between electrodes is 1.27 m between the tips. Every image shows a different discharge under the same conditions, but the images of the discharge development show a large similarity from discharge to discharge. The electrical signals of the voltage (U), cathode (I_{HV}) and anode (I_{GND}) current are represented in the bottom plot (p); these are the average over 65 discharges. The averaging is allowed because also the electrical characteristics between the individual discharges are very similar. For instance the details of the I_{HV} curve remain recognizable such as the first leap in between 0.2-0.3 μs . The trigger for the oscilloscopes and cameras is derived from the voltage as measured by the HV divider (figure 3.1). Even for the strongly fluctuating current I_{HV} on the HV electrode, the jitter over different discharges is only 50 ns.

On the time axis $t = 0 \mu\text{s}$ corresponds to the start of the voltage pulse. The solid vertical line z at $t = 0.47 \mu\text{s}$ in plot (p) indicates the shutter opening time of the camera. Dotted vertical lines (a)-(o) label the shutter closing times for the corresponding images. Thus, a single image is time-integrated from the starting time z until the shutter closing time between 25 (a) and 1650 (o) ns later. A faint speckle trace connecting the electrodes is visible in the first six images. It is caused by the huge brightness of the spark that appears after the camera shutter is closed. The electronic shutter is good but not perfect; some light of the arc leaks through the image intensifier even when it is off. But the speckle trace shows the final breakdown path even on pre-breakdown images. During the entire sequence we keep the camera sensitivity constant. The linear color coding scheme to the ICCD output is indicated by the color bar on the right. No gamma correction has been applied. The negative inception cloud is not included in this sequence; these images are shown later in 3.3.1.

At the beginning, a current of up to 40 A is measured on the high-voltage electrode between the times 0.15 and 0.32 μs , while the voltage rises to 180 kV; see figure 3.2 (p). The current leap corresponds to the first streamer burst or corona formation, where the current is the sum for all streamers from the tip and the edges of the protection disk. The high-voltage current decreases to zero at $t = 0.35 \mu\text{s}$, in spite of the voltage rising to 200 kV. The current zero indicates that the streamer growth stops momentarily. The second cathode current leap with the maximum amplitude 75 A and its associated streamer burst appears between $t = 0.35$ to 0.47 μs . The streamers are slightly visible in image (a) at 35 cm distance from the high-voltage electrode tip. Thus, two small

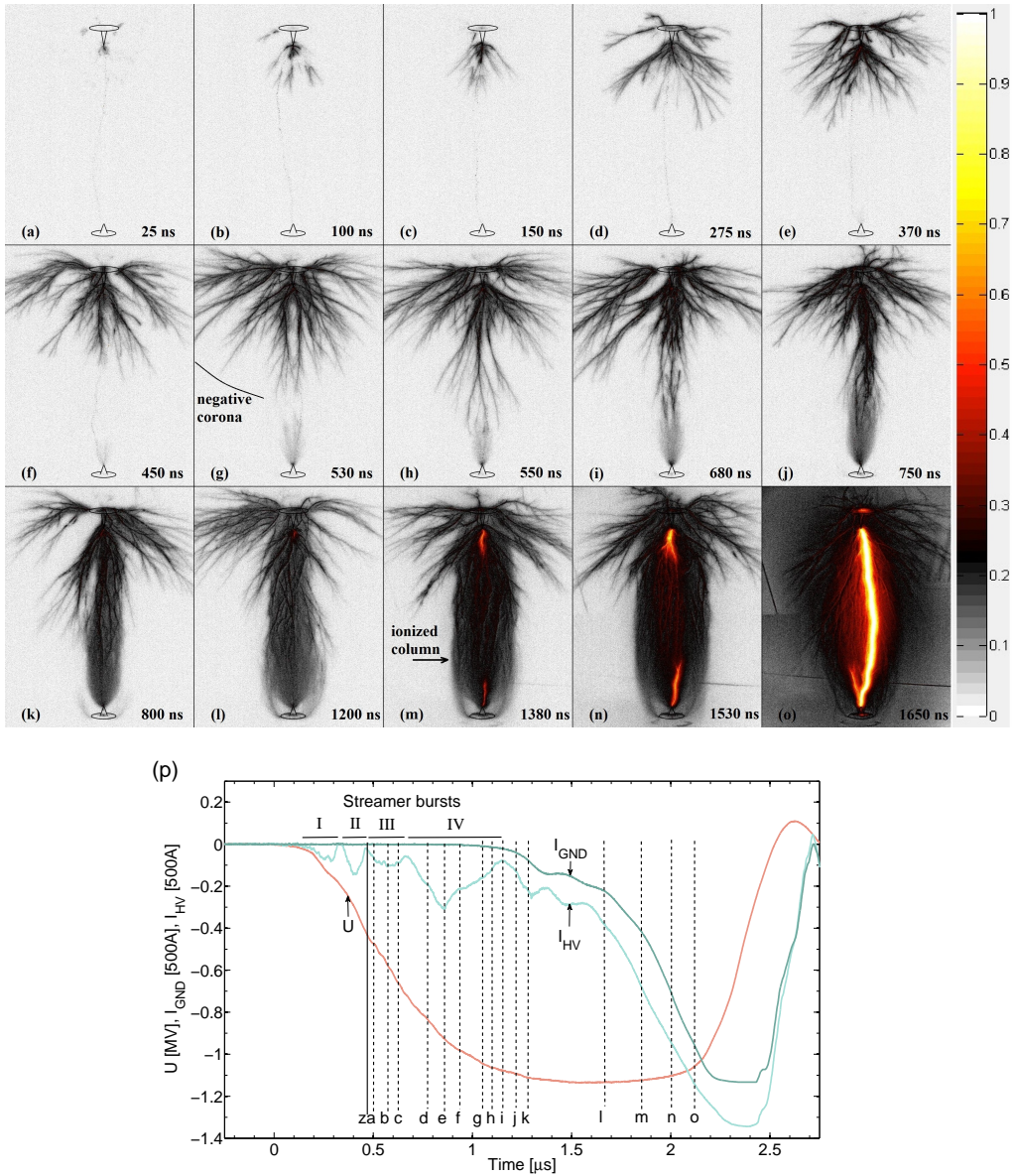


Figure 3.2: Time-integrated sequence of the development of a negative discharge over a gap length of 127 cm. Each picture shows a different discharge under the same conditions. The shutter always opens at $t = 0.47 \mu$ s (solid line z). The exposure time varies from 25 ns in panel (a) to 1650 ns in panel (o) and indicated at right bottom corner of each picture. The linear color coding scheme for the light intensity is indicated on the right side of the figure. Voltage (U), cathode (I_{HV}) and anode (I_{GND}) current are represented in the bottom plot (p). These measurements are averaged over 65 discharges.

streamer bursts with corresponding current pulses on the HV electrode preceded the sequence shown in figure 3.2.

In figure 3.2 (a)-(c) we see the third streamer burst. Because of the time-integration, image (b) comprises all light of (a) and so on. While the applied voltage keeps increasing, at $t = 0.7 \mu\text{s}$ the fourth and largest streamer burst starts. The corresponding image (d) shows a well-developed negative corona near the high-voltage electrode where the air is already ionized by previous streamers. From the continuity of the traces, we conclude that the outer-most streamer tracks are an extension of those existing earlier, in agreement with [Nij13]. Some of these streamers propagate quite far across the gap until close to the grounded electrode (images (d)-(g)). In image (e) a faint positive inception cloud [Bri08a, Cle13, Nij11b] is visible near the grounded electrode, because the approaching negative streamer charge raises the electric field at this electrode sufficiently. That inception cloud gradually develops (image (f)) to the moment when it destabilizes into positive streamers (image (g)). The positive counter-streamers merge with the approaching negative streamers and develop into a highly ionized column (images (k)-(n)) with a diameter of about 40 cm. Two bright leaders (images (m) and (n)) grow towards each other from the electrodes through the ionized column, until they connect and form a spark. The radius of the fully developed negative corona exceeds 1 metre in figure 3.2 (m). As we assumed earlier in [Ngu08], everything placed on shorter distance influences the discharge development by emitting unwanted streamers. In the present setup we moved sharp objects to a larger distance or covered them with conductive plastic, except for the grounded electrode.

Inception processes.

The first faint light comes from the inception cloud around the HV electrode tip immediately after we apply the high-voltage. Positive and negative inception clouds have been found and investigated previously in [Bri08a, Cle13, Nij11b]. Inception clouds of both polarities also appear in our experiments. They look similar although the current direction and electrode processes are quite different. Figure 3.3 (a) shows the negative inception cloud and the first streamers that emerge later from the disk rim. For this image we zoomed in on the HV electrode and enhanced the gain of the image intensifier. The camera shutter opening time is plotted in figure 3.3 (b), superimposed on the voltage and current waveforms. The radius of the inception cloud r_{ic} observed in figure 3.3 (a) is 1.6 cm. From the breakdown electric field $E_{cr} \sim 32 \text{ kV/cm}$ we estimate the necessary voltage: $U = r_{ic} \cdot E_{cr}$ and charge $Q = E_{cr} \times 4\pi\epsilon_0 r_{ic}^2$ in the simple model of a spherical and conducting inception cloud. The resulting voltage $U=50 \text{ kV}$, the charge inside the cloud is $Q=85 \text{ nC}$. This is consistent with the measurements: At the beginning of the waveform the current I_{HV} rises at the rate of 1 A/ns. Then the 85 nC charge is deposited in 13 ns or when the current attains 13 A. The measured voltage is indeed 50 kV at that moment. At the end of the camera exposure, the voltage has risen to 130 kV and the cloud has by then destabilized into streamers. The 120 A of observed current at the shutter closure time feeds the streamers emerging from the inception cloud and from the protection disk.

A positive inception cloud appears near the grounded electrode when the electric

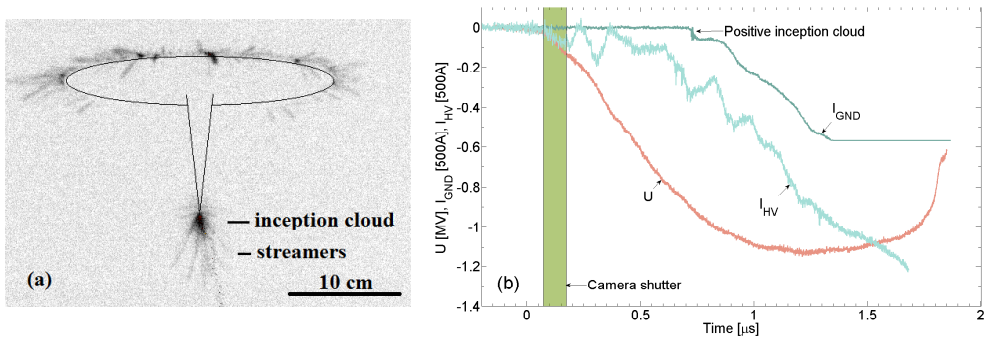


Figure 3.3: (a) Image of negative inception cloud and first streamer burst at the high-voltage electrode tip. The exposure time is 100 ns. The radius of the inception cloud around the electrode is 1.6 cm. Shutter opening time and moment of positive inception cloud formation are indicated in image (b). The gap distance is 107 cm.

field at the grounded electrode tip is sufficiently large. Such an event happens at time $t = 0.73 \mu\text{s}$ in figure 3.3 (b). In this particular discharge, the cloud formation causes the sudden rise of the current I_{GND} on the grounded electrode. Figure 3.4 shows two subsequent photos, each with 20 ns exposure, zoomed in on the grounded electrode tip, where both cameras have equal sensitivity. In the first photo, streamers emerge from the top of the positive inception cloud. The radius of the inception cloud is approximately 2 cm. The radius is consistent with the same E_{cr} for the charge of $80 \pm 50 \text{ nC}$ derived from the current I_{GND} . The large spread is due to the noise in the measurement. Of course, the relation between charge and voltage cannot be maintained for the grounded electrode. The cloud is warped due to the field inhomogeneity caused by the tip and to the presence of the negative streamer front. In the second photo (b) the cloud is not visible anymore. Apparently the excitation processes are not dominant anymore. Only a bright spot of several mm size remains near the electrode tip. The electrode emits a continuous current into the streamer corona, as also mentioned elsewhere for such a process [Bri08a, Cle13, Nij11b].

The streamers emerging from the negative inception cloud are relatively slow. With a speed of $4 \cdot 10^5 \text{ m/s}$ they cross a 13 cm distance from the cathode in figure 3.3 (a). The voltage at this moment is about 140 kV, thus the streamers have a so-called stability field of $140/13 \text{ cm} = 11 \text{ kV/cm}$ in agreement with previous measurements [Baz98]. For a recent critical discussion and new results on the theoretical understanding of the stability field, we refer to [Luq14]. We varied the distance between the electrodes and found that the delay between negative and positive clouds depends on this distance. Figure 3.5 shows the delay for distances between 1.0 m and 1.5 m. Naturally the voltage at which the positive inception cloud appears increases with distance between the electrodes. Still we can interpret the increased delay figure as an averaged streamer propagation speed over the gap. The straight line is a linear fit with a slope of $4.4 \cdot 10^5 \text{ m/s}$ and a determination coefficient R-squared of 0.97. This averaged speed is remarkably close to

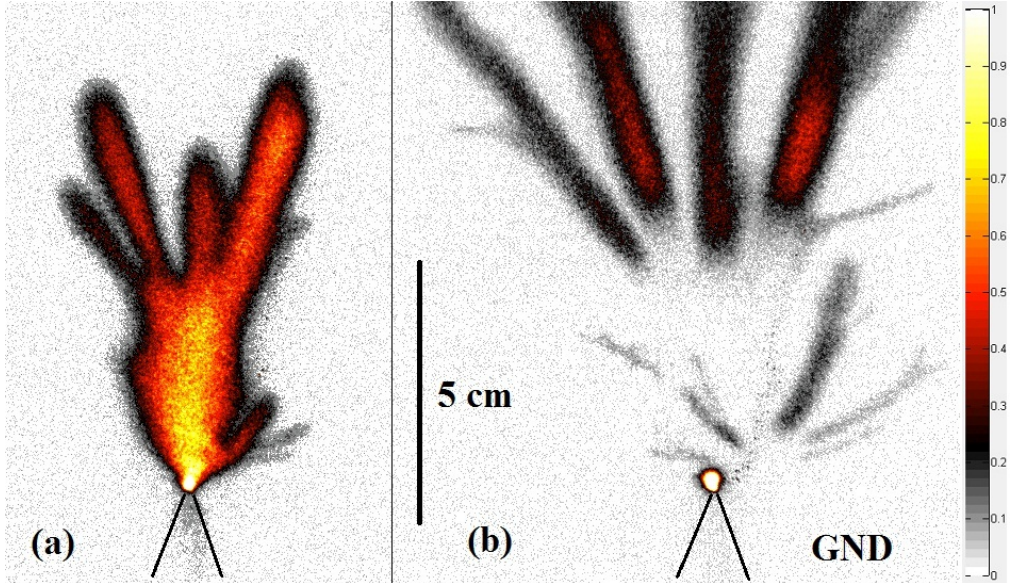


Figure 3.4: The positive inception cloud at the ground electrode is shown in two subsequent images, each with an exposure time of 20 ns. The inception cloud and the emerging streamers are visible in panel (a). Panel (b) shows the further growth of the streamers, and a bright dot of glow at the electrode that feeds the streamers and the now invisible cloud with current.

the speed of the first streamers emerging from the inception cloud as just mentioned.

Negative streamer propagation and streamer bursts.

We now analyze the negative streamer corona as shown in figure 3.2 (b) (h) as a half-sphere centered at the electrode tip. The radius of the corona sphere as a function of voltage is shown in figure 3.6 (a), and as a function of time in figure 3.6 (b). The straight line in panel (a) indicates so-called stability field $E_{min} = 12 \text{ kV/cm}$ for negative streamers in STP air [Bab97] and [[Bri08b], figure 7]. Observations [Baz98] show that the maximum streamer length is frequently determined by the applied voltage U divided by the stability field. But please note the experimental counter example in [Bri08b], with a theoretical substantiation in [Luq14]. Figure 3.6 shows the second, third and fourth streamer burst, indicated by II, III, and IV. In each burst, the streamers grow up to the maximal length supported by the voltage at that instant. The applied voltage increases slower than necessary to support a continuous streamer development. As a result, the streamers stop momentarily as indicated by the current zeros mentioned in figure 3.2 and 3.3.1. But voltage keeps rising. The 50 ns delay between second and third streamer burst in figure 3.6 (b) corresponds to a voltage rise of 100 kV. Streamers of the previous burst are then re-energized [Nij13] but also new streamers emerge from the high-voltage electrode, in particular from the rim of the disk. The process repeats until the fourth and last burst bridges the gap. The radii can be fitted by a curve $r_c = 95 \cdot t^2$, where r_c

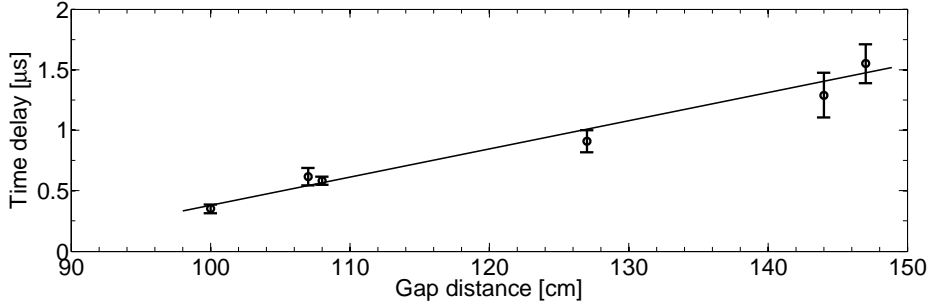


Figure 3.5: The time delay between the positive and the negative inception cloud as a function of the electrode distance, which can be interpreted as the averaged negative streamer propagation speed. The straight line with $4.4 \cdot 10^5$ m/s slope is a fit to the data.

is the corona radius in cm and t is time in μs . The last five data points are above the stability field line and that bursts appear when the gap is being bridged.

Branching angles of negative streamers.

The images show that most negative streamers split into two branches during their propagation. An example is shown in figure 3.7 (a). We analyzed how 500 branching events appear in the 2D image plane. We selected streamers with equal brightness on both branches without the gamma correction for the images. This selection emphasizes splits with both paths in a plane perpendicular to the camera viewing direction. Only outermost streamers were taken into account. The distribution of branching angles is shown in figure 3.7 (b). The branching angle may depend on gas parameters and electric field. It is clear that in our case the negative streamer tends to split at an angle of 29° with 5° standard deviation. Interaction and branching angles of positive streamers in different electrical environments were analyzed in [Bri08b, Nij08, Nij10]. To our knowledge, branching angles of negative streamers were not reported before.

3.3.2 Pre-breakdown in time-resolved image sequence

To illustrate the importance of short exposure images, we compare in figure 3.8 a long (a, 550 ns) and short (b, 25 ns) exposure. Many negative streamer traces are visible in figure 3.8 (a), but most of them have no visible traces in (b) just after the end of (a). This means that most negative streamer channels may still exist as conducting channels, but lost their light emitting properties for instance by lack of growth and optically active streamer head. Only positive streamers rise from the inception cloud

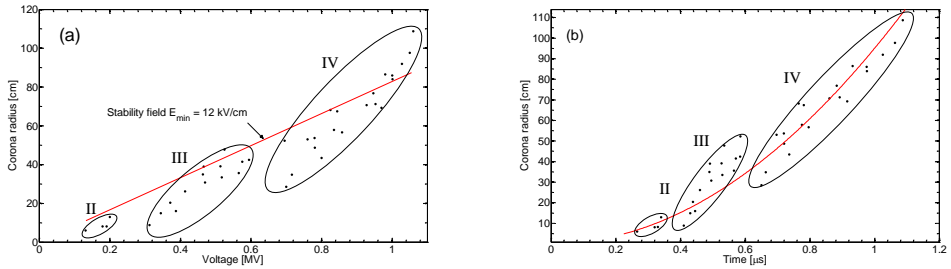


Figure 3.6: (a) The radius of the negative corona over the voltage in a gap of 127 cm length, obtained from 39 discharges. The so-called stability field of 12 kV/cm is indicated with a red line. The second, third and fourth streamer bursts are indicated with II, III, IV. (b) The corona radius now as a function of time. The time delay between bursts is 50 ns. A curve $r = 95 \cdot t^2$ is fitted to the data, where r is the corona radius in cm and t is time in μs .

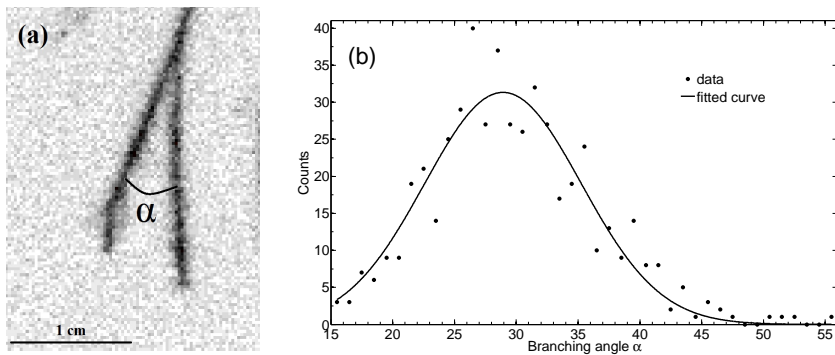


Figure 3.7: (a) Negative streamer branching. (b) The distribution of branching angles as it appears in the projection onto the image plane. The solid line indicates a Gaussian fit with mean angle $\alpha = 29^\circ$ with 5° standard deviation.

at the grounded electrode. The full discharge development is shown in figure 3.9 in a time-resolved sequence. Panel (h) shows the currents and voltage taken at the discharge of panel (f). The single red-blue (RB) pictures (a) - (g) is an overlay of two images from two cameras, each of 50 ns exposure. They have been taken directly after each other. The image of the first camera is placed on the red layer of the picture, the second image on the blue layer. The light level is reproduced as color intensity, where a gamma correction of 0.2 has been applied for better visibility of lesser bright parts. The HV current jump at $t = 0.4 \mu\text{s}$ already corresponds to the second streamer burst. From many other images not shown here, we find that the streamers bridge a distance of 30 cm with an average speed of $2 \cdot 10^6$ m/s, and then terminate at their maximal length allowed by the voltage, as discussed before.

Figure 3.9 (a) shows stages during the third burst accompanied by a current pulse with a maximum at $t = 0.55 \mu\text{s}$. The electrode distance is 127 cm as in figure 3.2. In going from the corona outer extent to the electrode, one first observes that the outermost blue streamer traces are shorter than the red ones. These streamers heads become slower - from $1.7 \cdot 10^6$ to $1.1 \cdot 10^6$ m/s - and eventually stop moving as discussed before. The outermost streamer traces extend to a distance of 38 cm from the high-voltage electrode at the end of the second camera exposure. The corresponding current jump is less intense but lasts longer than at the second burst; this is a consistent behavior as it also shows up in figure 3.2. The outermost traces appear as extension and branching of traces one layer deeper inside the corona, as has also been seen in figure 3.2 again. The separation between outermost red and inner blue traces shows that the latter are re-ignited streamers of the previous burst. There is only little overlap between the red and blue traces. Apparently the light from the streamer heads stems mostly from short lived i.e. less than 10 ns excited atomic and molecular states. Finally, near the electrode the third burst appears in image (a). Here, the red and blue traces largely overlap. This suggests that these streamers propagate less, and new ones may emerge and old ones are re-excited by the increasing current necessary to feed the outer streamers. However, we cannot exclude a possible role of longer living excitations.

After a substantial rise of the voltage the fourth streamer burst initiates in the pre-ionized medium near the electrode at $t = 0.7 \mu\text{s}$ (figure 3.9 (b)). The outer streamers propagate in a higher electric field; their speed now varies between $2 \cdot 10^6$ and $4 \cdot 10^6$ m/s. Meanwhile, a barely visible positive inception cloud appears at the grounded electrode during exposure (b). In figure 3.9 (c) the outermost streamers propagate farther in all directions over a half-sphere leaving diffuse and patchy structures behind. In part, these structures consist of positive streamers and ionized stationary traces that are reminiscent of 'secondary streamers' [Luq10, Liu10]. The outermost negative streamers reach their final extent at an average distance between 80 and 100 cm from the cathode. The voltage then is about 1 MV, and the size of the corona is again consistent with the stability field (3.3.1). Due to the proximity of the negative streamers, the electric field near the grounded electrode increases strongly and the inception cloud near the grounded electrode starts to emit positive streamers. In image (d) at $t = 1 \mu\text{s}$ many positive upward moving streamers appear. The positive streamers transform into a structure that resembles a space leader [Ree95] when they propagate through the zone pre-ionized by the previous negative streamer burst. The negative streamers that moved nearly horizontally from the high voltage electrode stop growing at this moment due to the

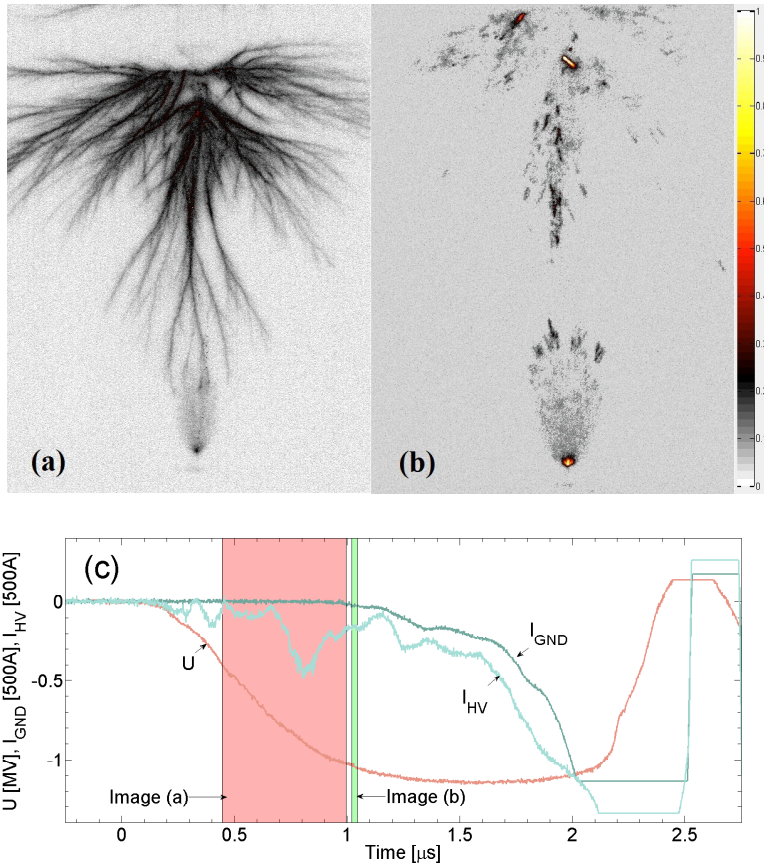


Figure 3.8: Long (a) and short (b) exposure images of pre-breakdown in a gap of 127 cm. Image (a) shows the light emitted during the fourth streamer burst between $t = 0.65 \mu\text{s}$ and $1 \mu\text{s}$. Image (b) shows the light from the ionization processes during a short time interval briefly later. The electrical characteristics of the discharge and the exposure times of the two images are indicated in panel (c). Because of the longer exposure time, image (a) is taken with a lower image intensifier gain than image (b).

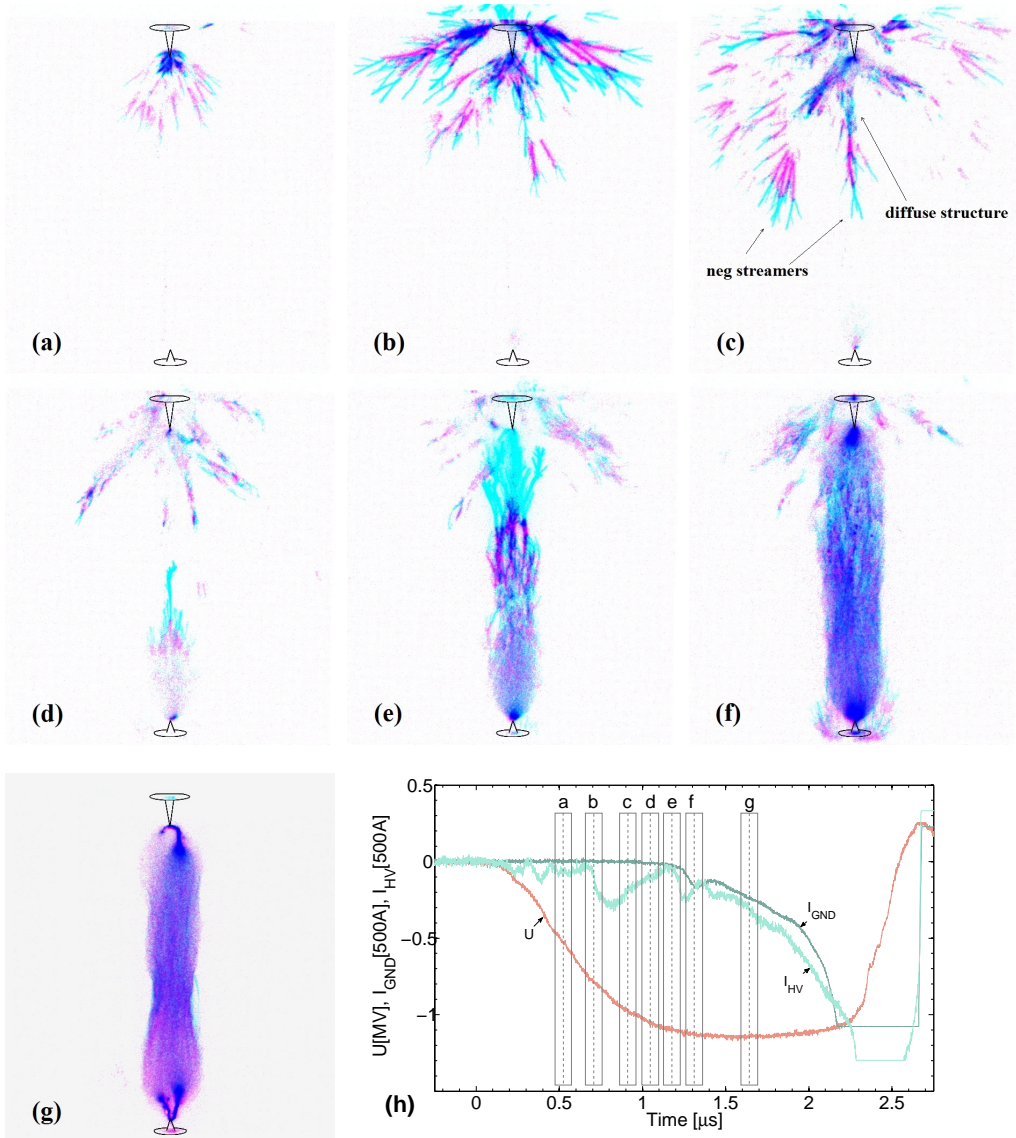


Figure 3.9: Time-resolved image sequence of the discharge development for an electrode distance of 127 cm. Every red-blue picture from (a) to (g) consist of two consecutive images with 50 ns exposure time. The first image is placed on the red layer of the RB picture and the second one is placed on the blue layer. When blue and red traces overlap they appear purplish. A gamma correction coefficient of 0.2 is applied to each picture. Panel (h) shows the electrode currents and voltage for panel (f).

rearrangement of the electric field by the positive charges from below.

Later, in image (*e*) the upward positive discharges merge with the ionized channels extending from the high-voltage electrode. Before (*e*) mostly the streamers heads emitted light. But now the channels become bright over their full length indicating strong Ohmic heating. These light emissions are also accompanied by a current pulse on the high-voltage electrode, often accompanied by high-frequency oscillations. These oscillations are similar to ones discussed earlier in [Koc12] for positive discharges. The light emission concentrates in the cylindrical region confined between the electrodes. First it has an inhomogeneous structure (image *e* and *f*) where streamer traces are still visible. But later it becomes diffuse (image (*g*)) with only slightly perceivable conducting channels. All streamer traces outside this region vanish. Those streamers deposited negative charge around the gap, and the electrons have two options: flow back via the ionized channel or get attached or recombine with the ions. Within the light emitting and conducting region, two leaders grow towards each other from both electrodes. They concentrate the current in a narrower and more heated region. In figure 3.9 (*h*) the final breakdown and spark occur after time $t = 2.3 \mu\text{s}$.

3.3.3 Detailed discharge structures near the high-voltage electrode

The resolution of the later images in figure 3.2 and figure 3.9 does not allow to resolve the details of the spaghetti-like discharge structures in the strongly pre-ionized region near the high-voltage electrode. When zooming in on that electrode, we observe several phenomena, a) light emitting fronts moving from and towards the electrode as well as b) stationary dots and c) stationary channels of varying brightness. Some of these have already been mentioned in [Ree95]. In order to have consistent names we use 'streamers' of both polarities for a), and 'pre-leaders' for c) because these stationary structures may finally transform into a real leader. We interpret these pre-leaders as re-excited conducting remainders of negative streamers, also called 'secondary streamers' in [Luq10, Liu10]. Items b) remain 'dots'. More theoretical and experimental investigations are required to understand the actual nature. The phenomena have been observed in many discharges and the images shown have been selected for clarity.

Figure 3.10 (*a*) shows positive and negative streamers moving towards and from the electrode; figure 3.10 (*b*) gives the corresponding electrical parameters. Both cameras had 3 ns exposure time, and the blue image was delayed by 10 ns. The arrows indicate the displacement from the red to the blue images. A slight horizontal dislocation in figure 3.10 (*a*) can be attributed to the different viewing angle of both cameras. The positive streamers move with a speed of about $2 \cdot 10^6$ m/s which is in a good agreement with the speed of positive streamers reported in [Koc12]. These propagate towards the high-voltage electrode and towards the negative pre-leader which is attached to the electrode. Upon their encounter high-frequency electromagnetic oscillations are detected by the current probes. An example is shown in figure 3.10 (*b*) at about $t = 0.65 \mu\text{s}$, marked as 'collision'. In [Koc12] we observed that such encounters are associated with x-ray emission. The radial luminous intensity of all positive streamers observed here can be fitted to a Gaussian profile with FWHM of 2 ± 0.4 mm. A few discharge channels

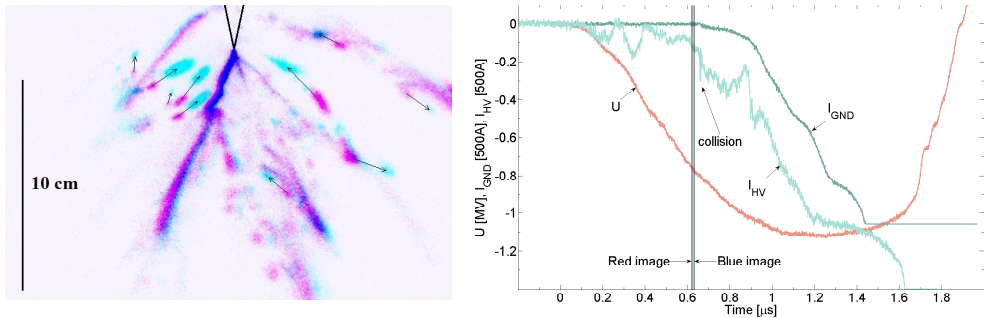


Figure 3.10: (a) Two images combined into one RB picture. The first image is placed on the red layer, and the second one on the blue layer. The exposure time is 3 ns for each image. The delay between the images is 10 ns. The gap distance is 107 cm. Arrows indicate the direction of motion, indicating that many 'streamers' move towards the cathode. A bright stationary discharge channel (leader) is attached to the electrode tip. (b) Currents and voltage, where the moment of collision of the positive 'streamers' of panel (a) with the cathode is indicated.

appear to be stationary, for instance both towards the lower left corner, one bright and one faint. They can play a role of ionization patches as described in [Liu12, Kos12].

The positive streamers come in bundles. Figure 3.11 (a) again shows the area near the high-voltage electrode, now with longer exposures of 50 ns for each camera and a delay of 50 ns. The gain of the image intensifier has been reduced with respect to figure 3.10 to avoid saturation. At least six tracks of positive streamer bundles can be seen. A stationary negative pre-leader extends from the right side of the high-voltage electrode. That pre-leader collects the right side bunch, and the electrode collects the left side bundle. The 'collision' in figure 3.11 (b) now indicates the moment the merging of positive and negative streamers, as in figure 3.9 (e).

In the previous Sections we showed that the streamers propagate in steps, probably because of the relatively slow rise of the driving voltage. Many images zoomed-in on the high-voltage electrode show that the steps themselves behave irregular as well, at least the later stages of discharge formation such as the fourth streamers burst. Figure 3.12 gives several images taken at the time as in figure 3.11 (b). The image intensifier gain is approximately equal to the one of figure 3.10 again. Some tracks are attached to the high-voltage electrode; streamers appear as separated tracks as in figure 3.9. The streamer luminosity varies over the track length. Some tracks split up into dots that often appear to be streamer branching points. The branching direction varies: most are downward, some upward. The branching direction depends on the streamer head polarity: positive ones moving upwards, negative downwards. We tentatively interpret the phenomena as follows: The luminosity variations over the track indicate irregular excitation and/or propagation. Charge accumulates in regions of more intense light, possibly even because of micro-stepping of the streamer. The accumulated charge or excitation promotes branching, similar to streamer emission from the inception cloud. The dots are then the visual stationary remainders of such accumulation.

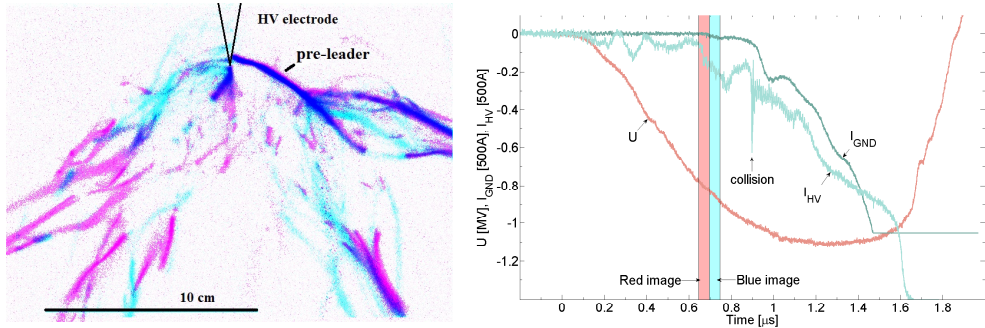


Figure 3.11: The RB picture consists of two images with 50 ns shutter opening time each. The first image is placed on the red layer of the RB picture and the second one is placed on the blue layer. A gamma correction coefficient of 0.2 is applied. The scales are the same as in 3.10. The timing of the images is indicated in panel (b).

The negative pre-leader does not form in a continuous way. The short exposure image with high image intensifier gain of figure 3.13 shows variations of the pre-leader thickness. A half-millimeter thin channel with broad ends is visible in the middle of the image, indicated by the arrow. The high-voltage current rises gradually as shown in figure 3.13 (b). A mix of streamers and their residues surrounds the composition. The camera's gain is set that high that leader and streamers are seen simultaneously, but the leader is overexposed into saturation. Since the saturation may lead to blooming in the CCD, the real thickness of the pre-leader may be smaller than observed.

3.3.4 Leader phase

Figure 3.14 (a) (c) show three examples of the formation and development of bright structures that develop on top of the positive streamers from the ground electrode. The camera sensitivity and exposure moment are the same as in figure 3.9 (e), but no gamma correction has been applied. The structure brightness is two up to four times larger than the streamer head traces. These structures are disconnected from the electrode, hence its name 'space leader' [Ree95]. It is clear that the central part of the structure in figure 3.14 (c) is brighter than its edges, indicating that the structure is stationary rather than moving. At both electrode the currents are almost equal to zero at this moment; compare with image (e) and (h) in figure 3.9. So the electrodes transfer only a small amount of energy and charge into the gap region. The enhanced brightness should then stem from the electrostatic energy stored locally and from the charge redistribution and associated current density near and inside the space leader. The multiple channels of the space leader persist in the final spark, as shown by the sill photograph of figure 3.14 (d).

Similarly bright leaders in figure 3.2 (n) appear later inside the heavily ionized column. Figure 3.9 (g) shows that both leaders grow simultaneously and remain attached at both electrodes. These leaders are formed out of streamer channels that are heated by the increasing currents from both electrodes. Because of the gradual heating of an already

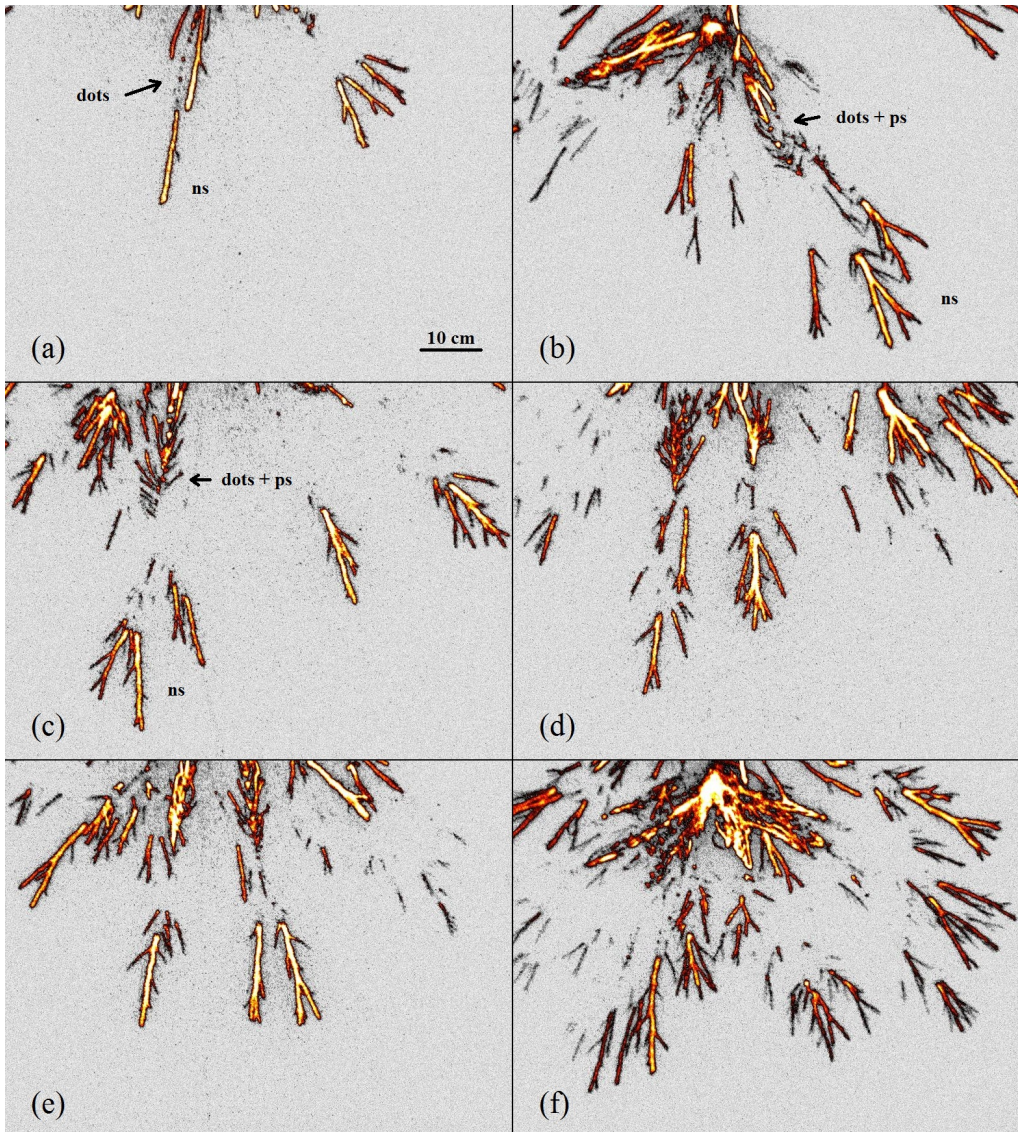


Figure 3.12: Typical images at the fourth streamer burst just below the high-voltage electrode. For all images time is the same as in 3.11. Exposure is 50 ns. (a) Negative streamers (ns) leave isolated dots behind. The dots act as a starting point for new positive (ps) cathode-directed streamers (b) - (f). Image (a) clearly represents a less intensive streamer burst than image (f).

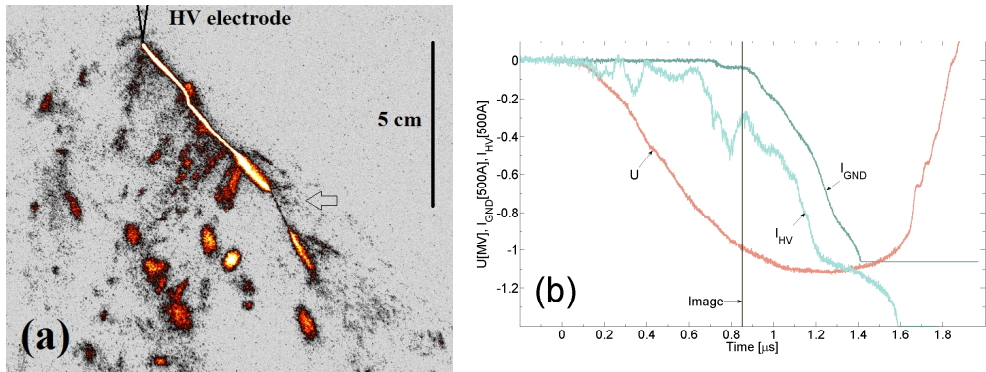


Figure 3.13: Fluctuations of the leader channel thickness. The gap distance is 107 cm, and the exposure time is 3 ns. The moment of the image is indicated in panel b that shows the electric characteristics of the event.

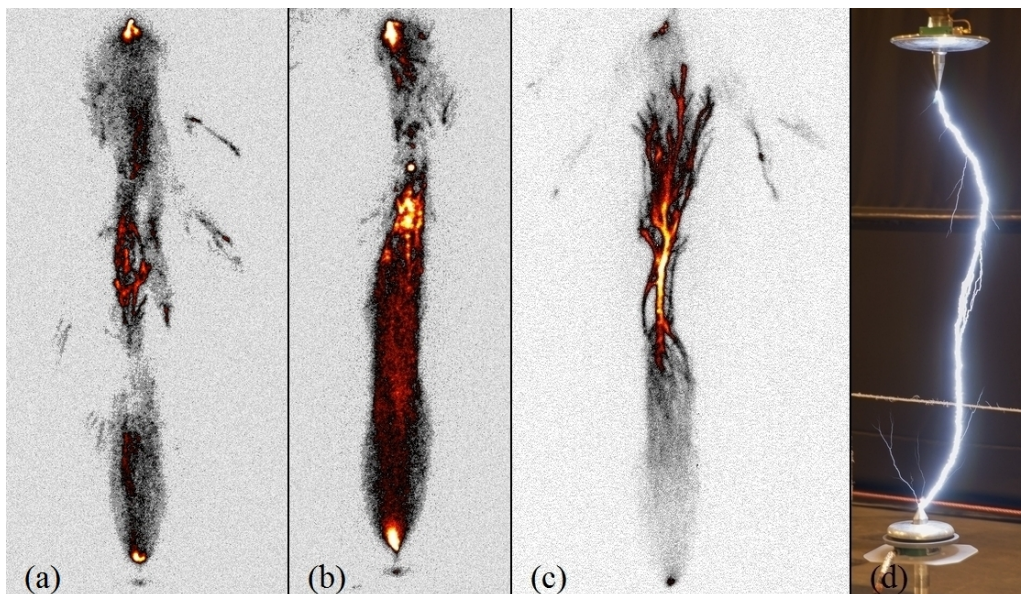


Figure 3.14: Space leaders observed in three different discharges. Images (a) (c) were taken at the same moment as in 3.9 (e). The exposure time is 100 ns, and the gap distance 150 cm. Image (d) is a photograph taken with shutter open during the whole discharge formation.

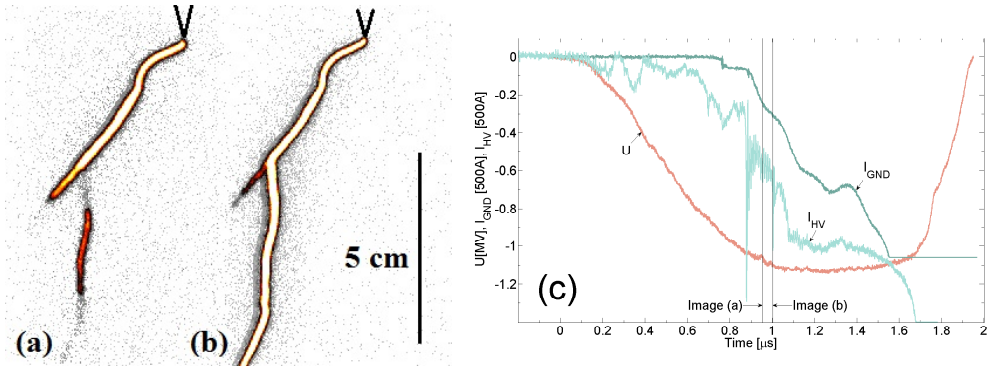


Figure 3.15: A stepping leader. The gap distance is 107 cm, and the exposure time is 0.5 ns for each image. The delay between the images is 50 ns. The electric characteristics in the right panel show that a peak in the high-voltage current is detected simultaneously with image (b) in the left panel.

existing channel, no 'leader velocity' can be defined here. The diameter of the column between two leaders in figure 3.9 (g) is about 40 cm as mentioned in 3.3.1. In images without gamma correction, the optical activity appears concentrated to a shield of about 12 cm diameter around the leader. Figure 3.2 (o) shows the ultimate development into an over-exposed spark.

3.3.5 Similarities between phenomena in the laboratory and in nature

In natural lightning the negative leader proceeds by steps. Figure 3.15 demonstrates that stepped phenomena also exist in an air gap of 107 cm. We reduced the sensitivity of the cameras to see only the brightest parts of the discharge suppressing streamers and glowing channels. The negative pre-leader is attached to the high-voltage electrode in image (a). The structure under it extends to the leader channel and downwards in image (b). This is accompanied by a rapid change in the high-voltage current. The earlier current distortion at $t = 0.88 \mu\text{s}$ is most likely associated with a similar process. An obvious similarity with natural lightning is the encounter of its downward leader and the upward leader originating at tall objects near the strike point. Our ground electrode acts as such an object.

Figure 3.16 compares a negative discharge in our laboratory (a) and a set of sprites observed by Cummer et al. [Cum06] (b). The similarity in appearance and evolution is striking, in spite of the differences in size, environment and polarity. A sprite is one of the transient luminous events (TLE's) that can develop above a thundercloud when triggered by an intense lightning strike. Sprites extend between 40 to 90 km altitude where air density varies over 3 orders of magnitude. They also grow in both directions out of a bright 'space leader', where the ionosphere acts as diffuse electrode. Concerning the dots we quote [Cum06]: "these dots are near branch points of the downward streamers, they

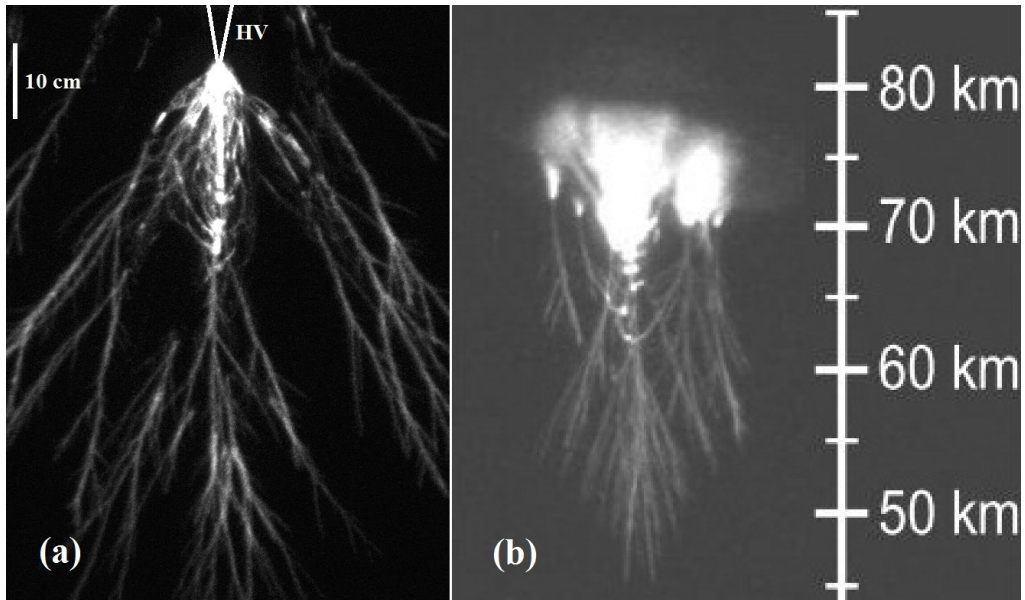


Figure 3.16: (a) Laboratory discharge with an exposure time of 100 ns, without color coding or gamma correction. (b) High speed image of a sprite discharge, adopted from [Cum06].

also appear in locations where no branching of the downward streamers is visible". This is in line with our discussion on dots in 3.3.3. As far as can be judged from figure 3.16 (b), also the branching angle is quite similar to figure 3.16 (a).

3.4 Discussion and conclusions

In this study we described nanosecond-fast photography of the development of negative discharges in STP air combined with the determination of the electrical parameters. The voltage source is a standard lightning impulse generator connected to a spark gap with conical electrodes separated by 1 up to 1.5 metre. The applied voltage is 1 MV with a rise time of 1.2 μ s. The discharge forms through a sequence of inception cloud, streamers, leaders and spark. The current measured on the high voltage electrode clearly shows up to four bursts of streamer formation at the HV electrode. Comparing the HV sources used in [Ree95] and [Nij11a] the occurrence of the bursts can be readily attributed to our slower voltage rise time and higher source impedance which is primarily inductive. The time-integrated images show that next-burst streamers are a continuation of the earlier [Nij13], and that new streamers are formed at the electrode. Outermost streamers of the first burst branch with the preferred angle of 29 ± 5 degrees. Their speed attains values between $2 \cdot 10^6$ and $4 \cdot 10^6$ m/s. This value is on order of magnitude larger than the average value derived from time-integrated images discussed in 3.3.1 and with figure 3.5. The fourth burst is accompanied by increased current density and ionization near the HV electrode. Generally, the zoom-images near the electrode are chaotic. Streamer

channels decay into 'dots', stationary items of increased luminosity. Such dots generate new streamer channels in both directions, away from and towards the HV electrode. Attached to the HV electrode luminous channels appear that transform into persistent pre-leaders with increasing brightness.

At the time of the fourth burst, the outermost streamers are halfway down the gap. The electric field at the grounded electrode has increased sufficiently to induce a positive inception cloud and streamers there. As for positive high voltage [Koc12] these streamers proceed with less variation in current intensity. When the positive streamers merge with the negative corona, the current on the HV electrode decreases first. At the merging point the locally stored electric energy causes a 'space leader', a set of highly luminous and conductive channels that finally extend to the HV electrode. Then the current on both electrodes rises quickly and strong re-excitation of all channels takes place. The conductive column of 40 cm diameter forms and contracts to 12 cm when a few channels transform into hot leaders starting simultaneously at both electrodes. Full breakdown occurs when the leaders meet. Remarkably the space leader filaments persist even at half height in the breakdown phase.

In natural lightning leaders proceed by streamer emission [Pet13]. It is worthwhile to investigate whether common factors with the laboratory experiments are 1) streamer and leader current restricted by the charge collection higher in the atmosphere and 2) micro-stepping of the leader through conversion of streamers into space leaders. As for the link with sprites we conclude that the visual resemblance with the chaos near the HV electrode and its growth pattern is striking, in spite of large difference in circumstances. The physical resemblance might be a matter of scaling [Ebe06].

CHAPTER 4

X-RAY BURSTS FROM NEGATIVE DISCHARGE

We investigate the development of meter long negative discharges and focus on their X-ray emissions. We describe appearance, timing and spatial distribution of the X-rays. They appear in bursts of nanosecond duration mostly in the cathode area. The spectrum can be characterized by an exponential function with 200 keV characteristic photon energy. With nanosecond-fast photography we took detailed images of the pre-breakdown phenomena during the time when X-rays were registered. We found bipolar discharge structures, also called "pilot systems", in the vicinity of the cathode. As in our previous study of X-rays from positive discharges, we correlate the X-ray emission with encounters between positive and negative streamers. We suggest that a similar process is responsible for X-rays generated by lightning leaders.

4.1 Introduction

Thunderstorms are held responsible for Terrestrial Gamma-Ray Flashes (TGFs) the most intensive pulses of electromagnetic radiation in the terrestrial atmosphere [Ina96]. TGFs were first detected from space [Fis94] and later at ground level [Dwy12a, Rin13]. The precise mechanism of their generation is still under discussion. The two most investigated theories are based upon relativistic feedback [Dwy03a] with its continuation as "dark lightning" [Dwy13], and upon production of energetic electron at the tip of a lightning leader [Mos06, Car09, Cel11, Koe14b].

Moreover, X-ray bursts emitted by lightning leaders are an intriguing but as yet unsolved problem in lightning physics [Dwy14]. The X-rays bursts have been detected both from natural and from rocket-triggered lightning. In natural lightning X-rays were detected during the stepping process of lightning leaders [Moo01], and they were later correlated with a single step [Dwy05a]. A negative leader often steps by forming a space

leader or space stem in front of it. The space leader is a bipolar structure that grows in both directions. The step occurs when the positive part attaches to the main leader. In triggered lightning X-rays originate from the tip of a dart leader [Dwy11] which also propagates in steps [Pet13].

In the laboratory negative metre-long discharges can also grow through a space stem/leader formation [Ste62, Les81, Ree95]. And, as was first shown in [Dwy05b] and later confirmed by several different high-voltage laboratories, long sparks also produce bursts of X-rays [Rah08, Dwy08, Ngu08, Mar11a]. While Relativistic Runaway Electron Avalanches (RREAs) cannot be responsible for the X-ray emission in laboratory sparks [Kut12], the thermal electron runaway mechanism provides a reasonable explanation for such emissions [Mos06, Cel11, Gur61, Gur07, Cha10, Li09, Cha08]. The thermal runaway electron mechanism relies on the assumption that some region with strong electric field is created by the discharge. In [Mos06, Cel11, Cha10, Li09, Cha08] it was shown that the tips of negative streamers can accelerate electrons into the run-away regime. Cooray et al. [Coo09] suggested that the run-away effect might be enhanced between positive and negative streamer tips approaching each other. In our previous study of long positive laboratory discharges with nanosecond-fast photography we confirmed this suggestion [Koc12].

In the present study we investigate source location, mechanism and characteristics of the X-ray bursts from *negative* discharges by measurements. In time-resolved photographs we show the space stem formation, the development into a pilot system and the attachment to negative leader/electrode.

4.2 Experimental setup

The setup is similar to that described in [Koc12, Koc14a] and represented in Figure 4.1. Here we describe only the essential elements. A 2 MV Marx generator delivers a standardized lightning pulse with 1.2/50 μ s rise/fall time when not loaded by the spark gap. The voltage is applied between conical electrodes, where the high-voltage electrode acts as cathode, and the grounded electrode as anode. We use three distances between the cone tips: 107, 145 and 175 cm. Only the first two lead to a full gap breakdown. The upper voltage limit is set to about 1 MV. Two Pearson 7427 current probes with 70 MHz bandwidth determine the currents through the high-voltage and the grounded electrodes. The probe for the high-voltage(HV) electrode has an optical transmission system to the oscilloscope. Appropriate attenuators and two antiparallel high-speed diodes protect the input of the transmitter. The diodes limit the linear response to 250 A. The grounded (GND) electrode current probe connected to the scope directly. Vaulted aluminum discs protect the probes against the spark current of 4 kA.

Two LaBr₃(Ce⁺) scintillator detectors (D1 and D2) manufactured by Saint-Gobain are mounted in EMC-cabinets and record the X-rays. The scintillator crystals are cylinders of 38 mm diameter and length, encased in 0.5 mm thick aluminum. The case is transparent for X-rays above 30 keV (attenuation 15% or less). The physical properties and the comparative performance have been discussed in [Ngu08, Dor04]. The signal cable is terminated into 50 Ohm at the input of the oscilloscope. The residual capacitance

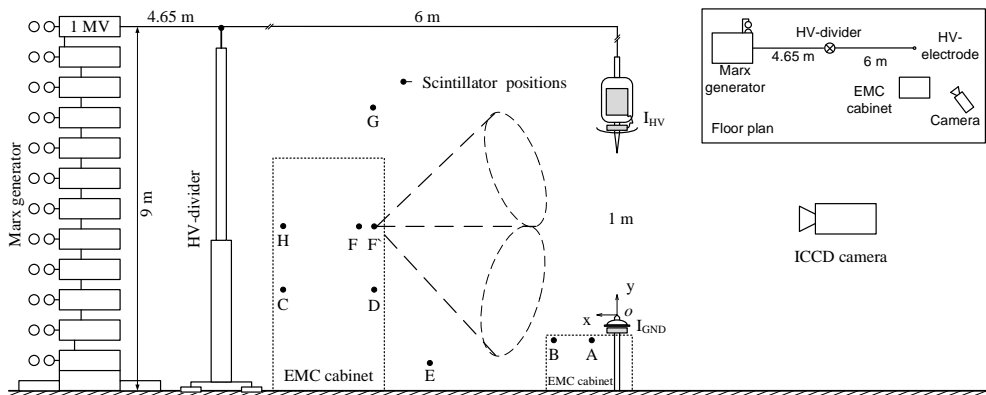


Figure 4.1: Schematic sketch of the spark gap geometry. Positions of the x-ray detectors are labeled from A to H. All the positions are in the same vertical plane. Dashed cones indicate the detector field of view when placed inside a lead cylindrical collimator. ICCD camera is located at 3.5-4.5 m distance from the gap. The distance between Marx generator and the spark gap is approximately 10.65 m. The upper right inset shows the correctly scaled floor plan.

between the 50 Ohm and the high-impedance input of the oscilloscope limits the rise time to about 1 ns, better than needed for our experiment. The scope high-impedance input is better protected against overload than the internal 50 Ohm setting; this is the reason why we choose external terminating resistor. Moreover, the LaBr3 detectors were equipped with special HV dynode dividers with additional capacitors in the upper dynodes to reduce saturation effects. The quality of the cabinets is such that the discharge formation does not interfere with the X-ray signals. The scintillators have a fast rise/decay time (11/16 ns) and a light yield of 63 photons/keV. The linearity of the detectors has been tested in [Ngu12] on ^{241}Am , ^{137}Cs , ^{60}Co and remains better than 6% at least up to 2.5 MeV. At higher energies saturation of the photomultiplier causes a slight deviation from linearity. By averaging many signals of the 662 keV photopeak from ^{137}Cs we obtained a noise free single photon response. The response as function of time allows distinguishing individual pulses even when pile-up occurs, as will be shown later in detail. The detectors are placed at different positions around the gap. To determine the origin of the X-ray signals in some experiments we restricted the detector field of view by 15 mm thick lead cylinders to a solid angle of 0.23 Sr, and we pointed them to different parts of the gap. Lead attenuators of different thickness helped us to determine the energy distribution.

The Picos4 Stanford Optics camera with an intensified CCD [Sta] is placed at 4 m distance from the spark gap and is directed perpendicular to the spark axis. The camera and all communication lines are properly shielded against electro-magnetic interference. The camera has a monochrome CCD; in contrast to [Koc14a] a single camera is employed. The lenses were either a Nikon 35 mm F2.8 fixed focus or a Sigma 70-300 mm F/4-5.6 zoom.

The electrical signal acquisition system consists of two Lecroy oscilloscopes with 1 GHz bandwidth. The negative edge of the signal from the high-voltage divider triggers

the oscilloscopes. One of the oscilloscopes transmits the trigger to the camera. The differences in the delays caused by the instruments and cables have been corrected to ns accuracy.

4.3 Results

Several reports on the observation of X-rays from long laboratory sparks have been published [Rah08, Dwy08, Ngu08, Mar11a], including blank tests where detectors without scintillators were used [Dwy05b]. Note that the background of the detector set at a discrimination level of 30 keV is approximately 50 counts per second. This includes the contributions from cosmic rays, the laboratory environment and the internal isotope decay. The probability to observe any background signal that might mimic an X-ray signal from the gap within an observation time of 500 ns is equal to $2.5 \cdot 10^{-5}$. This work is based upon 3281 negative discharges collected during three years of experimental investigation. The time interval between two discharges was at least 10 s. X-rays were observed in many, but not in all discharges.

4.3.1 Discharge development

The development of the negative discharges has been characterized in detail through ns-fast photography in [Koc14a]. For the sake of completeness we briefly recall the processes here. The pulses of the high-voltage current shown in Figure 4.2 indicate that the discharge development in a 107 cm gap can be divided into seven stages. All stages are very reproducible for different discharges with the same electrode configuration, and the curves in Figure 4.2 are actually averages over 302 discharge pulses. The first four stages coincide with four bursts of negative streamers. When we apply the high voltage, a negative streamer corona appears near the HV electrode and develops downwards and horizontally. It extends until the ratio of instantaneous potential over length is about $E_{min} = 12 \text{ kV/cm}$, which is the so-called stability field for negative streamer propagation; a new critical discussion and test of the stability field concept can be found in [Luq14]. As a negative streamer cannot propagate slower than the electron drift velocity at the enhanced electric field at the streamer tip [Luq08], it grows with a velocity of at least $5 \cdot 10^5 \text{ m/s}$ to the length determined by the instantaneous voltage. Meanwhile the voltage continues to rise, and eventually a second burst of negative streamers is emitted from the HV electrode and propagates further into the gap. The four stages of development correspond to four corona and streamer burst, each one propagating further into the gap, while the voltage rises. In addition, the inductive impedance caused by the long wires between HV divider and gap also contribute to limiting the current rise.

Stage 1 corresponds to the formation of a negative inception cloud around tip and protection disk of the high-voltage electrode. The inception cloud destabilizes and ejects negative streamers [Bri08b]. Stages 2, 3 and 4 correspond to the second, third and fourth streamer burst, respectively. They appear for all gap lengths larger than 1 m. When the outermost negative streamers approach the grounded electrode they bring part of the high voltage downward and enhance the local electric field there which, in turn, leads

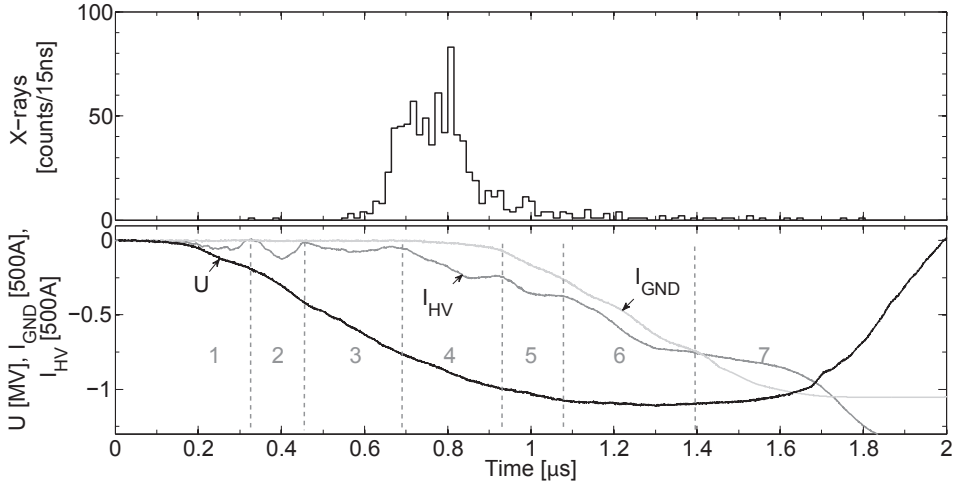


Figure 4.2: The development of the discharge in a 107 cm gap can be divided into 7 stages. Each stage begins with a rise of the current at the high-voltage electrode and ends with its drop. Voltage and current in the plot represent an average over 302 discharges. The X-ray counts per 15 ns represent data of 815 X-ray bursts detected during these 302 discharges. The maximum of the X-ray counts occurs at the beginning of the fourth stage.

to the formation of a positive inception cloud on the tip and on the sharp edges of the grounded electrode. The positive counter-streamers emerge from the positive inception cloud and move upwards, where they merge with the negative streamers. For the 107 cm gap the outermost streamers cross the gap at the fourth burst and then create a spark. In stage 5 the positive streamers from the grounded electrode reach to the high-voltage electrode, possibly along the traces of previous negative streamers. Then high amplitude HF oscillations in the cathode current may occur. A conductive channel between the electrodes is established and the currents on both electrodes increase quickly; this is the beginning of the leader phase (stage 6) and of complete breakdown (stage 7). It might be useful to recall at this point, that streamers emit light only in their growth region where additional ionization is created, and not in their conducting, current carrying parts. Only the high current in a leader or spark can create an optical signal; it can be distinguished spectroscopically from streamer heads.

4.3.2 Influence of the gap length on the electrical characteristics and on the X-ray time

In Figure 4.3 (a) to (c) we compare the electrical characteristics and X-ray emissions from gaps of 107 and 147 cm length, both at a maximum voltage of 1.1 MV. All curves are averaged over 302 or 72 discharges, respectively. The electrical characteristics of the individual discharges at the same gap length are so similar, that the averages show essentially the same features as the single measurements. The voltage rise time is

determined by the Marx generator and the HV divider circuit. Because the discharge current is strongly determined by the negative corona development and by the high inductive impedance of the wire between the top of the HV divider and the high-voltage electrode, the cathode current up to $1 \mu\text{s}$ is remarkably independent of the gap length. Most X-rays appear between 0.65 and $0.9 \mu\text{s}$, for both gap lengths (Figure 4.3 (d)); this time interval largely coincides with the fourth streamer burst. The voltage is then over 500 kV which apparently suffices to accelerate electrons sufficiently that their bremsstrahlung photons are within the energy range of our detectors. That the X-rays are detected within the same time span for both gap lengths implies that the anode region cannot contribute much to the X-ray generation. It takes $2 \mu\text{s}$ longer to break the 147 cm gap down than the 107 cm gap. As a result, the anode current also rises much later in the 147 cm gap, and about $1.5 \mu\text{s}$ after the X-ray detection. At breakdown the voltage fall time is determined by the resonance frequency of the capacitive HV divider and the inductive gap circuit.

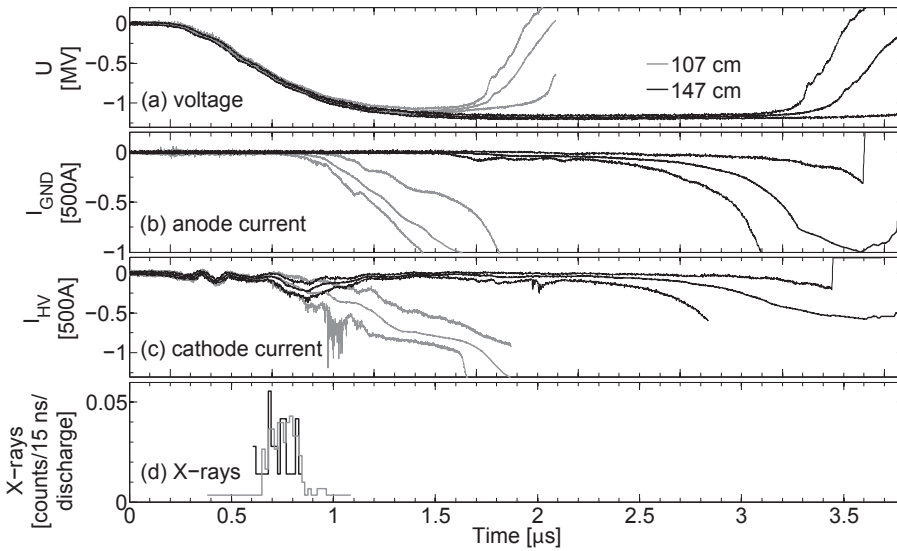


Figure 4.3: Electrical characteristics and X-ray registration time for discharge gaps of 107 cm (gray) and 147 cm (black). The measurements are averaged over 302 or 72 discharges, respectively. The electric breakdown in the 147 cm gap takes $2 \mu\text{s}$ longer than in the 107 cm gap. The cathode current curves (c) are remarkably similar up to $1 \mu\text{s}$, and also the temporal distribution of detected X-rays is similar for both gaps where most emissions also occur during the initial $1 \mu\text{s}$.

In the 147 cm gap, the streamers are not able to cross the gap at the fourth burst and a dark period without anode current occurs between 1.1 to $1.6 \mu\text{s}$ in Figure 4.3 (c). A fifth streamer burst does not occur anymore because the voltage does not rise anymore. There is no optical activity in the gap (the dark period) until positive streamers develop near the grounded anode. At this moment we see the current through the anode rising rapidly, as shown in Figure 4.3 (b) at about $2 \mu\text{s}$. Although there is hardly any light

during the dark period, this does not indicate that there is no current flowing, but only that hardly any ionization reactions occur.

The high-frequency oscillations of the cathode current in Figure 4.3 (c) at $t = 1$ to $1.1 \mu\text{s}$ correspond to the moment when positive streamers from the grounded electrode collide with the high-voltage electrode in the 107 cm gap. The same oscillations are visible at $t = 2$ to $2.1 \mu\text{s}$ for the 147 cm gap. Sometimes they are also accompanied by an X-ray signal.

4.3.3 X-ray measurements

A typical oscillogram with X-ray detection is shown in Figure 4.4. The gap distance between the electrodes is 107 cm. The voltage rises from 10 to 90% of its maximum value of 1.1 MV within $0.7 \mu\text{s}$, and breakdown occurs $1.6 \mu\text{s}$ after the start of the voltage pulse. In this measurement both X-ray detectors were placed next to each other at position H (Figure 4.1) with a centre to centre distance of only 6 cm as shown in Figure 4.5. When the X-rays are detected, in 82% of the cases the signal appears as a single pulse on one or both detectors simultaneously. In 17.5% of the cases we detect two X-ray pulses, well resolved in time during one discharge. And in the remaining 0.5% we detect three X-ray pulses. As shown in Figure 4.4, the X-ray signals appear simultaneously on both detectors. We conclude first that the X-rays are generated within nanosecond bursts, and secondly, taking into account that the scintillators have a diameter of 38 mm, that photon pile-up may occur in each detector. Still, all measured X-ray signals up to 0.5 MeV can be fitted with a single photon response. With a slight deviation from linearity, this is also possible for 2 MeV energy deposited in the detector; see for example Figure 4.6 (a). This 2 MeV signal can only be explained by pile-up since the maximum of the applied voltage is 1.1 MV, and since ionization with two elementary charges ($2e$) is negligible. The rising slope of the signal indicates that all X-ray photons arrived within 6 ns. Even much larger deposited energies occurred, as is shown in Figure 4.6 (b), where the oscilloscope channel clipped at its maximum of 5.5 MeV. The recorded detector signal can be fitted by two single photon responses with a delay of 40 ns, scaled to 10.3 and 7.5 MeV, respectively. However, as discussed in [Ngu12] deviations from linear response due to the saturation of the photomultiplier set in at 2.5 MeV. So the large signal may be additionally broadened due to different arrival times of the X-rays or by saturation. Both effects are difficult to distinguish, even in a non-clipped registration of the wave shape.

Correlation between X-ray bursts and high-frequency oscillations of the current

As in positive discharges (see Figure 4 in [Koc12]), the X-ray signals are accompanied by high frequency oscillations of the cathode current. In Figure 4.7 such oscillations are marked by arrows. They are also visible in Figure 4.4 as sharp spikes on the HV-current curve at the moment of X-ray detection. The more pronounced the oscillations are, the more likely they are accompanied by X-rays and the higher the amplitude of the X-ray

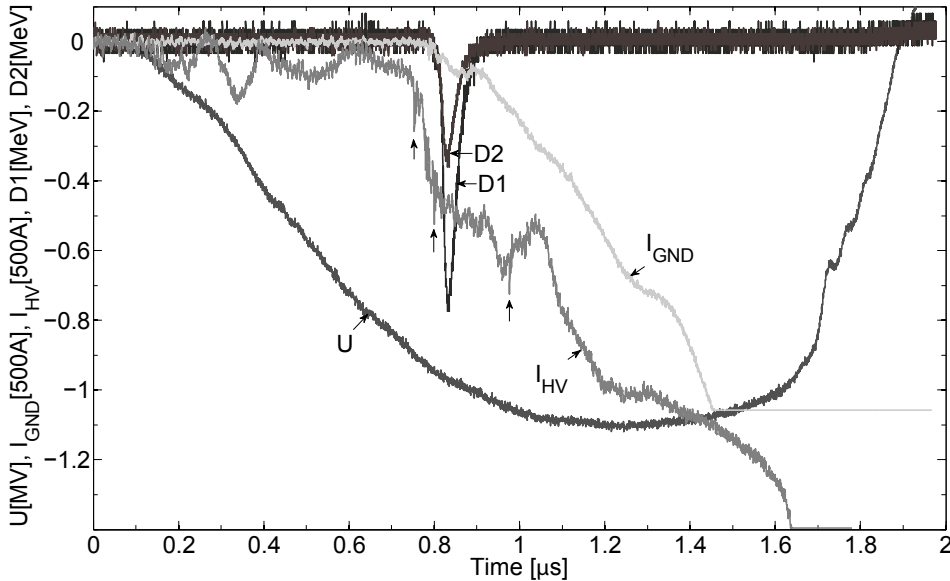


Figure 4.4: A typical recording of a single negative discharge. The voltage rises to 1.1 MV. The gap distance is 107 cm. Two LaBr_3 scintillation detectors D1 and D2 are placed next to each other at position H at 2 m distance from the spark gap. The X-ray detection coincides with the rise of the current I_{GND} on the grounded electrode. HF oscillations are indicated by vertical arrows.

signal is. As mentioned above, we do not detect X-rays in 100% of the discharges, but the oscillations are clearly visible in every discharge. Since the X-rays come in short bursts and are associated with high frequency oscillations, we assume that a ns-fast process is responsible for their generation, for instance the encounter of positive and negative streamers. This can happen at least three times (three X-ray bursts) during one discharge. As the X-rays appear in bursts, it is unlikely that the continuous propagation of streamers or leaders drives the process. However, any sudden process like stepping or collision is a candidate.

4.3.4 X-ray registration rate

By comparing the X-ray detections for different detector positions, we may derive where the X-rays are generated. Table 4.1 shows for each detector position the ratio of the number of discharges with X-ray detection over the total number of discharges. The gap between the electrodes is fixed at a length of 107 cm. The data for positions A, B, C and D were obtained in one series of measurements. Those for E, F and G were obtained in another series two months later. Those at position H were measured even later. For the detector at positions A and B we placed a small EMC cabinet under the grounded



Figure 4.5: How the two cylindrical LaBr_3 scintillation detectors are placed next to each other. The detectors register an X-ray signal simultaneously during some discharges. This proves that the photon flux is high enough to cause a multiphoton registration at one detector.

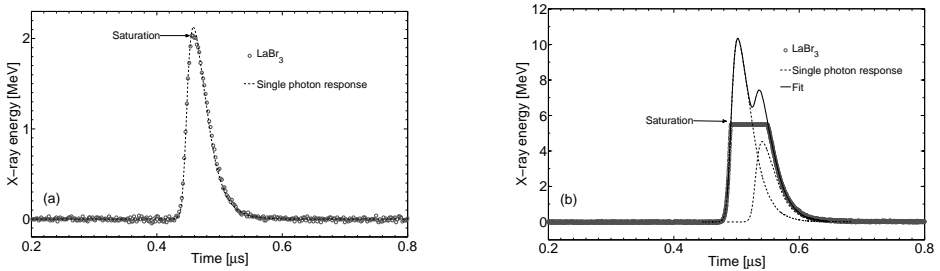


Figure 4.6: (a) An X-ray detector signal of 2 MeV. A single photon response fits the data well, while one would expect only multiple photons to generate a 2 MeV signal in a 1 MV discharge. At the peak the photomultiplier may be slightly saturated, or alternatively, the signal is a pile-up of two photons with 6 ns delay. (b) One of many possible fits to a measured signal. At least two X-ray bursts overlap each other, which leads to detector saturation. The signal of each burst, in turn, consists of multiple photons.

electrode (as shown in Figure 4.1); this cabinet remained there during all measurements in series I and II. In contrast to our previous study of positive discharges [Koc12], the cabinet did not influence the X-ray registration rate. This agrees with the observation that the grounded electrode essentially does not contribute to the X-ray generation in the present experiments.

The measurements with the collimated detectors F' up and F' down indicate that 2/3 of the X-rays come from the upper half of the gap. Besides that, the registration rates at positions A and B are similar or lower than those at positions D, E, F and G. Since they are all located at approximately the same distance from the cathode, the X-ray emission is on average isotropic in these experiments. To substantiate this further, we now assume that the X-ray source is point like and has a constant luminosity. With only geometrical decay, the registration rate should follow the inverse square law. For such a source, we can find its location based upon data of Table 4.1 by fitting the observed occurrences at detector position \vec{r} to the function $P(\vec{r})$:

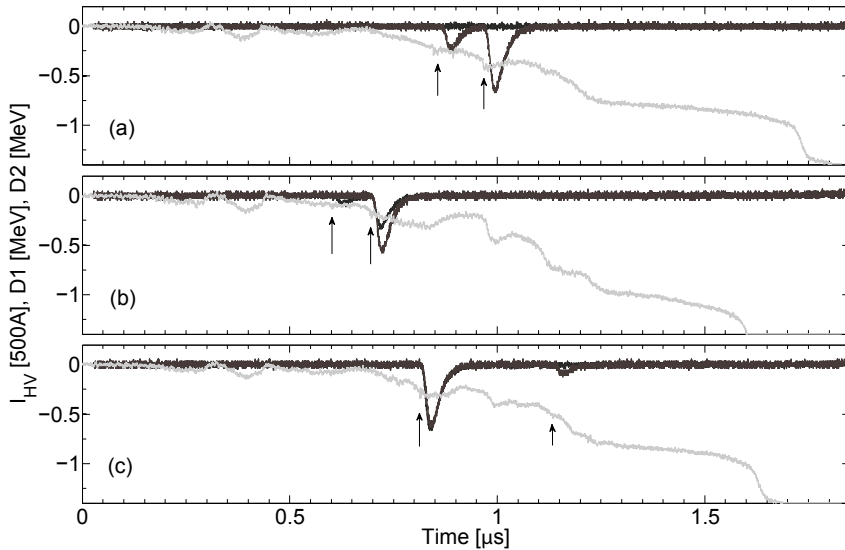


Figure 4.7: (a)-(c): Three different discharges in a gap of 107 cm. Plotted are cathode current (gray) and X-ray detections by two detectors at position H as a function of time. In all three cases two separate X-ray bursts are detected. All X-ray bursts are accompanied by high frequency oscillations of the current (marked by arrows).

$$P(\vec{r}') = \frac{P_0}{|\vec{r}' - \vec{r}_0'|^2} \quad (4.1)$$

where P_0 is the source amplitude or initial occurrence, and \vec{r}_0' its position vector. All detector positions in Table 4.1 were used; those for position F without collimator. The best fit \vec{r}_0' is indicated in Figure 4.8 by a star. The ellipse around the star represents the 95% confidence bound. Although R-square goodness of fit is low (60%), the location of the source is in accordance with the measurements with collimated detector at position F. It is remarkable that the source is off axis. This can have several reasons. First, the X-rays do not come from one fixed point in space. Second, and more importantly, the X-ray bursts from each electron acceleration event are not distributed isotropically, but are beamed in the direction of the main electron acceleration. A further investigation of the opening angle of such X-ray bursts and a reevaluation of the data is currently under way.

4.3.5 Ns-fast photography of the cathode area at x-ray time

The previous section demonstrated that the X-rays appear only during pre-breakdown. The majority came from the cathode region. In addition, the X-rays are correlated with high frequency oscillations of the cathode current, and their source location is near the

Table 4.1: The rate of discharges with X-rays detection for the different detector positions A to H (see Figure 4.1). The effective detection area of one detector is 11.3 cm^2 . The gap distance is 107 cm. The coordinate system is indicated in Figure 4.1.

Point	Coordinates x;y (m)	Occurrence out of surges	Occurrence P (%)
A ¹	0.15;-0.13	104/314	33
B ¹	0.35;-0.13	32/120	27
C ¹	2.10; 0.15	29/160	18
D ¹	1.50; 0.15	54/140	39
E ²	1.15;-0.3	3/10	30
F ²	1.50; 0.6	25/60	42
F' up ²	1.50; 0.6	8/50	16
F' down ²	1.50; 0.6	4/50	8
G ²	1.50; 2.0	14/50	28
H ³	2.10; 0.6	120/856	14

¹ Series I, ² Series II, ³ Series III.

cathode. For these reasons we pointed a nanosecond-fast ICCD camera to the vicinity of the cathode.

X-rays without final breakdown of the gap

When we increase the gap length to 1.75 m, no spark develops within the $50 \mu\text{s}$ of high voltage delivered by the Marx generator in the absence of electric breakdown. The electrical characteristics together with an image with 100 ns exposure time are shown in Figure 4.9; clearly the anode current - if there is any - remains hidden in the noise in the measurement. However, both scintillation detectors simultaneously register an X-ray signal at the same stage and time as in the smaller gaps. The camera shutter was opened just after the X-rays had been detected. As can be seen from image (b), there is streamer/leader activity around the high-voltage electrode. We conclude again that the grounded electrode is not directly involved in X-ray production.

The vicinity of the cathode during X-ray registration

Figure 4.10 shows the images for six different discharges, zooming in into the region just below the high-voltage electrode, at the moment when most X-rays are detected. All images have an exposure time of 50 ns, and the shutter in all images of Figure 4.10 and in Figure 4.9 (b) has been opened with the same delay after the beginning of the voltage rise (time zero in all plots). The images (a) to (f) have intentionally been ordered such as to illustrate the discharge development. Negative streamers (ns) leave isolated dots or beads behind during the propagation (image (a)). Later, the beads act as starting points for positive streamers (ps) (image (b)). We call these features positive streamers because they look like streamers, their velocity coincides with the velocity of positive streamers in our setup ($2 \cdot 10^6 \text{ m/s}$, see details in [Koc12, Koc14a]), they move towards

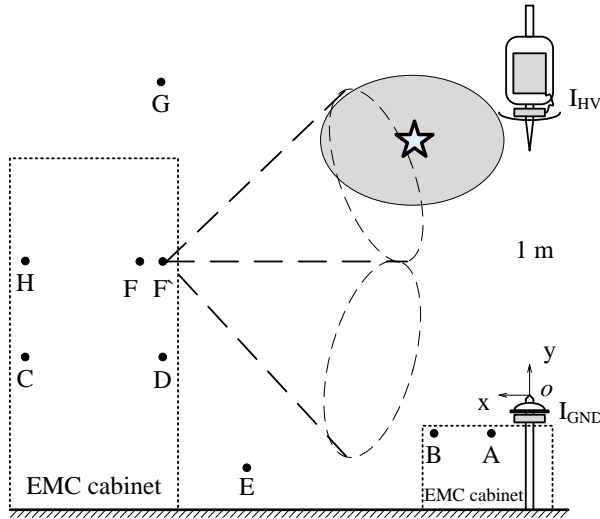


Figure 4.8: The source location with a confidence bound of 95% calculated with an inverse square law fit of the data shown in Table 4.1. Neither attenuation by air nor by detector/cabinet aluminum casings is taken into account. The approximate source location is near the HV electrode and off axis.

the negative high-voltage and they branch in this direction. Remarkably, the upward moving positive streamers co-exist with negative streamers that move downwards. Later positive and negative streamers collide (images (c) and (d)). X-rays are detected in discharge (a) 50 ns after the image; discharge (c) 40 and 110 ns after the image; and (d) 300 ns after the shutter was closed. Even when the streamer encounter is clearly visible on the image, this does not guarantee X-ray detection. And vice versa - when we detect an X-ray signal, the streamer encounter, which is possibly responsible for it, might not be located in the camera field of view. Apart from that, it is a matter of luck to take a snapshot - point the camera to the right place, open its shutter at the right moment and keep it open as short as possible. Even though we cannot link a single encounter with a single X-ray burst and prove their correlation, similar collisions between positive and negative streamers have been observed in positive discharges, also simultaneously with X-ray registration.

The entire structure that eventually develops out of the negative streamers, beads and positive streamers is a pilot system in the nomenclature of [Ree95, Gal02]; a schematic representation of the pilot system is shown in Figure 4.11. Images (e) and (f) in Figure 4.10 show that such pilot structures are common features in negative discharges in the laboratory. The structures were also observed in other experiments [Ste62, Les81, Ree95]. In larger gaps of a few meters, the pilot system can even develop into a space leader. In the center of images (d) and (e) two of these structures are clearly visible, but more than ten were counted in image (f).

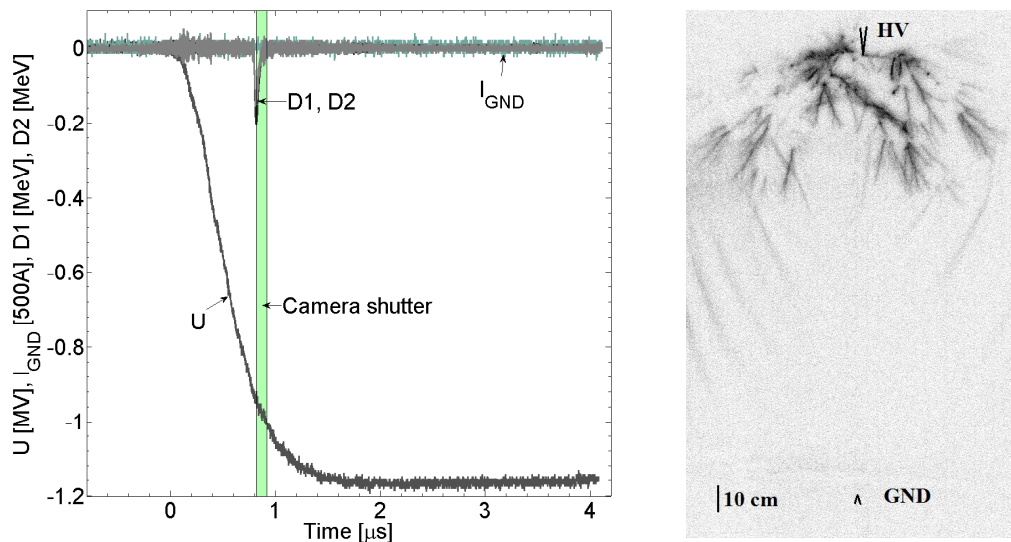


Figure 4.9: Here the distance between HV and GND electrodes is as large as 175 cm. X-rays are detected during the fourth streamer burst of the pre-breakdown phase. No current through the GND electrode is registered, and no light from the GND electrode detected. The discharge does not develop into a spark. The X-rays were detected by two LaBr3 detectors just before the picture was taken with an exposure time of 100 ns.

4.3.6 Energy spectra and attenuation curves

In order to get a statistically meaningful X-ray spectrum, we analyzed the amplitudes of 636 X-ray signals collected with a single detector at position H in Figure 4.1. We found that the X-ray energy depends neither on the instantaneous voltage nor on the current. Thus, they are apparently generated by independent events. So, when two or three X-ray bursts were detected during a discharge we count them separately. As we have previously shown, even a small deposited energy could be the sum of several photons. Because of multiphoton registration and overlapping X-ray bursts, we can only get a pseudo-spectrum with our detector. Such a spectrum is shown in Figure 4.12, where we divided the energy scale in bins of 55 keV. As mentioned above, detected energies of up to 0.5 MeV can be fitted by a single photon response. Energies larger than this value are more likely multiphoton registration and/or burst overlap. Up to about 0.5 MeV the pseudo-spectrum can be fitted by an exponential function $dn/d\epsilon \sim \exp(-\epsilon/\epsilon_c)$ with a characteristic energy $\epsilon_c = 0.2$ MeV. This ϵ_c agrees well with the energies reported in [Dwy08, Ngu08, Mar11a]. The average deposited energy over the entire spectrum is 0.55 MeV. So, on average we detect 2 - 3 X-ray photons by our detector per burst. If we assume that the X-rays within one burst are distributed isotropically, we get approximately 10^5 photons per burst over the complete solid angle of 4π .

In order to get more information on the distribution of the single photon energies we performed a series of measurements with lead attenuators in front of the detector. One detector was mounted in the small EMC cabined located below the grounded electrode at position A, the other in the large cabined at position D (see Figure 4.1). The detectors were wrapped in a 15 mm thick lead cylinder and the scintillator crystals were covered by lead caps with varying thicknesses of 1.5, 3, 4.5, 6 and 7.5 mm. Each cap was placed right in front of the scintillator, touching it. For each cap thickness we determined the X-ray detection in 50 discharges. The data are shown in Table 4.2. The detections without attenuator indicate the initial intensity of the source at the specific location. As expected, the amount of detected X-rays decreases with increasing cap thickness.

Table 4.2: *The amount of discharges (% out of 50) when x-rays are detected.*

	Lead thickness, mm					
	0	1.5	3	4.5	6	7.5
Point A	31	6	2	0	0	0
Point D	32	8	5	0	0	2

If for the moment we neglect multiphoton registration and burst overlap, the attenuation (removal) of photons from the initial burst as they pass through the attenuator would follow the equation:

$$\frac{I}{I_0} = e^{-\mu(\epsilon) \cdot x} \quad (4.2)$$

where I_0 is the initial source intensity, I the intensity after the lead attenuator, $\mu(\epsilon)$ the linear attenuation coefficient at energy ϵ , and x the lead thickness. The attenuation

coefficient μ is the sum of individual attenuation coefficients for photoelectric absorption and Compton scattering: $\mu = \mu_{ph} + \mu_{comp}$

We can neglect Rayleigh scattering and pair production in our energy range. Moreover, since we put the lead caps right in front of our detector, and since the attenuator thickness is significantly thinner than the detector size, many Compton scattered photons will penetrate into the scintillator and interact with it. We also proved experimentally in [Koc12] that we can neglect Compton scattering in our setup and only consider the photoelectric absorption inside the lead attenuator. Taking the detectors quantum efficiency at energy ϵ into account, we have the following general relationship:

$$I = \int_{\epsilon_{min}}^{\epsilon_{max}} \eta(\epsilon) \cdot I_0(\epsilon) \cdot e^{-\mu_{ph}(\epsilon) \cdot x} d\epsilon. \quad (4.3)$$

where $I_0(\epsilon)$ is the incident energy spectrum, $\eta(\epsilon)$ is the quantum efficiency of the detector (about 100% at our energy range), and the absorption function μ_{ph} is taken from NIST [Ber98]. Now we can calculate the attenuation curves for different detector positions. In Figure 4.13 we compare the measured attenuation curves (dashed lines) with those calculated under the assumption that single photons are registered (solid lines). The measured attenuation curves are below the ones calculated, which confirms that the real X-ray spectrum is softer than that indicated by the detectors. This means that in each burst we detect several lesser energetic photons simultaneously rather than one single hard X-ray photon. A monoenergetic X-ray beam of 0.2 MeV photons would undergo attenuation similar to the one measured at point A. In this analysis we neglected the attenuation by 2 m of air since the additional attenuation is only 3% at 200 keV and 8% for 30 keV which is the lower limit of the detectors. A more thorough investigation including Monte Carlo simulations of X-ray propagation through the air and of the interaction with the detector will be presented in a future paper.

4.4 Discussion

Although negative and positive laboratory discharges possess similar features - streamers, leaders, counter-streamers and counter-leaders - their development is quite different. The photography with nanosecond fast cameras shows that laboratory discharges with positive polarity grow in a more continuous way [Koc12]. Negative discharges have a more complex structure and development mechanism [Koc14a], in particular, they do not propagate continuously in the present set-up, but in four streamer bursts, and they form space-stems ahead of the negative streamers/leaders - at least in the fourth burst near the cathode. The X-rays from both discharges appear in short bursts. The measurements with the LaBr3 detectors fix the upper limit of the burst duration at 6 ns for signals of up to 2 MeV. Other measurements with the faster BaF₂ [Ngu12] and with plastic detectors show that the bursts likely last as short as 1 ns. This made us look whether the images contain indication of such fast processes, which can be held responsible for the X-rays. The best candidate is the encounter of streamers. Streamer heads of both polarities are observed simultaneously near the cathode. The streamers move with approximately 2 mm per ns in these images; the measured diameter is 2

to 4 mm. Models suggest that the electric field in front of a streamer is about 100 - 160 kV/cm [Nai09]. When two long streamers of opposite polarity approach each other, the electric field between their tips dramatically enhances. This mechanism is suggested by Cooray et al in [Coo09] and in general is confirmed here and in [Koc12] by time resolved photography with simultaneous X-ray measurements. Note, however, that in positive discharges, the encountering streamers are primary streamers propagating through non-preionized air near the grounded electrode, while in the negative discharges they are near the HV electrode pre-treated by several earlier streamer bursts.

An electric field enhancement can also occur when streamers approach an electrode, in the so-called proximity effect. In this intense field the electrons from the negative streamer or electrode can overcome the friction barrier at about 200 eV kinetic energy over a fraction of a millimeter and run away [Dwy04a]. The photographs in Figures 4.9 and 4.10 show that such encounters occur near the cathode, so there is ample voltage difference left with respect to the environment for the electrons to attain large energy, if the electrodes are not screened by plasma. In our setup with voltages over 500 kV, electrons can accelerate into the relativistic regime, and lose their energy rapidly through X-ray bremsstrahlung. It should be noted that much of our understanding of streamers relates to the first streamers propagating through virgin air, while in the present experiments, the fourth streamer burst produces most X-rays. Inhomogeneous background ionization created by the previous streamer bursts can create the bead structure near the cathode [Luq11] that can be seen in the images.

X-ray bursts in laboratory discharges of both polarities are accompanied by high-frequency oscillations; see [Koc12] and this work. The frequency is far above the 70 MHz working range of the current probes. We attribute these electrical signatures to the electrodes acting as oscillating antenna excited by the sudden current changes caused by the streamer encounters. Perhaps even the conductive streamers may act as such an antenna. Although we did not register X-rays from every discharge, we always observed the oscillations. Moreover, the oscillations coincide with X-rays if detected. In addition, the amplitudes of the oscillations are positively correlated with the probability of X-ray detection. We therefore presume that X-rays occur in nearly all measurements and that the detection is a matter of probability given by the limited number of photons and energy limit of our detectors 30 keV. Another possible explanation of the lower X-ray detection rate is that the X-ray bursts have a finite opening cone, and that X-rays are detected only if the detector is in the cone. Investigations of this question are now under way.

In short gaps of 1 meter or less, the X-ray bursts coincide with the onset of current at the grounded electrode, as is for example shown in Figure 4.2. High-frequency oscillations are then also visible in the anode current. Table 4.1 for the position F' down shows that about one third of the X-rays occur in the anode region. We again attribute this to the encounter of negative streamers with positive streamers, but now near the anode.

The fact, that the final breakdown is not necessary for the X-ray production allows us to compare the negative laboratory discharge with the X-rays produced by a negative stepped lightning leader. It has been shown that natural negative lightning generates X-rays during the stepping of the leader [Moo01, Dwy05a]. The stepped leader propagates by creating space leaders. The space leader is a bipolar structure that develops in both

directions in front of the lightning leader. When the positive part of it connects to the negative leader the step occurs. Recent high-speed video observation of the stepping process [Pet13] allows us to suppose that X-rays from negative stepped leaders can be generated in the same way as described in this manuscript. The pilot systems observed in this work develop into space leaders in longer gaps and in natural lightning.

The attenuation curve shows that most large energy signals are due to pile-up. However, the fact that we still detected an X-ray signal behind 7.5 mm of lead indicates that a high energy tail exists in the electron and X-ray distribution. Photons of 200 keV have a chance of less than 1% to pass the attenuator; at 500 keV it is more than 10%.

It will be an interesting experimental task to create a single streamer encounter under controllable conditions and with sufficient energy pumped in.

4.5 Conclusions

Based upon observations of more than three thousand long negative laboratory discharges we arrive at the following conclusions:

- Nanosecond-fast X-ray bursts happen during the pre-breakdown process; the final breakdown of the gap is not necessary.
- It is most likely that streamer encounters are responsible for the X-rays, because the field enhancement between streamers tips makes it easier for the electrons to run away (thermal run-away mechanism [Gur61]).
- Since lightning leaders propagate in a similar stepped manner, we propose that streamer encounters are responsible also for the X-rays from the leader.
- The X-ray spectrum in our measurements can be approximated by an exponential distribution function with a characteristic energy of about 200 keV. In order to calculate the precise spectrum and the initial number of high-energy electrons, simulations would be required. These simulations should include the relevant processes and many details of the setup.
- The X-ray bursts seem to be correlated with current oscillations, but current oscillations occur also without X-ray detections. A possible explanation is that the X-ray bursts have a finite opening cone and that the detector is not always inside the cone.

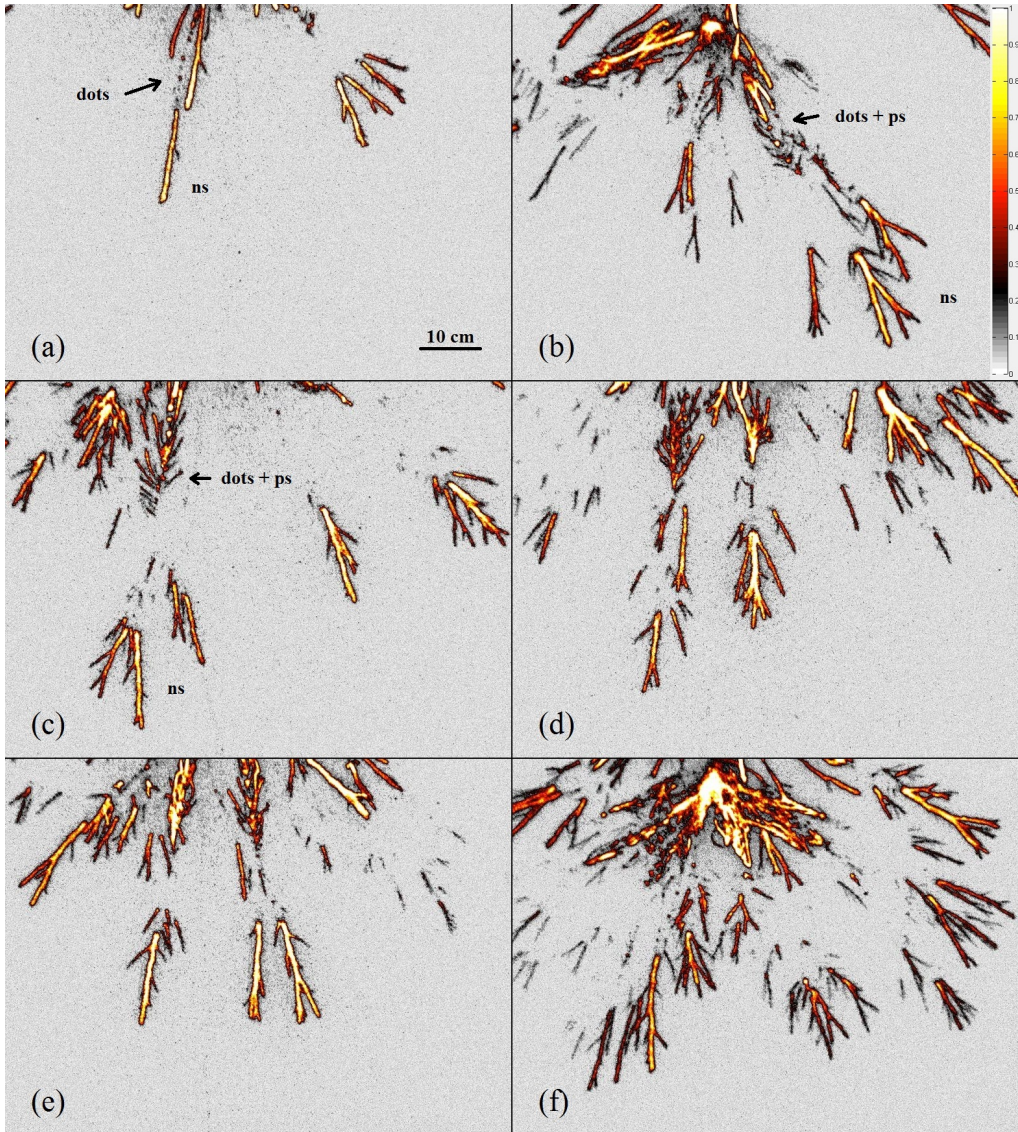


Figure 4.10: Images of the vicinity of the cathode at the time of X-ray detection with an exposure time of 50 ns. For all images the camera shutter is opened at the same time as in Figure 4.9 (b). (a) Negative streamers (ns) leave beads behind in pre-ionized medium. The dots act as starting points for new positive (ps) cathode-directed streamers (b)(f). A possible collision between negative and positive streamers is visible in (c) and (d).

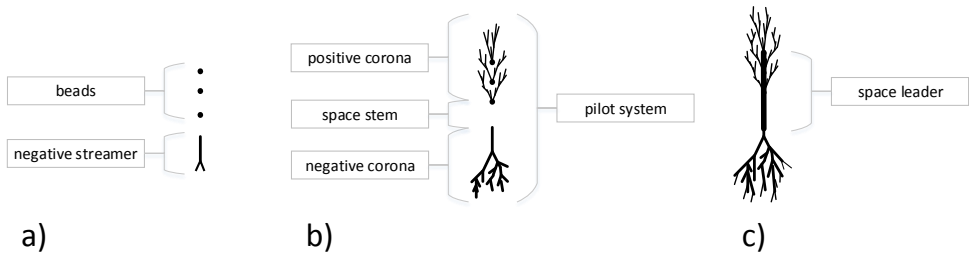


Figure 4.11: Schematic of the development of a pilot system. It is a bipolar structure that can develop into a space leader in sufficiently long gaps and apparently into lightning leaders.

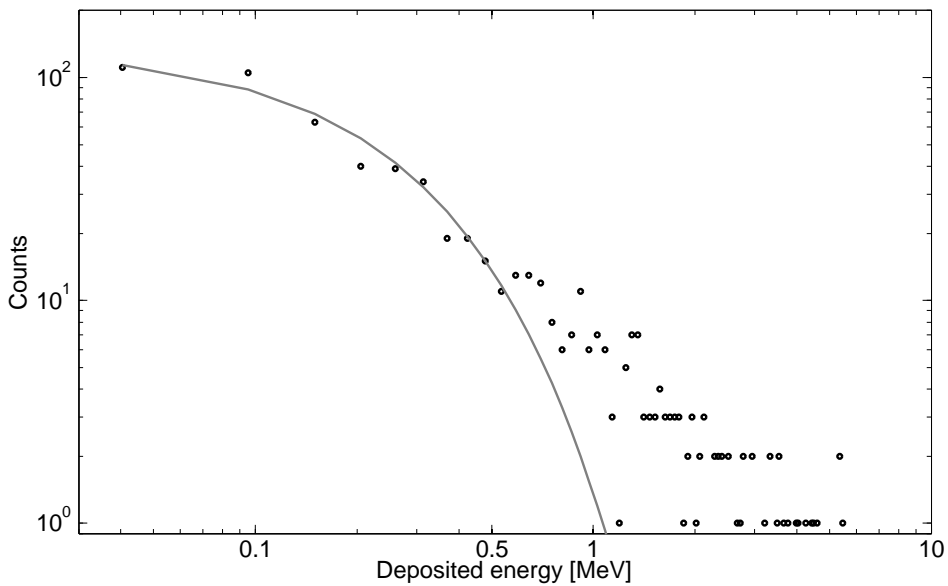


Figure 4.12: The pseudo-spectrum of X-rays (dots) collected by two LaBr3 detectors at position H (Figure 4.1), indicating the energy deposition in a detector which also can be due to the pile-up of multiple photons in an X-ray burst. The energy bins are 55 keV wide, and the statistics is over 636 X-ray bursts. The solid line is a fit with $dn/d\epsilon \sim \exp(-\epsilon/\epsilon_c)$, where ϵ_c equals 0.2 MeV. While the low energetic part of spectrum fits well up to 0.5 MeV, the high-energetic part lies above the fit. This happens due to multiphoton counts within one X-ray burst, or due to the overlap of two or more X-ray bursts.

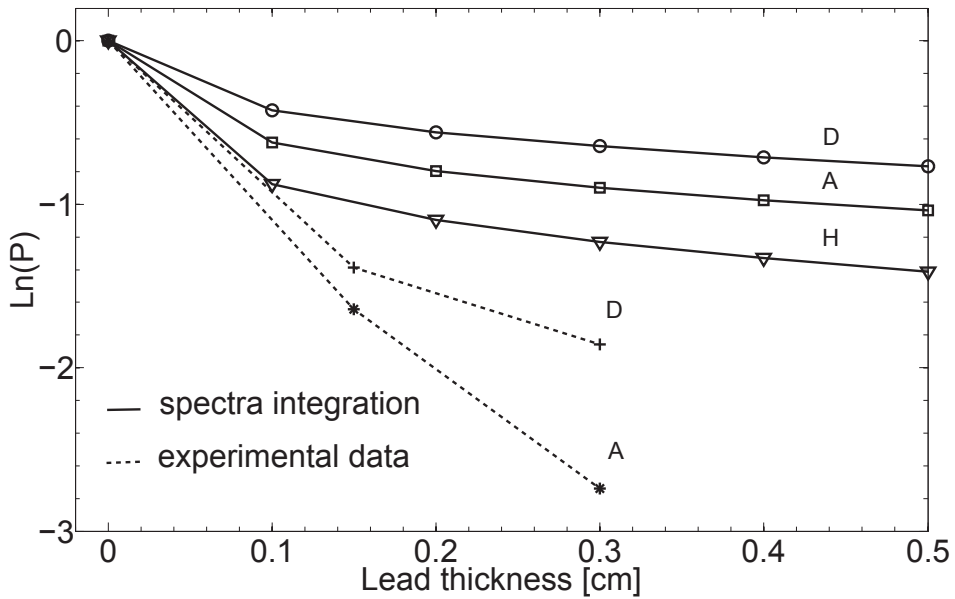


Figure 4.13: Experimental (dashed) and calculated (solid) attenuation curves at positions A, D and H. The calculated values are above the measured ones because of multiphoton registration and of overlapping X-ray bursts.

CHAPTER 5

MONTE CARLO SIMULATION OF X-RAY EMISSION

Long laboratory discharges generate bursts of x-rays. The bursts are short and intense, which makes it a challenging task to measure their characteristics correctly. In this work we try to determine the initial intensity and energy composition of the bursts. We create a detailed Geant4 model of the LaBr₃ detector and compare the results of the simulation with measured in the lab. Isotropic x-ray bursts near the high-voltage electrode with $7 \cdot 10^4$ initial photons in 4π and mean energy of about 160 keV give the spectra and attenuation curves close to measured. This Chapter will be merged with a Chapter 5 of Chris Koehn's PhD Thesis "The production of X-rays in air by monoenergetic electron beams with energies of 1 MeV or less" and submitted as a journal publication.

5.1 Introduction

Long laboratory sparks emit x-rays [Dwy05b, Mar11a, Rah08, Ngu08, Dwy08]. Previously we showed that most of the x-rays appear in short (1 ns or less) and intense bursts, consist of photons with about 200 keV characteristic energy and come from cathode area. We also concluded that the most likely candidate for the x-ray source is a streamer encounter [Koc12, Koc14b].

In this work we pursue two goals: 1) create a model of the x-ray emission, propagation and detection and 2) find some basic properties of the x-rays such as the initial number of photons and the spectrum. The model has to prove or disprove our understanding of the problem and might be extended to a future model for the high energy radiation of a lightning leader. The model is based on Geant4 software.

Geant4 (for GEometry ANd Tracking) is a toolkit for the simulation of the passage of particles through matter. It is widely used in high energy physics (Hadron Production Experiment at CERN), nuclear physics, as well as in medicine and space science. It includes facilities for handling geometry, tracking, detector response, visualization and many others. In this work we simulate the detector response when a particle passes through the scintillator volume and thereby approximate how a real detector would respond.

5.2 Experimental setup

A 2 MV Marx generator at Eindhoven University of Technology delivers a IEC standardized lightning impulse voltage waveform of $1.2/50 \mu\text{s}$ rise/fall time when not loaded. The generator is connected to a spark gap with cone-shaped electrodes. Distance between electrodes is 1 meter. The setup is similar to the one described in [Koc12, Koc14a, Koc14b].

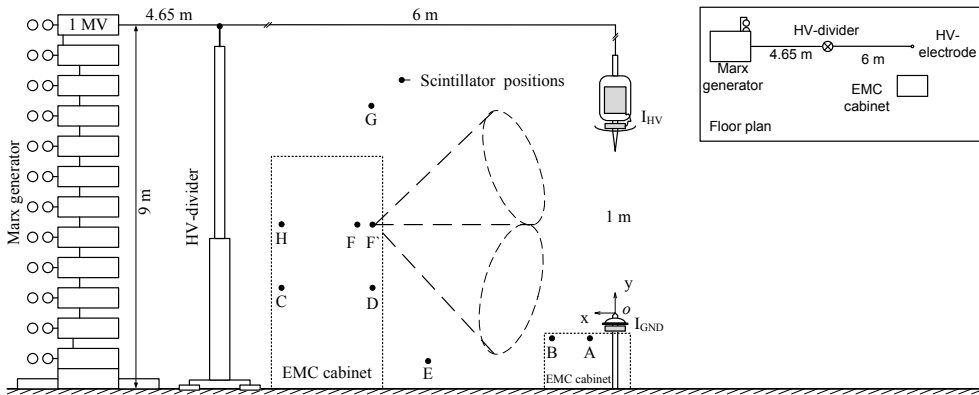


Figure 5.1: Schematic sketch of the spark gap geometry. Positions of the x-ray detectors are labeled from A to H. All positions are in the same vertical plane. Dashed cones indicate the detector field of view when placed inside a lead cylindrical collimator. Two ICCD cameras are located at 3.5-4.5 m distance from the gap. The distance between Marx generator and the spark gap is 10.65 m. The upper right inset shows the correctly scaled floor plan.

Two $\text{LaBr}_3(\text{Ce}^+)$ scintillator detectors manufactured by Saint-Gobain were mounted in EMC cabinets and recorded the x-rays. Scintillators are cylinders of 38 mm in diameter and height. Any interference on their signals due to the discharge initiation can be excluded, since such interference would most likely manifest itself as oscillatory signal, and not mimic a clear scintillator signal. Also, in many discharges only the signal channel noise floor was measured. The scintillators have a fast primary rise/decay time (11/16 ns) and a high light yield of 63 photons/keV, which is 165% of the more common $\text{NaI}(\text{TI})$. The linearity of the detectors tested on ^{241}Am , ^{137}Cs , ^{60}Co and remains perfect up to 2505 keV, which is the total absorbed energy from two gamma quanta of the ^{60}Co source in the scintillator [Ngu12]. The slight deviation from linearity at higher energies is attributed to saturation of the photomultiplier. The output of the photomultiplier is recorded directly on the oscilloscope without any waveshaping electronics usually

employed in photon counting. This allows to distinguish individual pulses even when pile-up occurs within the decay time of the scintillator. In some series of measurements the detectors were located inside separate EMC-cabinets; one detector was placed in a small cabinet at positions A and B and the other detector was placed in the large cabinet at positions E, D, F, G, H as indicated in figure 5.1. The total aluminum thickness between the scintillator and surrounding area is $550 \mu\text{m}$.

5.3 Experimental data

The x-rays we detect in our experiments are generated by Bremsstrahlung interaction of high-energy electrons with air molecules. As was shown previously in [Koc12] and [Koc14b] the source is located near negatively charged electrode. The most likely candidate so far is a streamer encounter. When two streamers of opposite polarity approach each other an electric field between them quickly increases. When it reaches a critical value free electrons between the streamers gain more energy from the field than they lose on mainly ionization processes. They come into so-called run-away regime [Dwy04a]. They can be accelerated to relativistic energies and quickly escape the region between streamers. After that, they collide with an air molecule and emit accumulated energy in x-ray form. These x-rays are captured by our detectors. The entire process lasts of the order of nanosecond. It is unlikely that the high-energy electrons escape the high-field region isotropically. They might be beamed or have other anisotropic shape. But as shown in [Koe14a], that electrons with several keV energies emit x-rays rather isotropically. At least the level of anisotropy decreases after Bremsstrahlung scattering. Since we could not find any direct evidence of anisotropy in our measurements, we can safely assume isotropic x-ray bursts. In the laboratory we measure a registration rate, spectra and attenuation curves at different positions of the detectors (see figure 5.1). We do not detect x-rays in every discharge. For example, when a single LaBr_3 detector shows x-ray signature in 30 out of 100 discharges, we say that the registration rate at this position is 30%. The registration rate contains information about the initial amount of x-ray photons that can bring us to the initial amount of high-energy electrons necessary to produce the x-ray burst. As was shown in [Koc14b], an x-ray burst can be intense enough that the detector can be hit by several photons simultaneously within 1 ns or less. In such case we cannot distinguish between one 200 keV photon and two 100 keV photons - the photomultiplier gives an identical electrical output. Which means that we do not measure a spectrum but rather pseudo-spectrum and the question about the true energy composition of the burst remains open. We also measured attenuation curves that contain information about the true energy composition of the x-rays which, in turn, can lead us to a spectrum of the initial high-energy electrons.

5.3.1 Registration rate

We measured the registration rate by one LaBr_3 detector at different positions that are indicated in figure 5.1. Moreover, in position F we covered two detectors by lead tubes of 15 mm thickness and pointed them to different parts of the gap - up and down. The

detector angles of view do not overlap. The measured registration rates are shown in table 5.1.

Table 5.1: Occurrence of x-rays detection in different positions. The effective area of one detector is 11.3 cm^2 . The gap distance is 107 cm .

Point	Coordinates x;y (m)	Occurrence out of surges	Occurrence P (%)
A ¹	0.15;-0.13	104/314	33
B ¹	0.35;-0.13	32/120	27
C ¹	2.10; 0.15	29/160	18
D ¹	1.50; 0.15	54/140	39
E ²	1.15;-0.3	3/10	30
F ²	1.50; 0.6	25/60	42
F' up ²	1.50; 0.6	8/50	16
F' down ²	1.50; 0.6	4/50	8
G ²	1.50; 2.0	14/50	28
H ³	2.10; 0.6	120/856	14

¹ Series I, ² Series II, ³ Series III.

Series II has been measured two months later then Series I, series III half a year later. The electrical parameters of the discharge remained constant during all series. As can be seen, two times more events are detected when the detector is pointed to the top of the gap (F' up) than when it is pointed to the bottom (F' down). The same behavior was observed in positive discharges, for which the cathode area produced twice the number of x-rays compared to the anode [Koc12]. It is also remarkable that the farthest positions C and H show the lowest registration rate. In general tree main processes contribute to the registration rate: 1) the generation rate, 2) the geometrical decay and 3) the attenuation by air, the detector hull and the EMC-cabinet. Below we consider each of them in detail. The generation rate is the source property only.

Generation rate

Usually we detect a single x-ray burst during one discharge, but sometimes we even see up to five. The x-ray signatures of 20 discharges are shown in figure 5.2. First nine discharges show no x-rays. Three x-ray bursts are generated in discharge #10. Discharges #13, 17 and 20 show a single x-ray burst. In total, x-rays are detected from 4 discharges. The registration rate in this particular case is $4/20=20\%$. By analysis of 950 discharges performed in 4 days in a row we noticed that a ratio between single, double and triple x-ray bursts does not depend on the detector position, which means that it mainly determined by the source. The chance to see k number bursts in a single discharge can be described by the Poisson distribution as seen from figure 5.3. The best fit of the measured data is achieved with $\lambda = 0.85$. The registration rate in this terms is sum of all none-empty discharges:

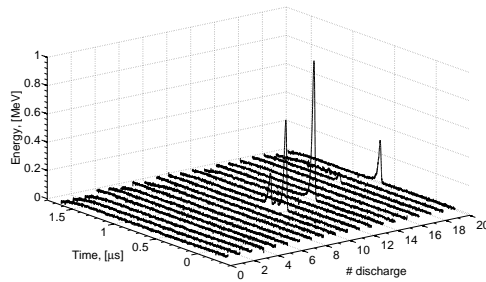


Figure 5.2: Oscillograms of 20 discharges measured in a row. The first nine discharges show no x-rays. Discharge #10 shows three x-rays burst. Four discharges contain an x-ray signature. The registration rate then equal to 20%.

$$RR(k) = \sum_{k>0} \frac{\lambda^k e^{-\lambda}}{k!}, \quad (5.1)$$

with $RR(k)$ - the registration rate and λ - the Poisson distribution parameter. It also means that not every single discharge generates x-rays but, according to equation 5.1, only 57% of them. The parameter λ is a characteristic of our setup in general and the HV electrode shape in particular. Obviously, it is different in different lab experiments. In [Koc12] we demonstrated how we can increase the amount of x-rays by just changing the cathode shape.

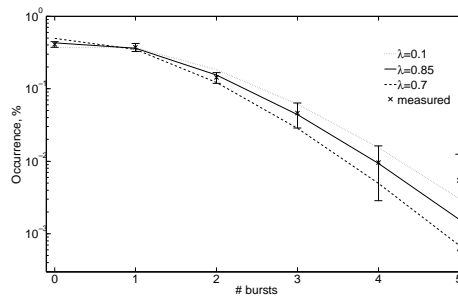


Figure 5.3: The number of bursts is a single discharge. A Poisson distribution with $\lambda = 0.85$ best fits the measured data.

Geometrical decay

In [Koc14b] we show that x-ray source is located near the HV electrode. It is also clear from the measurements with collimators at position F (up and down) in table 5.1. Due to the cylindrical symmetry of the gap and averaging over many discharges we can

consider the source location at a straight vertical line connecting both electrodes in our calculations. Next to the generation rate, we should consider the impact of geometrical decay on the registration rate, especially at large distances. By geometrical decay we mean the inverse square law for isotropic x-ray bursts. As can be seen from table 5.1, the registration rate decreases with the distance from the gap. For the sake of simplicity we just take the distance as counted from the electrode tip. Consider an x-ray burst that emit n_{ph} number of photons in 4π . If we move the detector towards the gap, at some distance r_s (s stays for *single*) a flux through the detector equal to one or more photons per burst. At this distance and closer we are in a single and multiphoton registration regime when, at least one or more photons hit the detector simultaneously. At these distances the registration rate is only limited by the generation rate. In other words, we see each burst that is generated by the discharge. The maximum registration rate is equal to about 57% in our configuration (equation 5.1) and we obviously cannot see more than has been generated. If we put our detector further than r_s , the registration rate decays according to inverse square law starting from its maximum:

$$RR(k, r) \sim \frac{1}{r^2} \cdot RR(k), r > r_s \quad (5.2)$$

The photon flux through the detector at distance r can be estimated by the following equation:

$$F(r) = \frac{n_{ph}}{4\pi} \cdot \frac{1}{r^2} \cdot \pi r_d^2 \quad (5.3)$$

Where F - amount of photons per detector area at distance r , r_d - detector scintillator radius, n_{ph} - total amount of initial photons emitted in 4π . For simplicity here we just use geometrical scintillator radius instead of an effective detection area which is energy dependent and will be considered in the next Section.

Then registration rate can be determined as following:

$$RR(k, r) = \begin{cases} F(r) \cdot RR(k), & r > r_s \\ RR(k), & r \leq r_s \end{cases} \quad (5.4)$$

Now the registration rate can be calculated for different initial amount of photons (n_{ph}) and compared to the measured in table 5.1. The result is shown in figure 5.4.

As can be seen from figure 5.4, the initial amount of photons is of the order of 10^4 in 4π . But more processes have impact on the registration rate and they are energy dependent.

Attenuation and detector efficiency

The attenuation is an energy-dependent process and accounting for it will increase the amount of initial photons calculated above. The attenuation caused by air and the aluminum hull of the detector and EMC-cabinet is mostly important for low energy photons. The attenuation is described by following equation:

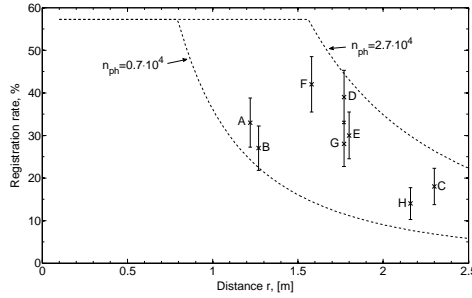


Figure 5.4: The registration rate versus distance from the x-ray source to the detector. It is limited from the top by the generation rate and follows an inverse square law at distances where photon flux through the detector is smaller than one photon. Measured registration rates at different locations are also indicated.

$$\frac{n'_{ph}}{n_{ph}} = e^{-(\mu_{air}r + \mu_{al}d)} \quad (5.5)$$

Where n_{ph} - initial amount of photons generated by x-ray burst in 4π , n'_{ph} - the amount of photons that can reach a sphere (isotropic burst) of radius r , μ - linear attenuation coefficients, d - total aluminum thickness. The attenuation coefficients are energy dependent.

The detector efficiency is an absorption efficiency and reflects the ability of the detector to absorb the incident radiation. The higher the x-ray photon energy the higher a chance of its penetration through the detector without any interaction with the scintillator. The detector efficiency graphs can be found in the manufacturer's specification.

5.3.2 Spectrum and attenuation curves

Due to extreme short duration and the intensity of an x-ray burst, the determination of the spectrum is not trivial. As we mentioned above, the main problem of our detector is that we cannot distinguish between single 200 keV photon and two 100 keV photons arrived simultaneously. The only validation procedure we have is a comparison of the x-ray signature with a single photon response function measured on calibration sources. But even if the measured signal fits perfectly to the single photon response function we cannot guarantee that it was a single photon. So what is measure in our experiments is a pseudo-spectrum and it is harder than the real x-ray spectrum due to multiphoton registration. The pseudo-spectrum measured at position H by two identical LaBr₃ detectors placed next to each other is shown in figure 5.5. Only x-ray signatures that match a single photon response function have been included.

In order to get more information about the true energy composition of the x-ray bursts we measured attenuation curves. The detector was placed inside a lead tube of

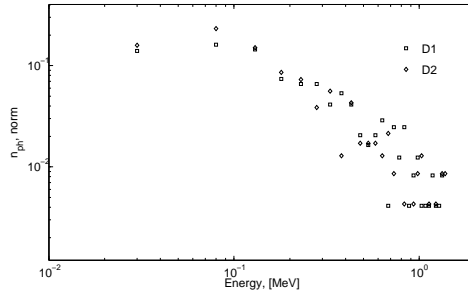


Figure 5.5: Measured spectra by two identical LaBr_3 detectors D1 and D2 located next to each other at position H. Bin width is 50 keV.

15 mm thickness and was covered by lead caps of various thicknesses: 1.5, 3, 4.5, 6 and 7.5 mm. The registration rate was measured at positions A and D. For every thickness we made 50 to 100 discharges. The result is shown in table 5.2.

Table 5.2: The amount of discharges (%) when x-rays are detected.

	Lead thickness, mm					
	0	1.5	3	4.5	6	7.5
Point A	31	6	2	0	0	0
Point D	32	8	5	0	0	2

As expected, the registration rate quickly decreases with increasing absorber thickness. The slope of the decrease contains information about the energy composition of the bursts. The faster it decays the softer the spectrum. In order to confirm the approach described above and to find the initial amount of photons in a single burst and its true energy composition, we ran a Monte Carlo simulation in Geant4.

5.4 Model

The model consist of a detailed description of a LaBr_3 detector. The model was validated in the lab using three radiation sources - ^{241}Am , ^{137}Cs and ^{60}Co . We placed the sources at 25 cm distance from the detector and measured their spectra and attenuation curves with lead absorbers of different thickness. A background correction was applied to the measured values. The same situation was simulated in Geant4.

5.4.1 Model validation

Figure 5.6 compares the measured and simulated spectra. Photo peaks are well visible together with Compton edge and Compton spectrum.

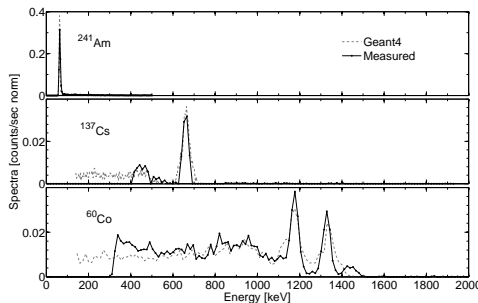


Figure 5.6: Comparison of measured and simulated spectra of ^{241}Am , ^{137}Cs and ^{60}Co radiation sources. Photo peaks and Compton edges are visible. Background radiation is subtracted from the measured spectra.

Figure 5.7 compares the measured and simulated attenuation curves. The LaBr_3 detector is placed in a lead tube and covered by lead absorbers of different thickness in Geant4 as well as in the experiments. The radiation source ^{137}Cs was placed at 25 cm distance from the detector. The experimental and the simulated attenuation curves show acceptable similarity.

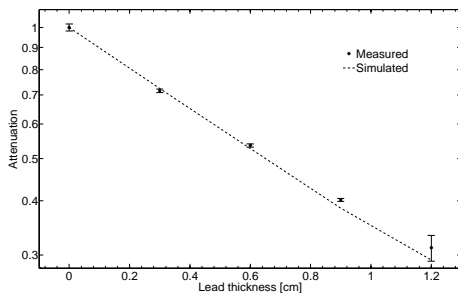


Figure 5.7: Comparison of measured and simulated attenuation curves. The LaBr_3 detector is placed in a lead tube and covered by lead absorbers of different thickness in the same way as during experiments. Radiation source ^{137}Cs is located at 25 cm distance from the detector. The same procedure was performed in Geant4. Measured and simulated attenuation curves show sufficient similarity.

With this experimental validation we conclude that the model is sufficiently good and can be used to simulate the processes in the actual discharge.

5.5 Results

We simulate isotropic x-ray bursts near the HV electrode (± 25 cm from the electrode tip in horizontal direction). The spectrum is chosen of $dn_{ph}/d\epsilon \sim e^{(-\sqrt{\epsilon}/\epsilon_{av})}$ shape which is derived from electron simulations performed by Chris Koehn in his thesis; it is not shown here. The energy is set from 1 keV to maximum theoretically available in our setup 1 MeV. By varying the amount of initial photons and the mean energy ϵ_{av} we want to find the best fit of the attenuation curves and the measured spectrum. The results of the simulation are shown in figures 5.8 and 5.9.

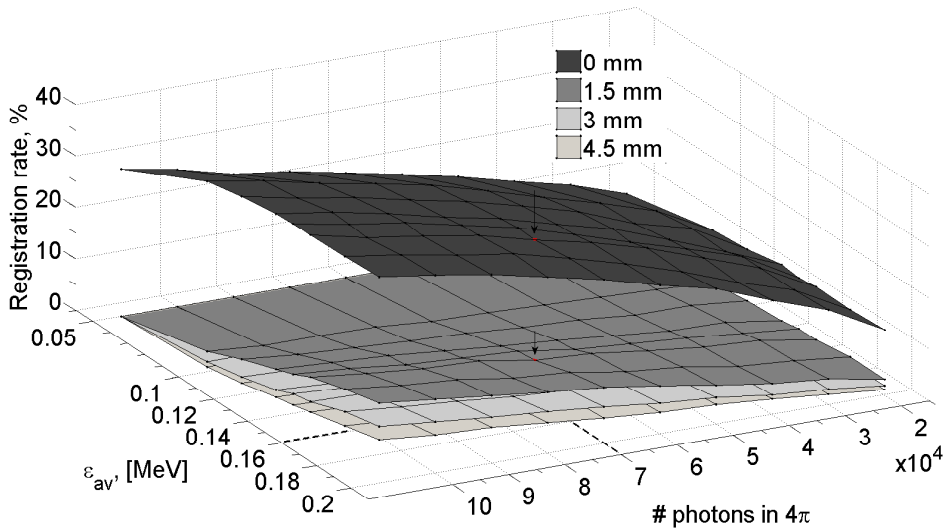


Figure 5.8: The registration rate vs source intensity n_{ph} vs mean photon energy ϵ_{av} calculated at position D . Four planes are simulated for different attenuator thicknesses in front of the detector. Points on the planes marked by arrows correspond to the best fit to the measured attenuation curve (see table 5.2).

The place where measured attenuation rate coincides with the simulated is indicated by arrows. The best agreement between measured and simulated data we found with the following parameters:

- isotropic distribution
- $\lambda = 0.85$
- $\epsilon_{av} = 0.16$ MeV
- $n_{ph} = 7 \cdot 10^4$

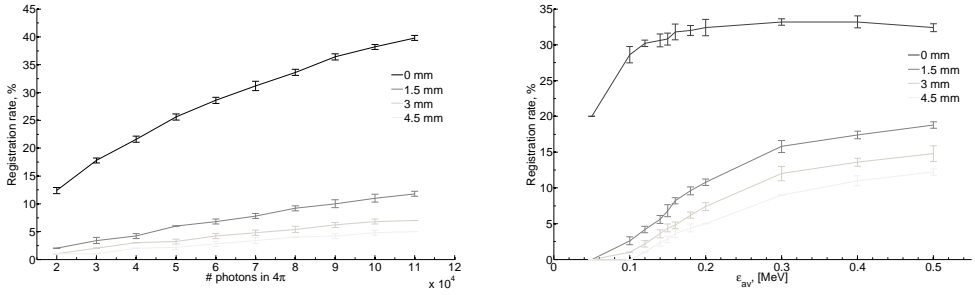


Figure 5.9: (Left) The registration rate versus source intensity for different attenuator thicknesses. Average energy ϵ_{av} is fixed to 0.16 MeV. The registration rates at $7 \cdot 10^4$ photons coincide with those measured at the lab. (Right) The registration rate versus mean photon energy ϵ_{av} for different attenuator thicknesses. The initial amount of photons is fixed to $7 \cdot 10^4$ in 4π . At $\epsilon_{av} = 0.16$ MeV the registration rates coincide with those measured in the lab.

5.5.1 Spectrum

Figure 5.10 shows comparison between simulated and measured pseudo-spectra.

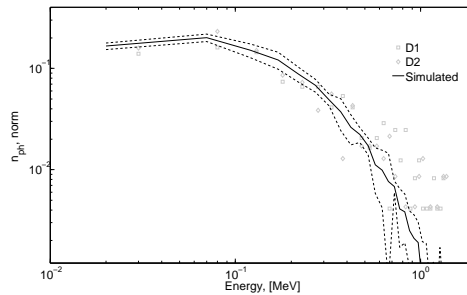


Figure 5.10: Simulated and measured by detectors D1 and D2 spectra at position H. Bin width is 50 keV. The initial amount of photons is equal to 10^5 in 4π and the average energy ϵ_{av} is equal to 0.15 MeV.

As can be seen from figure 5.10, the simulated and measured spectrum are close to each other at low and moderate energies with slight deviation at higher energies. As we mentioned above, the only criteria to decide whether it is a single burst or not is the fit to the single photon response function. But when two x-ray bursts happen simultaneously (bursts overlaying) we are not able to resolve them as separate. Multiphoton registration is accounted in the Geant4 model but not the x-ray bursts overlaying. This causes the deviation at high energy.

5.6 Discussion and conclusions

In our previous works we investigated long laboratory spark development process in particular focusing on its x-ray generation. Here we attempt to describe the x-ray source quantitatively based on experimental data. We described the main source characteristics - generation rate, initial amount of photons and their spectrum. The amount of x-ray bursts in a single discharge follows Poisson distribution with mean value $\lambda = 0.85$. We found three main processes contribute to x-ray detection. These are: generation rate, geometrical decay and attenuation. By creating a precise model of LaBr_3 detector we simulate its response. It is consistent with measurements.

Although this study is based on negative discharges the same thoughts are applicable for x-rays from positive discharges [Koc12]. Registration rate in positive discharges is about double as such in negative *in our setup*.

Although simple mathematical model predicts about $3 \cdot 10^4$ initial photons (see figure 5.4), detailed Monte Carlo simulation shows $7 \cdot 10^4$ photons are needed. This is because we included photons down to 1 keV in the simulation. Their significant amount and strong attenuation by air and detector hull makes this difference.

CHAPTER 6

IN-FLIGHT MEASUREMENTS OF HIGH ENERGY RADIATION FROM THUNDERCLOUDS AND LIGHTNING

In the certification procedure aircraft builders carry out so-called icing tests flights, where the zero degree Celsius altitude is deliberately sought and crossed in or under thunderstorms. Airbus used these flights to test ILDAS, a system aimed to determine lightning severity and attachment points during flight from high speed data on the electric and magnetic field at the aircraft surface. We used this unique opportunity to enhance the ILDAS systems with two x-ray detectors coupled to high speed data recorders in an attempt to determine the x-rays produced by lightning in-situ, with synchronous determination of the lightning current and electric fields. Such new data highly interest geophysicists studying lightning physics. In addition, the data may provide clues to the x-ray dose for personnel and equipment during flights. The icing campaign ran in April 2014; in eight flights we collected data of 62 lightning strikes on an Airbus flight test aircraft. In this communication we briefly describe the system and show some selected first results.

6.1 Introduction

We describe a system ILDAS designed to determine the lightning current waveform and trajectory through an aircraft in-flight. The new feature is that ILDAS has been extended and now also measures the x-rays that are generated by the lightning strike with high time resolution and accuracy, in high synchronicity with the lightning data. At higher altitude, the aircraft is a part of the still growing lightning channel and may be considered as a step in the formation. We present first observations of x-rays inside the

cloud during lightning leader propagation. X-rays from lightning leaders have earlier been measured on ground level [Moo01, Dwy03b, Dwy05a]. Flights through thunderstorms with aircraft [McC85] and balloon [Eac96] proved that x-rays are associated with the lightning discharge. In addition, thunderstorms present a longer lasting glow of x- and gamma rays of a fraction of a minute that terminates with the cloud discharge [Kel10].

First we compare our measurements with cosmic rays background at different altitudes and show very consistent results with those measured in 1910's [Kol13, Car12]. Then we select two lightning strikes into the airplane and show them in the highest resolution available. We identify current flow pattern through the airplane for one particular case and assign it to plausible lightning attachment and propagation scenario. X-rays are detected during attachment and propagation phases and are associated with lightning stepped and dart-stepped leaders.

6.2 The ILDAS system

Aircraft manufacturer Airbus occasionally performs icing flights with test aircraft, also in the scope of certification of new aircraft, prolonged flights at an altitude of zero degree Celsius in or under thunderstorms. The flights also gave an opportunity to test and improve the system ILDAS, acronym for "In Flight Lightning Damage Assessment System" [ILD]. ILDAS includes a number of electric (E) and magnetic (H) field sensors with on-board data recording, and on-ground data analysis after the flight. The goal of ILDAS is to increase knowledge on lightning-aircraft interaction and evaluating a possible future commercial adaptation for use in regular airline operations as a real-time lightning damage assessment system. ILDAS is capable to determine intensity and attachment points of the lightning current which reduces maintenance time on the aircraft when hit by lightning. The ILDAS system was earlier developed in an EU FP6 project with many partners [EU FP6-030806] and has been described in detail in a series of contributions to the ICOLSE conferences [Zwe09, Boe11, Boe13]. Figure 6.1 gives the position of E and H-sensors and x-ray detectors in an A350 aircraft. All sensors are inside the fuselage, or the temperature and pressure controlled environment.

The E-field antenna is a capacitive probe attached to a window. The H-sensor employs an aircraft window as thick 'slotted' antenna. The sensor determines the voltage over the window at mid-height due to the current density pattern K around the window; see figure 6.2. In the window frame the sensor captures the magnetic flux entering and exciting both window halves; [Deu11a] provides a detailed analysis of the sensitivity for an aircraft with a thin metallic hull such as an Airbus A320 or A380. A horizontal wire is sensitive to the horizontal component of the current density K , a vertical wire to the vertical component of K , be it with different sensitivity. Both E- and H-sensors are followed by a combined passive/active integrator to redress the frequency response.

ILDAS continuously monitors each signal in an individual Sensor Assembly Electronics box (SAE). The sampling rate of H and E sensors is 83.3 MS/s (12 ns sampling time) and 100 MS/s (10 ns sampling time) of X-ray sensors. Dynamic range is 96 dB over a bandwidth up to 10 MHz (H-sensor) and 500 kHz (E-sensor). The characteristic lightning induced variation of the electric and magnetic field at the aircraft surface provides a

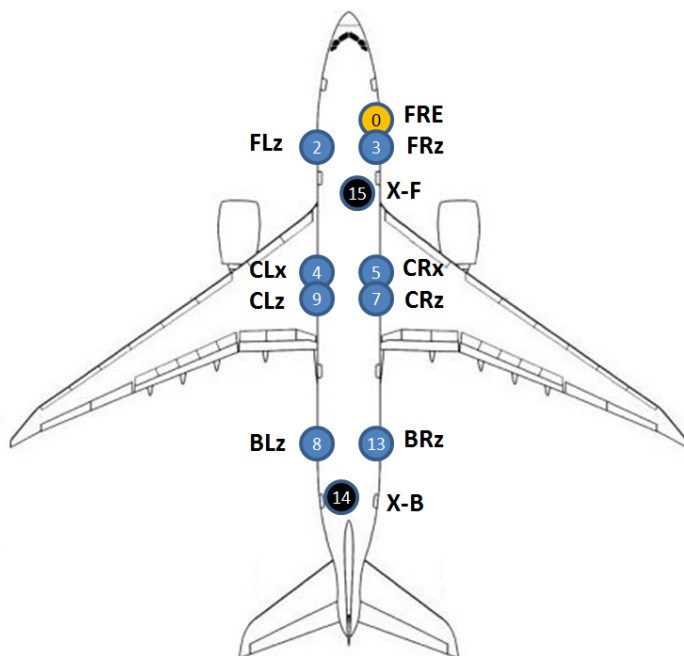


Figure 6.1: *ILDAS sensors location map for A350 aircraft.*

trigger for ILDAS. Upon triggering the systems stores pre- and post-trigger data over a time span of 1.2 seconds for H and E sensors, and 1 second for X-ray sensors. In the process all SAEs are synchronized to within 1 sample. For our experiments the ILDAS system has been enhanced with two x-ray detectors with $\text{LaBr}_3(\text{Ce})$ scintillators of 38 mm diameter and 38 mm length [Dor04]. The 100 Ms/s sample speed suffices to see individual pulses and to discriminate real signals from interference. The fuselage walls absorb x-rays with energy below 20 keV. As a result we only see the harder part of the spectrum. Cosmic rays cause a never-interrupted background of high energy x- and gamma-rays and charged particles. As a result the x-ray detectors cannot be included in the triggering. The background also varies strongly with aircraft altitude. Three special counters in the SAE determine the number of 10 ns sample periods where the x-ray signal exceeds three preset energy levels over consecutive periods of 15 ms. During flights the counter data are stored in continuous data files, CDF for short. The CDFs later provide information about the background and to a limited extent about its energy spectrum. The three preset levels are 0.29, 1.37 and 13.50 MeV for X14 and 0.64, 1.96 and 15.30 MeV for X15.

A first test flight occurred in December 2013, when the full ILDAS system was flown in an A350 between Bergerac and Foix in Southern France over a range of 300 km. The flight lasted a little over 2 hours, and was at 9 km altitude for 20 minutes. No thunderstorms were crossed, which allowed us to test the x-rays detectors on the cosmic ray background. Figure 6.3 on the left shows the plot of the CDF data for detector X14,

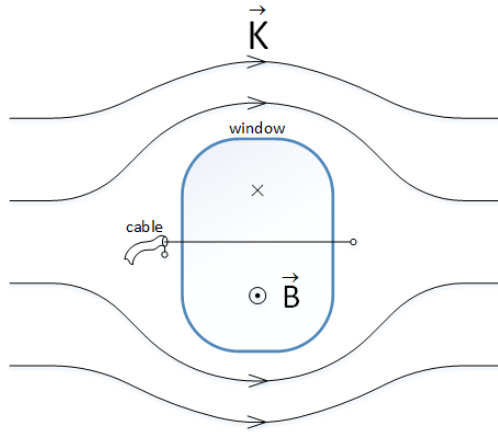


Figure 6.2: Schematic view of window sensor with lightning current density K through the aircraft fuselage. Magnetic field direction is indicated by \times and \odot . The sensor generates negative signal for this current pattern.

where we plotted the average number of 10 ns sample periods that the detector output exceeded the lowest level of 0.29 MeV; the X15 results are identical. The horizontal axis is the aircraft altitude. The general similarity with the original 1913-14 cosmic ray data [Kol13, Car12] is striking. At ground level there is a strong contribution to soil emission of radioisotopes. At higher altitudes cosmic rays dominate. Both plots show a minimum around 1 km altitude. The major difference is that our data either show excess at lower altitude, or lack at higher altitudes. But one should consider that we compare unequal quantities: period counts in the CDF files averaged over 75 s (left) versus number of ion pairs created per second (right). The general conclusion is that the system including the x-ray detectors works as desired. Up to 4 km altitude, the average background count is 2 sample periods per 15 ms. This counter value is equivalent to the detection of about 20 single photons or charged particles per second.

6.3 Two selected lightning strikes

We selected 2 strikes out of 62 recorded during the flight campaign. They contain most of the observed features.

Figure 6.4(a) shows 0.5 s of the measurements during the A350 flight on April 24, 2014. A lightning strike occurred at 16:22:20 UTC, our event code #203C2BF0. During this flight season, the zero degree Celsius altitude is at about 4 km. The E and H come from sensor E00 and H02 respectively, the x-ray data from X14. Positive H-field corresponds to a positive current flow from tail to nose (figure 6.1). With the radius of the aircraft of about 3 m, the conversion of H-field into fuselage current becomes 2 kA per 100 A/m. The high speed data record starts with the characteristic E-field variation; the actual trigger at $t = 0$ is the first magnetic field pulse due to a stroke. Several strokes or current pulses occurred; most were accompanied by E-field steps. In the 0.5 s time

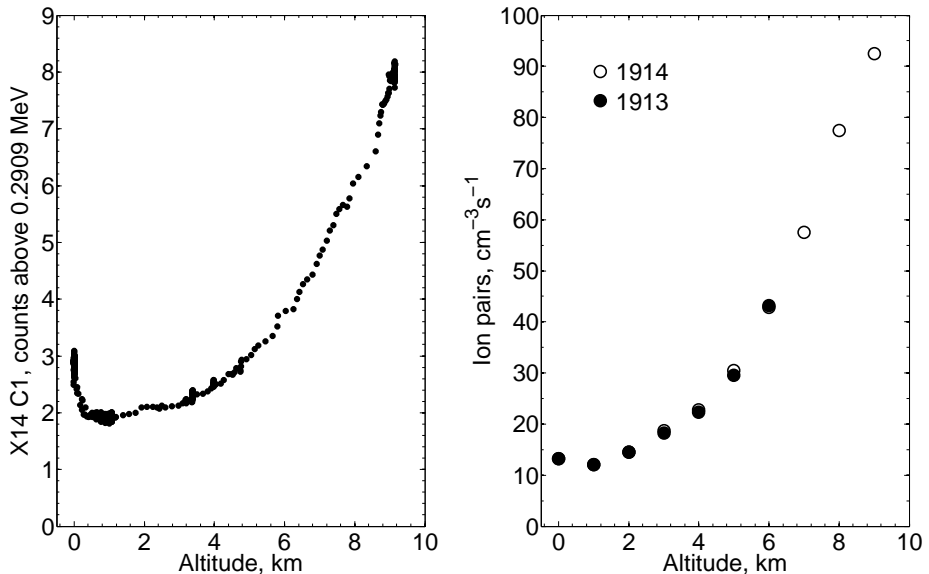


Figure 6.3: (Left) The average number of 10 ns sample periods that the x-ray detector output exceeded the lowest level of 0.29 MeV. (Right) The rate of atmospheric ionization as a function of altitude, as measured by Werner Kolhöster in 1913-14.

span, the aircraft moved about 80 m. As a result different strokes may have a different current pattern. After trigger the majority of the current pulses are accompanied by x-rays. On the other hand, not all x-ray signals match with a current pulse and may be due to background or distant lightning events. For instance, the 10 MeV pulse at $t = +0.084$ s is a single pulse of 75 ns full width at half maximum, not related to any sudden change in E- or H-signal.

Figure 6.4(b) zooms in on the attachment phase. At $t = -81.6$ ms the E-field starts to rise in 3 ms and then decays stepwise. The steps go with a current pulse of the order of 500 A; two current pulses coincide with a single x-rays pulse of about 2 MeV. In a tentative interpretation, the leader attaches at a single point of the aircraft at step A; a second attachment forms at the second step after A and the aircraft becomes a part of the current path. The 200 μ s between steps near A is a commonly observed time span between steps during lightning leader growth.

Figure 6.4(c) zooms in on the 10 MeV x-ray pulse at $t = 0.302$ s. It is known that these large energies lead to some saturation of the detector photomultiplier [Ngu12]. Still, the signature of individual x-ray pulses can be discerned. Even the main peak seems to consist of at least two equally large pulses within 100 ns. The x-rays occur at the rise of the current up to 5 kA maximum and near the largest E-field. Minor oscillations appear in the H-field at the period of about 300 ns that can be attributed to the excitation of an electromagnetic mode of the aircraft.

Figure 6.4(d) shows the more structured x-ray burst of about $1 \mu\text{s}$ duration near $t = 0.319 \text{ s}$. The appearance suggests two overlapping shorter duration bursts. The x-rays again occur before the largest current of 3 kA, but now at the largest E-field variation. Figure 6.4(e) shows a similar burst of lesser x-ray energy. The current attains 1.5 kA.

Figure 6.5 shows a current flow through all H-field sensors for the strokes represented in figure 6.4(c) and (d). The pattern suggests "right-wing-to-tail" scenario, when lightning attaches to the right wing of the aircraft and leaves it from the tail. It is interesting to note that the stroke (e) has its current pattern completely reversed in all sensors.

Figure 6.6(a) shows a different strike on an A350 recorded at 12:42:05 UTC on April 30, 2014, our event code #5049BB21. A particular subsequent stroke of 5 kA occurs quite late, near $t = 0.333 \text{ s}$. Based on the signals of all H-field sensors, the probable current pattern is from the right wing to both nose and tail. Both X14 and X15 detectors recorded several x-ray bursts. The single peak of 8 MeV on X14 at $t = 0.345 \text{ s}$ can be attributed to background. Figure 6.6(b) zooms in on the major subsequent stroke, and shows separate x-ray burst on both detectors; each burst lasts about $4 \mu\text{s}$. The x-ray pattern on both detector signals shows some similarity, with the foremost detector X15 delayed over approximately $1.5 \mu\text{s}$ with respect to X14. Similar delay of about $1.5 \mu\text{s}$ are found between the various H-field sensors. These delays cannot be explained by travel times over the 66 m long aircraft, but rather suggest several, at least three, lightning attachment points with different current pattern as function of time as just mentioned.

We attribute the X15 signals later than $425 \mu\text{s}$ in Figure 6.6(b) to interference from the magnetic field. The signals clearly do not resemble photomultiplier pulses. The X15 detector is placed between the nose and the wing box where one may expect a concentration of the lightning current and enhanced magnetic fields. Also the interference on the X14 detector is less. Nevertheless, it shows that some modification of the combination x-ray detector - SAE is desirable.

6.4 Continuous data file

Figure 6.7 shows the continuous data file recorded on April 30, 2014 along with the estimated background level calculated from the flight altitude profile and the curve shown in figure 6.3(a). The airplane takes off at about 10:50, gains altitude and reaches a thundercloud at about 11:50. Then it descends to zero-degree level (about 4 km height) and keeps the altitude with slight variations. Because of the averaging over 5000 periods the x-rays from the lightning strokes do not show up in this figure. After 17:10 the aircraft gains altitude to fly back to the base and finally lands at about 18:20. As can be seen, no evidence of long gamma-ray glow can be found in the CDF data.

6.5 Discussion

The current pattern over the aircraft varies between strokes, or subsequent strokes do not necessarily follow the same ionized channel through air. This is in part due to the

movement of the aircraft, which is of the order of 150 m/s in our records. The timing shows that x-rays are generated during the first attachment of the lightning channel to the aircraft and also later in the attachment of subsequent discharges. X-rays mostly occur in bursts that last a few microseconds. On such time scale the aircraft displacement can be neglected. The aircraft is a large intrusion into the charged cloud with strong field enhancement near the relatively sharp edges. It is plausible that only a small region near the attachment point is responsible for the x-rays. This was known at lower altitudes [Dwy11], but is now also demonstrated at altitudes up to 4 km. It is also in line with our findings on metre long discharges in the laboratory [Koc12, Koc14b], where the x-ray come from a region near the cathode. The recorded energy in single detector pulses ranges from a few tens of keV to 10 MeV. This agrees with soil based measurement on x-rays stemming from dart leaders in triggered lightning. However, it cannot be excluded that the larger energies are partly caused by pile-up of several lower energy pulses.

A continuous glow of x-rays has been observed at km distances from the thundercloud. The glow abruptly stops upon the lightning discharge, to be built up again slowly. The glow should in principle be observable in the CDF with the aircraft at constant altitude, but does not become apparent in our data because of the altitude variations in searching the thunderstorm zero degree level. As mentioned earlier, the background varies with altitude.

When the aircraft is inside a thunderstorm the non-averaged CDFs shows a few (less than five) hits crossing the largest preset level of 13.5 MeV (X14) or 15.3 MeV (X15) over a total period of about 10 minutes. No accompanying lightning trigger and high speed record were found. The cosmic ray background is a plausible explanation for the large energy. However, also TGFs might be responsible for such events [Smi11].

It would be also interesting to obtain the x-ray dose and its statistics. The campaign with the A350 is closed now. The ILDAS system with the x-ray extension is versatile and can easily be installed in other aircraft. We can only speculate on new flight plans through thunderstorms, for instance at different altitude.

We conclude with the remark that a large fraction of the observed x-rays in the high speed data are caused by the presence of the aircraft in the thundercloud. Still, the x-ray observations at 4 km altitude are similar to on-ground measurements in spite of the different air density. However, the relation between our data and the natural x-rays occurrence without aircraft requires more investigations.

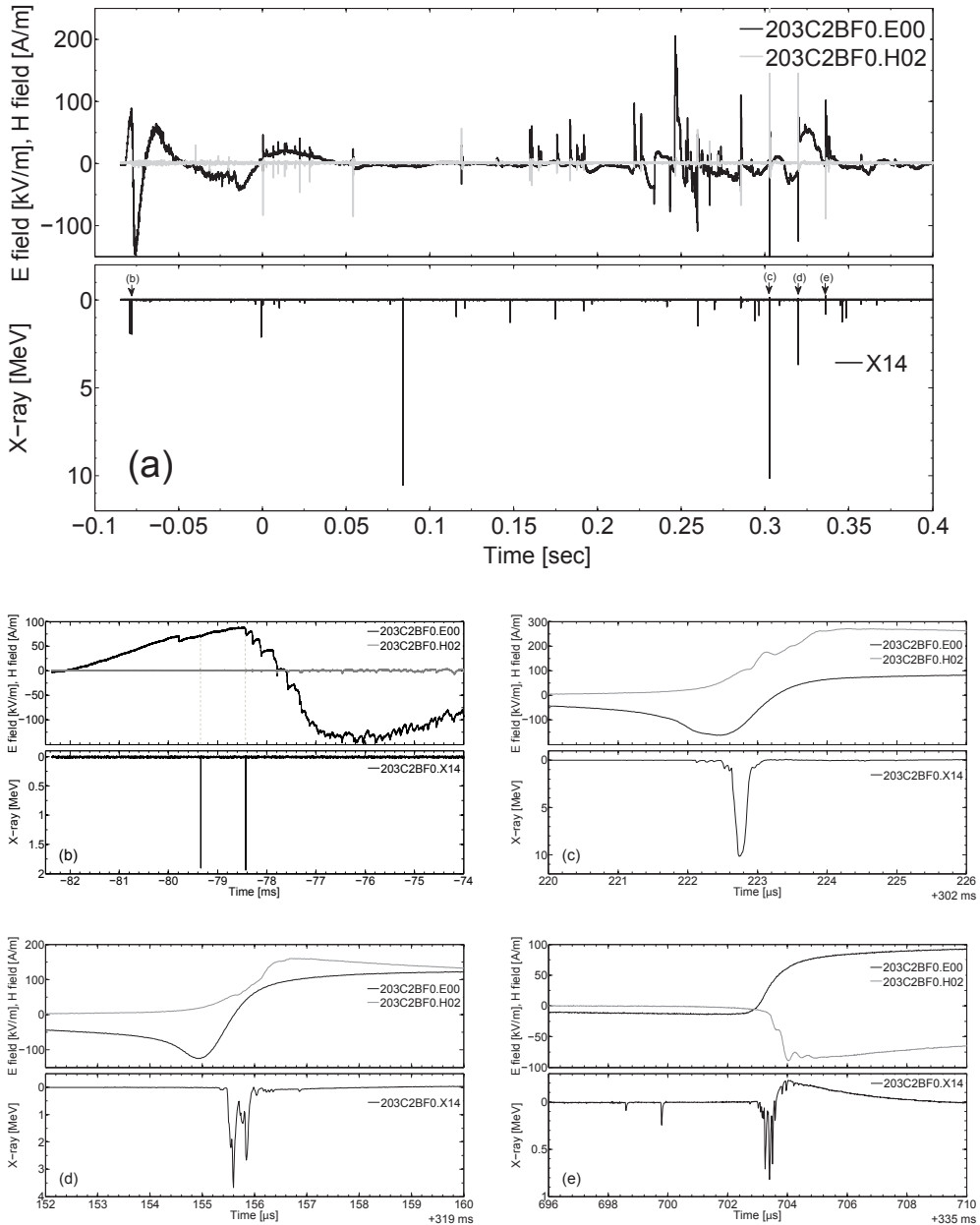


Figure 6.4: (a) Shows 0.5 s of the measurements during the A350 flight on April 24, 2014. A lightning strike occurred at 16:22:20 UTC, our event code #203C2BF0. (b) Zooms in on the attachment phase at $t = -0.08$ s. (c) Zooms in on the 10 MeV x-ray pulse at $t = 0.302$ s. (d) The more structured x-ray burst of about 1 μ s duration near $t = 0.319$ s. (e) Similar burst of less x-ray energy.

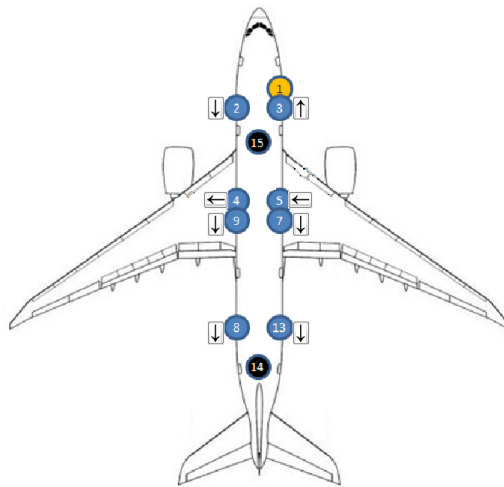


Figure 6.5: Current pattern for the events shown in figure 6.4(c) and (d). Arrows indicate the current directions. The event (e) has inverse current directions in all H-field sensors.

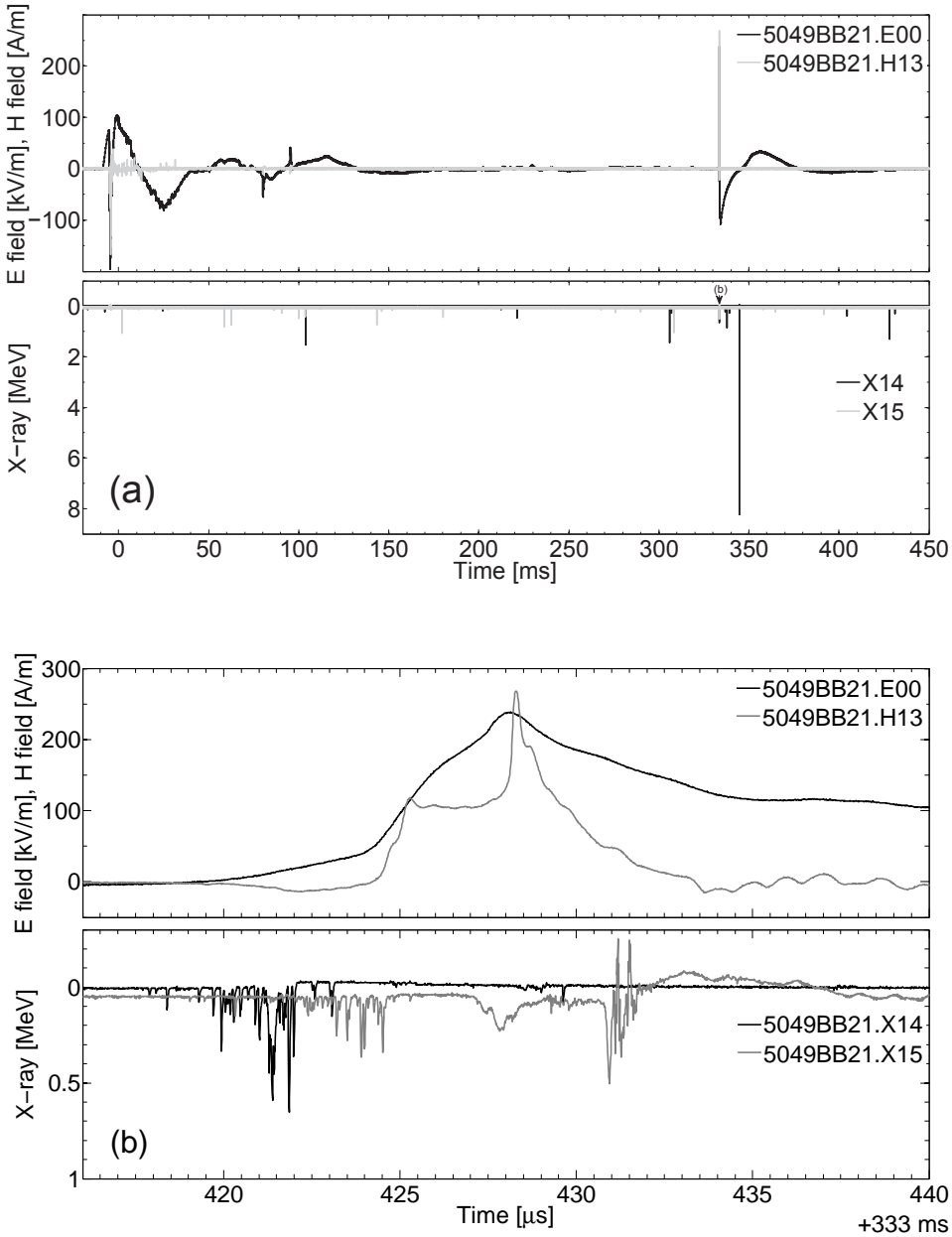


Figure 6.6: (a) Shows a different strike on an A350 recorded at 12:42:05 UTC on April 30, 2014, our event code #5049BB21. (b) Zooms in on the major subsequent stroke, and shows separate x-ray burst on both detectors; each burst lasts about 4μ s.

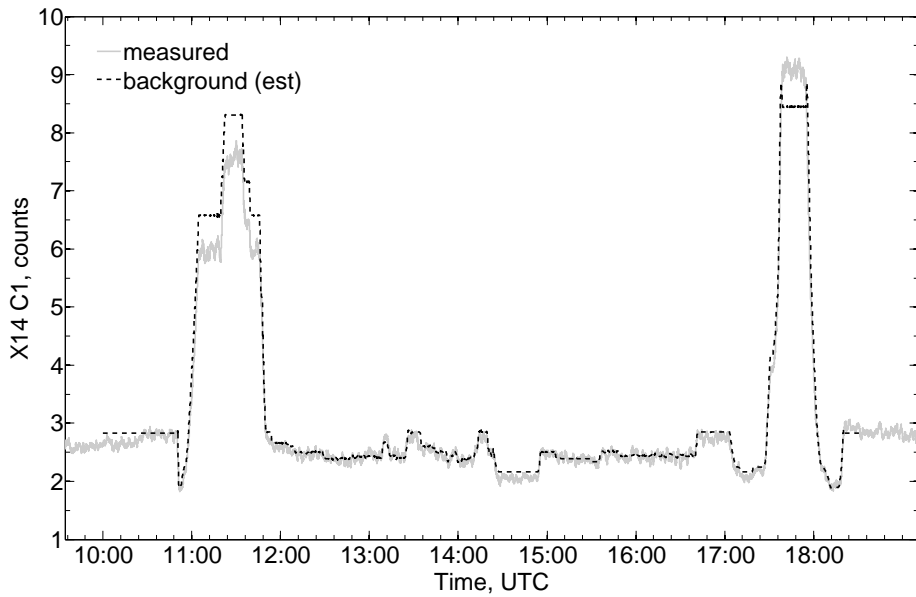


Figure 6.7: *Measured and estimated radiation. No evidence of long gamma-ray glow has been detected.*

CHAPTER 7

CONCLUSIONS AND OUTLOOK

7.1 Conclusions

We investigated structure and evolution of long positive spark breakdown. We showed at which stage pulses of hard x-rays are emitted. The discharge evolution was imaged with a resolution of tens of nanoseconds with an intensified CCD camera. $\text{LaBr}_3(\text{Ce}^+)$ scintillation detectors recorded the x-rays emitted during the process. The voltage and the currents on both electrodes were measured synchronously. All measurements indicate that first a large and dense corona of positive streamers emerges from the high voltage electrode. When they approach the grounded electrode, negative counter-streamers emerge there, and the emission of hard x-rays coincides with the connection of the positive streamers with the negative counter-streamers. Leaders are seen to form only at later stages. In general, we confirm the suggestion voiced in [Coo09] that streamer encounter might be responsible for the detected x-ray emission.

We studied the development of a negative discharge driven by a Marx generator of about 1 MV in an air gap of 1 up to 1.5 meter, at standard temperature and pressure. We showed the evolution of the discharge with nanosecond-fast photography together with the electrical characteristics. The negative discharge develops through four well-distinguished streamer bursts. The streamers have different velocities and life times in different bursts. The last burst triggers a positive inception cloud on the positive grounded electrode and a burst of positive counter-streamers emerges. The pre-discharge then bridges the gap and leaders grow from both electrodes. Finally a spark is formed. Looking closer into the pre-ionized zone near the cathode, we find isolated beads which are potential branching points. These beads act as starting points for positive streamers that move back towards the high-voltage electrode. We also find such phenomena as space leaders and leader stepping in our laboratory sparks.

The negative discharge development process with focus on its x-ray emission was investigated. We described x-ray appearance, timing and spatial distribution. It has been

observed that the x-rays appear in bursts of nanosecond duration in the cathode area. No anisotropy has been observed in the spatial distribution when averaged over many discharges. The spectrum can be characterized by an exponential function with 200 keV characteristic photon energy. By using ns-fast photography we made detailed images of pre-breakdown phenomena in x-ray registration time. We found bipolar discharge structures, also called "pilot systems", in vicinity of the cathode. As in our previous study on x-rays from positive discharges, we associate the x-ray emission with encounters between positive and negative streamers. We suggest that a similar process is responsible for x-rays generated by lightning leader.

We created a detailed Geant4 model of the LaBr₃ detector and compared the results of the simulation with measurements in the lab. Isotropic x-ray bursts near the high-voltage electrode with $7 \cdot 10^4$ initial photons in 4π and mean energy of about 160 keV give the spectra and attenuation curves close to ones obtained from the measurements. The question about emission anisotropy remains open for laboratory sparks as well as for natural lightning.

We used an unique opportunity provided by Airbus to measure the x-rays produced by natural lightning *in-situ* on board of an aircraft, with synchronous determination of the lightning current and electric fields. Such new data highly interest geophysicists studying lightning physics. In addition, the data provide clues to the x-ray dose for personnel and equipment during flights. The flights ran from April till May 2014; in eight flights we collected data of 62 lightning strikes on an A350 aircraft. We briefly described the system and showed some selected first results. No gamma-ray glows of thunderclouds were detected during the flights, but the massive x-ray bursts were detected and associated with dart lightning leaders.

By this work we contributed to at least three questions among the top ten in lightning research [Dwy14]: regarding lightning propagation, its x-ray emission and we also shed some light on TLEs sprites.

7.2 Outlook

This is the second thesis on x-rays from long sparks with a SSG laid out for standard lightning impulse. The SSG will not be transferred to new building. Time to have some philosophy on research that would further deepen understanding, given freedom of choice of HV equipment. We assume fast photography, or sequential photography present together with fast current probes, E-field measurements (antennas and capacitive plates) and x-ray detection.

7.3 Fundamental research on HV discharge initiation versus lightning research

Streamer microphysics is a very broad topic. A number of fundamental questions related streamer microphysics and lightning remained or become unanswered in the research

described in this thesis. Several of the most challenging and interesting questions are outlined below.

- What is the local electric field in front of a single streamer head?
- What is the electric field between two streamer heads just before they collide?
- Does streamer stepping still occur at shorter voltage rise time?
- Can positive streamer(s) step?
- Can the run-away electrons (timing, number, distribution of energy and direction) be detected directly other than by plastic scintillators?
- Is the x-ray emission isotropic?
- What causes the high-frequency oscillations observed together with the x-rays?
- Do the high-frequency oscillations in the laboratory relate to certain phenomena such as the dE/dt steps in real lightning?
- In the laboratory we observed millimeter to decimeter structures near the cathode at x-ray time. Are similar structures involved in the production of x-rays in real lightning?

Based upon our practical experience collected during the last 6 years of active experimentation we are ready to accept the challenge. Primarily one needs a high-voltage generator able to create 0.6 to 1 MV pulses of 0.1 to 1 μs rise time and appropriately designed electrodes to address most of the questions. By varying the high-voltage pulse amplitude and duration the complex streamer dynamic can be studied. As medium we prefer air, to preserve the relation with lightning.

Among lightning related questions we would like to highlight the following:

- Streamer to leader transition.
- Leader propagation and branching.
- Leader stepping mechanism.
- Stepped leader x-ray emission.

To perform this investigation a similar HV generator is needed but with a pulse duration of the order of milliseconds rather than microseconds. Possibly we could seek cooperation with other laboratories: at UPC, Terassa (1 MV SSG with 600 ns rise time) and Pau (1 MV with long duration).

Airbus expressed interest to continue the measurements with ILDAS + x-rays. Flights with a Dassault aircraft are foreseen in May 2015. Further cooperation can be embedded within EUFAR organization (www.eufar.org). A practical goal of the measurements is to establish the dosimetry for avionics and personnel. The data will also lead to a better basic understanding of the lightning attachment on fast moving objects and of the high energy processes like x-rays generation.

BIBLIOGRAPHY

- [Bab97] N. Y. Babaeva, G. V. Naidis and I. I. N. U. M. Odel. “Dynamics of Positive and Negative Streamers in Air in Weak Uniform Electric Fields”. *IEEE Transactions on Plasma Science*, vol. 25, no. 2 pp. 375--379, 1997.
- [Bab03] Babich L.P. *High-Energy Phenomena in Electric Discharges in Dense Gases*. Futurepast Inc, 2003.
- [Bar11] G. Bargboer. *Measurements and modeling of EMC, applied to cabling and wiring*. Ph.D. thesis, Eindhoven University of Technology, 2011.
- [Baz98] E. M. Bazelyan and Y. P. Raizer. *Spark Discharge*. CRC Press LLC, Boca Raton, New York, 1998.
- [Bel95] T. F. Bell, V. P. Pasko and U. S. Inan. “Runaway electrons as a source of Red Sprites in the mesosphere”. *Geophysical Research Letters*, vol. 22, no. 16 pp. 2127--2130, 1995.
- [Ber98] M. J. Berger, J. H. Hubbell, S. M. Seltzer, J. Chang, J. S. Coursey, R. Sukumar and D. S. Zucker. “XCOM: Photon Cross Sections Database”. *NIST Standard Reference Database 8 XGAM*, vol. NBSIR 87-3, 1998.
- [Bia11] C. J. Biagi and M. Uman. “Observations and modeling of long negative laboratory discharges : identifying the physics important to an electrical spark in air (LLNL-TR_520260)”. Tech. Rep. November, Lawrence Livermore National Laboratory, 2011.
- [Blo97] P. P. M. Blom. *High-Power Pulsed Corona*. Ph.D. thesis, Eindhoven University of Technology, 1997.
- [Boe11] A. de Boer, M. Bardet, C. Escure, G. Peres, V. Srithammavanh, K. Abboud, T. Abboud, J. Boissin, F. Flourens, A. Toufic, T. Vorreux, L. Riccio and A. P. J. V. Deursen. “In-flight Lightning Damage Assessment System (ILDAS):

- Initial in-flight lightning tests and improvement of the numerical methods”. In *ICOLSE 2011*, September. 2011.
- [Boe13] A. de Boer, S. Bardet, J. Boissin, A. P. J. V. Deursen, F. Flourens and A. Herve. “IN-FLIGHT LIGHTNING DAMAGE ASSESSMENT SYSTEM (ILDAS): FURTHER IN-FLIGHT VERIFICATION, WITH MULTI-SENSOR CONFIGURATION”. In *ICOLSE 2013*, vol. 3, pp. SEA2013--44.1. 2013.
- [Bri08a] T. M. P. Briels, E. M. Van Veldhuizen and U. Ebert. “Positive streamers in air and nitrogen of varying density: experiments on similarity laws”. *Journal of Physics D: Applied Physics*, vol. 41, no. 23 p. 24, 2008.
- [Bri08b] T. M. P. Briels, E. M. van Veldhuizen and U. Ebert. “Time resolved measurements of streamer inception in air”. *IEEE Transactions on Plasma Science*, vol. 36, no. 4 pp. 908--909, 2008.
- [Cam08] C. G. Camara, J. V. Escobar, J. R. Hird and S. J. Putterman. “Correlation between nanosecond X-ray flashes and stickslip friction in peeling tape”. *Nature*, vol. 455, no. 7216 pp. 1089--1092, 2008.
- [Car09] B. E. Carlson, N. G. Lehtinen and U. S. Inan. “Terrestrial gamma ray flash production by lightning current pulses”. *Journal of Geophysical Research*, vol. 114 p. A00E08, 2009.
- [Car12] P. Carlson. “A century of cosmic rays”. *Physics Today*, vol. 65, no. 2 p. 30, 2012.
- [Cel11] S. Celestin and V. P. Pasko. “Energy and fluxes of thermal runaway electrons produced by exponential growth of streamers during the stepping of lightning leaders and in transient luminous events”. *Journal of Geophysical Research*, vol. 116, no. A3 p. A03315, 2011.
- [Cha08] O. Chanrion and T. Neubert. “A PIC-MCC code for simulation of streamer propagation in air”. *Journal of Computational Physics*, vol. 227, no. 15 pp. 7222--7245, 2008.
- [Cha10] O. Chanrion and T. Neubert. “Production of runaway electrons by negative streamer discharges”. *Journal of Geophysical Research*, vol. 115 p. A00E32, 2010.
- [Cha14] O. Chanrion, Z. Bonaventura, D. Çinar, a. Bourdon and T. Neubert. “Runaway electrons from a beam-bulk model of streamer: application to TGFs”. *Environmental Research Letters*, vol. 9, no. 5 p. 055003, 2014.
- [Cle13] T. T. J. Clevis, S. Nijdam and U. Ebert. “Inception and propagation of positive streamers in high-purity nitrogen: effects of the voltage rise rate”. *Journal of Physics D: Applied Physics*, vol. 46, no. 4 p. 45202, 2013.
- [Coo09] V. Cooray, L. Arevalo, M. Rahman, J. Dwyer and H. Rassoul. “On the possible origin of X-rays in long laboratory sparks”. *Journal of Atmospheric and Solar-Terrestrial Physics*, vol. 71, no. 17-18 pp. 1890--1898, 2009.

- [Cum06] S. A. Cummer, N. Jaugey, J. Li, W. A. Lyons, T. E. Nelson and E. A. Gerken. "Submillisecond imaging of sprite development and structure". *Geophysical Research Letters*, vol. 33, no. 4 p. L04104, 2006.
- [Cum11] S. a. Cummer, G. Lu, M. S. Briggs, V. Connaughton, S. Xiong, G. J. Fishman and J. R. Dwyer. "The lightning-TGF relationship on microsecond timescales". *Geophysical Research Letters*, vol. 38, no. 14 pp. 1--6, 2011.
- [Deu11a] A. P. J. V. Deursen. "Inductive Sensor for Lightning Current Measurement , Fitted in Aircraft Windows Part II : Measurements on an A320 Aircraft". vol. 11, no. 1 pp. 205--209, 2011.
- [Deu11b] A. P. J. V. Deursen and V. Stelmashuk. "Inductive Sensor for Lightning Current Measurement , Fitted in Aircraft Windows Part I : Analysis for a Circular Window". vol. 11, no. 1 pp. 199--204, 2011.
- [Dor04] P. Dorenbos, J. de Haas and C. van Eijk. "Gamma ray spectroscopy with a O19x19 mm³ LaBr₃:0.5% Ce³⁺ scintillator". *IEEE Transactions on Nuclear Science*, vol. 51, no. 3 pp. 1289--1296, 2004.
- [Dwy03a] J. R. Dwyer. "A fundamental limit on electric fields in air". *Geophysical Research Letters*, vol. 30, no. 20 p. 2055, 2003.
- [Dwy03b] J. R. Dwyer, M. a. Uman, H. K. Rassoul, M. Al-Dayeh, L. Caraway, J. Jerauld, V. a. Rakov, D. M. Jordan, K. J. Rambo, V. Corbin and B. Wright. "Energetic radiation produced during rocket-triggered lightning." *Science (New York, N.Y.)*, vol. 299, no. 5607 pp. 694--7, 2003.
- [Dwy04a] J. R. Dwyer. "Implications of x-ray emission from lightning". *Geophysical Research Letters*, vol. 31, no. 12 p. L12102, 2004.
- [Dwy04b] J. R. Dwyer, H. K. Rassoul, M. Al-Dayeh, L. Caraway, B. Wright, A. Chrest, M. A. Uman, V. A. Rakov, K. J. Rambo, D. M. Jordan, J. Jerauld and C. Smyth. "Measurements of x-ray emission from rocket-triggered lightning". *Geophysical Research Letters*, vol. 31, no. 5 p. L05118, 2004.
- [Dwy05a] J. R. Dwyer. "X-ray bursts associated with leader steps in cloud-to-ground lightning". *Geophysical Research Letters*, vol. 32, no. 1 p. L01803, 2005.
- [Dwy05b] J. R. Dwyer, H. K. Rassoul and Z. Saleh. "X-ray bursts produced by laboratory sparks in air." *Geophysical Research Letters*, vol. 32, no. L20809 p. L20809, 2005.
- [Dwy08] J. R. Dwyer, Z. Saleh, H. K. Rassoul, D. Concha, M. Rahman, V. Cooray, J. Jerauld, M. A. Uman and V. A. Rakov. "A study of X-ray emission from laboratory sparks in air at atmospheric pressure". *Journal of Geophysical Research*, vol. 113, no. D23 p. D23207, 2008.
- [Dwy11] J. R. Dwyer, M. Schaal, H. K. Rassoul, M. A. A. Uman, D. M. Jordan and J. D. Hill. "High-Speed X-ray Images of Triggered Lightning Dart Leaders". *Journal of Geophysical Research*, vol. 116, no. D20 p. D20208, 2011.

- [Dwy12a] J. R. Dwyer, M. M. Schaal, E. Cramer, S. Arabshahi, N. Liu, H. K. Rassoul, J. D. Hill, D. M. Jordan and M. A. Uman. “Observation of a gamma-ray flash at ground level in association with a cloud-to-ground lightning return stroke”. *Journal of Geophysical Research: Space Physics (1978-2012)*, vol. 117, no. A10303 p. A10303, 2012.
- [Dwy12b] J. R. Dwyer, D. M. Smith and S. a. Cummer. “High-Energy Atmospheric Physics: Terrestrial Gamma-Ray Flashes and Related Phenomena”. *Space Science Reviews*, vol. 173, no. 1-4 pp. 133–196, 2012.
- [Dwy13] J. R. Dwyer, N. Liu and H. K. Rassoul. “Properties of the thundercloud discharges responsible for terrestrial gamma-ray flashes”. *Geophysical Research Letters*, vol. 40, no. 15 pp. 4067–4073, 2013.
- [Dwy14] J. R. Dwyer and M. a. Uman. “The physics of lightning”. *Physics Reports*, vol. 534, no. 4 pp. 147–241, 2014.
- [Eac96] K. B. Eack, W. H. Beasley, W. D. Rust, T. C. Marshall and M. Stolzenburg. “Xray pulses observed above a mesoscale convective system”, 1996.
- [Ebe97] U. Ebert, W. V. Saarloos and C. Caroli. “Propagation and structure of planar streamer fronts”. *Physical Review E*, vol. 55, no. 2 pp. 1530–1549, 1997.
- [Ebe06] U. Ebert, C. Montijn, T. M. P. Briels, W. Hundsdorfer, B. Meulenbroek, a. Rocco and E. M. V. Veldhuizen. “The multiscale nature of streamers”. *Plasma Sources Science and Technology*, vol. 15, no. 2 pp. S118–S129, 2006.
- [Ebe10] U. Ebert, S. Nijdam, C. Li, A. Luque, T. M. P. Briels and E. M. van Veldhuizen. “Review of recent results on streamer discharges and discussion of their relevance for sprites and lightning”. *Journal of Geophysical Research*, vol. 115 p. A00E43, 2010.
- [Fis94] G. J. Fishman, P. N. Bhat, R. Mallozzi, J. M. Horack, T. Koshut, C. Kouveliotou, G. N. Pendleton, C. A. Meegan, R. B. Wilson, W. S. Paciasas, S. J. Goodman and H. J. Christian. “Discovery of intense gamma-ray flashes of atmospheric origin”. *Science (New York, N.Y.)*, vol. 264, no. 5163 pp. 1313–1316, 1994.
- [Fra66] S. Frankel, V. Highland, T. Sloan, O. van Dyck and W. Wales. “Observation of X-rays from spark discharges in a spark chamber”. *Nuclear Instruments and Methods*, vol. 44, no. 2 pp. 345–348, 1966.
- [Gal02] I. Gallimberti, G. Bacchiega, A. Bondiou-Clergerie and P. Lalande. “Fundamental processes in long air gap discharges”. *Comptes Rendus Physique*, vol. 3, no. 10 pp. 1335–1359, 2002.
- [Grc05] L. Grcsev, A. P. J. van Deursen and J. B. M. van Waes. “Lightning current distribution to ground at a power line tower carrying a radio base station”. *IEEE Transactions on Electromagnetic Compatibility*, vol. 47, no. 1 pp. 160–170, 2005.

- [Gur61] A. V. Gurevich. “On the theory of runaway electrons”. *J. Exp. Theor. Phys.*, vol. 12 pp. 904–912, 1961.
- [Gur92] A. Gurevich. “Runaway electron mechanism of air breakdown and preconditioning during a thunderstorm”. *Physics Letters A*, vol. 165, no. 5-6 pp. 463–468, 1992.
- [Gur96] A. V. Gurevich, J. A. Valdivia, G. M. Milikh and K. Papadopoulos. “Runaway electrons in the atmosphere in the presence of a magnetic field”. *Radio Science*, vol. 31, no. 6 p. 1541, 1996.
- [Gur07] A. V. Gurevich, K. P. Zybin and Y. V. Medvedev. “Runaway breakdown in strong electric field as a source of terrestrial gamma flashes and gamma bursts in lightning leader steps”. *Physics Letters, Section A: General, Atomic and Solid State Physics*, vol. 361, no. 1-2 pp. 119–125, 2007.
- [Hel95] M. van Helvoort. *Grounding structures for the EMC-protection of cabling and wiring*. Ph.D. thesis, Eindhoven University of Technology, 1995.
- [Hor98] F. van Horck. *Electromagnetic compatibility and printed circuit boards*. Ph.D. thesis, Eindhoven University of Technology, 1998.
- [Hou90] M. van Houten. *Electromagnetic compatibility in high-voltage engineering*. Ph.D. thesis, Eindhoven University of Technology, 1990.
- [IEC97] IEC 1997. “Electromagnetic compatibility (EMC) Part 5: Installation and mitigation guidelines Section 2: Earthing and cabling”. Tech. rep., Geneva, IEC, 1997.
- [ILD] “<http://ildas.nlr.nl>”.
- [Ina96] U. S. Inan, S. C. Reising, G. J. Fishman and J. M. Horack. “On the association of terrestrial gamma-ray bursts with lightning and implications for sprites”. *Geophysical Research Letters*, vol. 23, no. 9 pp. 1017–1020, 1996.
- [Kap05] S. Kapora. *Protection by open systems: an EMC study*. Ph.D. thesis, Eindhoven University of Technology, 2005.
- [Kel10] N. Kelley, A. Lowell, D. M. Smith, J. R. Dwyer, S. Cummer, G. Lu and R. Blakeslee. “Rare TGFs and common glows: a systematic survey of data from the first flights of ADELE”. In *AGU Fall Meeting*, pp. AE11A--0332. 2010.
- [Kle73] R. W. Klebesadel, I. B. Strong and R. A. Olson. “Observations of Gamma-Ray Bursts of Cosmic Origin”. *The Astrophysical Journal*, vol. 182 p. L85, 1973.
- [Koc12] P. O. Kochkin, C. V. Nguyen, A. P. J. van Deursen and U. Ebert. “Experimental study of hard x-rays emitted from metre-scale positive discharges in air”. *Journal of Physics D Applied Physics*, vol. 45, no. 42 p. 425202, 2012.
- [Koc14a] P. O. Kochkin, A. P. J. van Deursen and U. Ebert. “Experimental study of the spatio-temporal development of metre-scale negative discharge in air”. *Journal of Physics D: Applied Physics*, vol. 47, no. 14 p. 145203, 2014.

- [Koc14b] P. O. Kochkin, A. P. J. van Deursen and U. Ebert. “Experimental study on hard X-rays emitted from metre-scale negative discharges in air.” *Journal of Physics D: Applied Physics*, 2014.
- [Koe14a] C. Koehn and U. Ebert. “Angular distribution of Bremsstrahlung photons and of positrons for calculations of terrestrial gamma-ray flashes and positron beams”. *Atmospheric Research*, vol. 135-136 pp. 432--465, 2014.
- [Koe14b] C. Koehn, U. Ebert and A. Mangiarotti. “The importance of electron-electron bremsstrahlung for terrestrial gamma-ray flashes, electron beams and electron-positron beams”. *Journal of Physics D: Applied Physics*, vol. 47, no. 25 p. 252001, 2014.
- [Kol13] W. Kolhorster. “Durchdringende Strahlung”. *Physik. Zeitschr.*, vol. 14 p. 1153, 1913.
- [Kos12] B. C. Kosar, N. Liu and H. K. Rassoul. “Luminosity and propagation characteristics of sprite streamers initiated from small ionospheric disturbances at subbreakdown conditions”. *Journal of Geophysical Research*, vol. 117, no. A8 p. A08328, 2012.
- [Kut12] I. M. Kutsyk, L. P. Babich, E. N. Donskoi and E. I. Bochkov. “Analysis of the results of a laboratory experiment on the observation of a runaway electron avalanche in air under high overvoltages”. *Plasma Physics Reports*, vol. 38, no. 11 pp. 891--898, 2012.
- [Leh96] N. G. Lehtinen, M. Walt, U. S. Inan, T. F. Bell and V. P. Pasko. “ γ -Ray emission produced by a relativistic beam of runaway electrons accelerated by quasi-electrostatic thundercloud fields”. *Geophysical Research Letters*, vol. 23, no. 19 p. 2645, 1996.
- [Les77] Les Renardières. “Positive Discharges in long air gaps at Les Renardières: 1975 results and conclusions”. *Electra*, vol. 53, no. 53 pp. 31--128, 1977.
- [Les81] Les Renardières. “Negative Discharges in long air gap discharges”. *Electra*, vol. 74 pp. 67--216, 1981.
- [Li09] C. Li, U. Ebert and W. Hundsdorfer. “3D hybrid computations for streamer discharges and production of run-away electrons”. *Journal of Physics D: Applied Physics*, vol. 42, no. 20 p. 202003, 2009.
- [Liu10] N. Liu. “Model of sprite luminous trail caused by increasing streamer current”. *Geophysical Research Letters*, vol. 37, no. 4 p. L04102, 2010.
- [Liu12] N. Liu, B. Kosar, S. Sadighi, J. R. Dwyer and H. K. Rassoul. “Formation of Streamer Discharges from an Isolated Ionization Column at Subbreakdown Conditions”. *Physical Review Letters*, vol. 109, no. 2 p. 025002, 2012.
- [Luq08] A. Luque, V. Ratushnaya and U. Ebert. “Positive and negative streamers in ambient air: modeling evolution and velocities”. *Journal of Physics D: Applied Physics*, vol. 41, no. 23 p. 18, 2008.

- [Luq09] A. Luque and U. Ebert. “Emergence of sprite streamers from screening-ionization waves in the lower ionosphere”. *Nature Geoscience*, vol. 2, no. 11 pp. 757--760, 2009.
- [Luq10] A. Luque and U. Ebert. “Sprites in varying air density: charge conservation, glowing negative trails and changing velocity”. *Geophysical Research Letters*, vol. 37, no. 6 p. L06806, 2010.
- [Luq11] A. Luque and F. J. Gordillo-Vázquez. “Sprite beads originating from inhomogeneities in the mesospheric electron density”. *Geophysical Research Letters*, vol. 38, no. 4 p. L04808, 2011.
- [Luq14] A. Luque and U. Ebert. “Growing discharge trees with self-consistent charge transport: the collective dynamics of streamers”. *New Journal of Physics*, vol. 16, no. 1 p. 013039, 2014.
- [Mal13] S. a. Mallios, S. Celestin and V. P. Pasko. “Production of very high potential differences by intracloud lightning discharges in connection with terrestrial gamma ray flashes”. *Journal of Geophysical Research: Space Physics*, vol. 118, no. 2 pp. 912--918, 2013.
- [Mar10] M. et al Marisaldi. “Detection of terrestrial gamma ray flashes up to 40 MeV by the AGILE satellite”. *Journal of Geophysical Research*, vol. 115, no. A14 pp. 1--12, 2010.
- [Mar11a] V. March and J. Montanyà. “X-rays from laboratory sparks in air: The role of the cathode in the production of runaway electrons”. *Geophysical Research Letters*, vol. 38, no. 4 p. L04803, 2011.
- [Mar11b] M. Marisaldi, F. Fuschino, C. Labanti, A. Bulgarelli, F. Gianotti, M. Trifoglio, M. Tavani, A. Argan, E. D. Monte, F. Longo, G. Barbiellini, A. Giuliani, A. Trois and f. t. A. Collaboration. “AGILE Observations of Terrestrial Gamma-Ray Flashes”. *arXiv*, vol. astro-ph.H, 2011.
- [McC85] M. McCarthy and G. K. Parks. “Further observations of X-rays inside thunderstorms”. *Geophysical Research Letters*, vol. 12, no. 6 p. 393, 1985.
- [McH07] M. G. McHarg, H. C. Stenbaek-Nielsen and T. Kammae. “Observations of streamer formation in sprites”. *Geophysical Research Letters*, vol. 34, no. 6 p. L07810, 2007.
- [Moo01] C. B. Moore, K. B. Eack, G. D. Aulich and W. Rison. “Energetic radiation associated with lightning”. *Geophysical Research Letters*, vol. 28, no. 11 pp. 2141--2144, 2001.
- [Mos06] G. D. Moss, V. P. Pasko, N. Liu and G. Veronis. “Monte Carlo model for analysis of thermal runaway electrons in streamer tips in transient luminous events and streamer zones of lightning leaders”. *Journal of Geophysical Research*, vol. 111, no. A2 p. A02307, 2006.

- [Nai09] G. V. Naidis. “Positive and negative streamers in air: Velocity-diameter relation”. *Physical Review E - Statistical, Nonlinear, and Soft Matter Physics*, vol. 79, no. 5 p. 057401, 2009.
- [Ngu08] C. V. Nguyen, A. P. J. van Deursen and U. Ebert. “Multiple x-ray bursts from long discharges in air”. *Journal of Physics D: Applied Physics*, vol. 41, no. 23 p. 234012, 2008.
- [Ngu10] C. V. Nguyen, A. P. J. van Deursen, E. J. M. van Heesch, G. J. J. Winands and a. J. M. Pemen. “X-ray emission in streamer-corona plasma”. *Journal of Physics D: Applied Physics*, vol. 43, no. 2 p. 025202, 2010.
- [Ngu12] Nguyen C V. *Experimental Study on Hard Radiation from Long Laboratory Spark Discharges in Air*. Phd thesis, PhD Thesis Eindhoven University of Technology, 2012.
- [Nij08] S. Nijdam, J. S. Moerman, T. M. P. Briels, E. M. van Veldhuizen and U. Ebert. “Stereo-photography of streamers in air”. *Applied Physics Letters*, vol. 92, no. 10 p. 101502, 2008.
- [Nij10] S. Nijdam, F. M. J. H. Van De Wetering, R. Blanc, E. M. Van Veldhuizen and U. Ebert. “Probing photo-ionization: Experiments on positive streamers in pure gasses and mixtures”. *Journal of Physics D: Applied Physics*, vol. 43, no. 14 p. 145204, 2010.
- [Nij11a] S. Nijdam. *Experimental Investigations on the Physics of Streamers*. Ph.D. thesis, PhD Thesis Eindhoven University of Technology, 2011.
- [Nij11b] S. Nijdam, K. Miermans, E. M. van Veldhuizen and U. Ebert. “A peculiar streamer morphology created by a complex voltage pulse”. *IEEE Transactions on Plasma Science*, vol. 39, no. 11 pp. 2216--2217, 2011.
- [Nij13] S. Nijdam, E. Takahashi, A. H. Markosyan and U. Ebert. “Investigation of positive streamers by double pulse experiments, effects of repetition rate and gas mixture (submitted to Plasma Sources Sci. Technol.) arXiv:1310.4307v2”. pp. 1--27, 2013.
- [Ogi11] A. Oginov, K. Shpakov, E. Oreshkin and S. Chaikovsky. “Experimental study of the initial phase of atmospheric discharges”. In *International Conference on Multimedia Technology*, pp. 6357--6360. P.N. Lebedev Physical Institute of RAS, Moscow, Russia, Hangzhou, 2011.
- [Pet13] D. A. Petersen and W. H. Beasley. “High-speed video observations of a natural negative stepped leader and subsequent dart-stepped leader”. *Journal of Geophysical Research: Atmospheres*, vol. 118, no. 21 pp. 12110--12119, 2013.
- [Rah08] M. Rahman, V. Cooray, N. A. Ahmad, J. Nyberg, V. a. Rakov and S. Sharma. “X rays from 80-cm long sparks in air”. *Geophysical Research Letters*, vol. 35, no. 6 p. L06805, 2008.

- [RD96] R. Roussel-Dupré and A. V. Gurevich. “On runaway breakdown and upward propagating discharges”. *Journal of Geophysical Research*, vol. 101, no. A2 p. 2297, 1996.
- [Ree95] T. Reess, P. Ortega and A. Gibert. “An experimental study of negative discharge in a 1.3 m point-plane air gap: the function of the space stem in the propagation mechanism”. *Journal of Physics D*, vol. 28, no. 11 pp. 2306–2313, 1995.
- [Rin13] R. Ringuette, G. L. Case, M. L. Cherry, D. Granger, T. G. Guzik, M. Stewart and J. P. Wefel. “TETRA observation of gamma-rays at ground level associated with nearby thunderstorms”. *Journal of Geophysical Research: Space Physics*, vol. 118, no. 12 pp. 7841–7849, 2013.
- [Rob12] E. Robert, V. Sarron, D. Riès, S. Dozias, M. Vandamme and J.-M. Pouvesle. “Characterization of pulsed atmospheric-pressure plasma streams (PAPS) generated by a plasma gun”. *Plasma Sources Science and Technology*, vol. 21, no. 3 p. 034017, 2012.
- [Sar11] V. Sarron, E. Robert, S. Dozias, M. Vandamme, D. Ries and J. M. Pouvesle. “Splitting and mixing of high-velocity ionization-wave-sustained atmospheric-pressure plasmas generated with a plasma gun”. *IEEE Transactions on Plasma Science*, vol. 39, no. 11 PART 1 pp. 2356–2357, 2011.
- [Smi05] D. M. Smith, L. I. Lopez, R. P. Lin and C. P. Barrington-Leigh. “Terrestrial gamma-ray flashes observed up to 20 MeV.” *Science*, vol. 307, no. 5712 pp. 1085–1088, 2005.
- [Smi11] D. M. Smith, J. R. Dwyer, B. J. Hazelton, B. W. Grefenstette, G. F. M. Martinez-Mckinney, Z. Y. Zhang, A. W. Lowell, N. A. Kelley, M. E. Splitt, S. M. Lazarus, W. Ulrich, M. Schaal, Z. H. Saleh, E. Cramer, H. Rassoul, S. A. Cummer, G. Lu, X. M. Shao, C. Ho, T. Hamlin, R. J. Blakeslee and S. Heckman. “A terrestrial gamma ray flash observed from an aircraft”. *Journal of Geophysical Research D: Atmospheres*, vol. 116, no. 20, 2011.
- [Sta] Stanford Computer Optics. “<http://www.stanfordcomputeroptics.com/>”.
- [Sta06] M. A. Stanley, X. M. Shao, D. M. Smith, L. I. Lopez, M. B. Pongratz, J. D. Harlin, M. Stock and A. Regan. “A link between terrestrial gamma-ray flashes and intracloud lightning discharges”. *Geophysical Research Letters*, vol. 33, no. 6, 2006.
- [Ste62] I. S. Stekolnikov and A. V. Shkilev. “New information on the development of a negative spark and its comparison with lightning”. *Dokl. Akad. Nauk SSSR*, vol. 145 pp. 782–5, 1962.
- [Ste08] V. Stelmashuk and A. P. J. Van Dursen. “Sensors for lightning measurements on aircraft”. In *Proceedings of IEEE Sensors*, pp. 1036–1039. 2008.
- [Van98] P. C. T. Van Der Laan and A. P. J. Van Deursen. “Reliable protection of electronics against lightning: Some practical applications”, 1998.

- [Wika] “http://en.wikipedia.org/wiki/Gamma_ray_burst”.
- [Wikb] Wiki. “Distribution of lightning”.
- [Wike] Wiki. “Upper-atmospheric lightning”.
- [Wil25] C. T. R. Wilson. “The electric field of a thunderstorm and some of its effects”. *Proceedings of the Royal Society of London*, vol. 37, no. 32D, 1925.
- [Xu12] W. Xu, S. Celestin and V. P. Pasko. “Source altitudes of terrestrial gamma-ray flashes produced by lightning leaders”. *Geophysical Research Letters*, vol. 39, no. 8, 2012.
- [Zen13] R. Zeng and S. Chen. “The dynamic velocity of long positive streamers observed using a multi-frame ICCD camera in a 57 cm air gap”. *Journal of Physics D: Applied Physics*, vol. 46, no. 48 p. 485201, 2013.
- [Zwe09] R. Zwemmer, M. Bardet, A. de Boer, J. Hardwick, K. Hawkins, D. Morgan, N. Marchand, J. Ramos, I. Revel and W. Tauber. “In-flight Lightning Damage Assessment System (ILDAS) Results of the Concept Prototype tests”. In *ICOLSE 2009*, September, pp. 15--17. 2009.

LIST OF PUBLICATIONS

Journal publications

2014

- P.O. Kochkin, A.P.J. van Deursen and U. Ebert. “Experimental study of the spatio-temporal development of metre-scale negative discharge in air”. *J. Phys. D: App. Phys.*, vol. 47, no. 14, 145203 , 2014.
- P.O. Kochkin, A.P.J. van Deursen and U. Ebert. “Experimental study on hard X-rays emitted from metre-scale negative discharges in air”. *Submitted to J. Phys. D: App. Phys.*.
- P.O. Kochkin, C. Köhn, A.P.J. van Deursen and U. Ebert. “A GEANT4 Monte Carlo simulation of X-ray emission from meter-scale laboratory discharges in STP air”. *In preparation.*
- P.O. Kochkin, A.P.J. van Deursen, A.I. de Boer, M. Bardet and J.F. Boissin. “In-flight measurements of energetic radiation from lightning and thunderclouds”. *In preparation.*

2012

- P.O. Kochkin, C.V. Nguyen , A.P.J. van Deursen and U. Ebert “Experimental study of hard x-rays emitted from metre-scale positive discharges in air”. *J. Phys. D: App. Phys.*, vol. 45, no. 42, 425202 , 2012.

Conference publications

2014

- P.O. Kochkin, A.P.J. van Deursen and U. Ebert. “Development of positive discharge in meter-scale STP air gap.”. *In Proceedings 31st URSI General Assembly*

and Scientific Symposium (31st URSI GASS), Beijing, China, 2014.

- P.O. Kochkin, A.P.J. van Deursen and U. Ebert. “Development of negative discharge in meter-scale STP air gap.”. *In Proceedings 31st URSI General Assembly and Scientific Symposium (31st URSI GASS)*, Beijing, China, 2014.
- A.P.J. van Deursen, P.O. Kochkin, A.I. de Boer, M. Bardet and J.F. Boissin. “In-flight measurements of high-energetic radiation from thunderstorms.”. *In Proceedings 31st URSI General Assembly and Scientific Symposium (31st URSI GASS)*, Beijing, China, 2014.

Conference oral and poster presentations

2014

- P.O. Kochkin, A.P.J. van Deursen and U. Ebert. “Similarities in appearance between natural sprites and pilot systems in the lab.” *2nd TEA-IS Summer School, 2014, Collioure, France.*
- P.O. Kochkin, A.P.J. van Deursen and U. Ebert. “Observation of X-rays from long laboratory negative discharge in STP air.” *European Geosciences Union General Assembly 2014 (EGU2014), 2014, Vienna, Austria.*
- A.P.J. van Deursen, P.O. Kochkin, A.I. de Boer, M. Bardet and J.F. Boissin. “In-flight measurements of Terrestrial Gamma-Ray Flashes.” *European Geosciences Union General Assembly 2014 (EGU2014), 2014, Vienna, Austria.*
- P.O. Kochkin, A.P.J. van Deursen and U. Ebert. “X-ray emission generated by streamer encounter.” *26th NNV-Symposium on Plasma Physics and Radiation Technology (26NNV), 2014, Lunteren, The Netherlands.*

2013

- P.O. Kochkin, A.P.J. van Deursen and U. Ebert. “From long laboratory spark to lightning.”. *American Geosciences Union Fall Meeting (AGU2013), 2013, San Francisco, USA.*
- P.O. Kochkin, A.P.J. van Deursen and U. Ebert. “On the origin of hard X-rays in the growth of meter long sparks.” *10th Frontiers in Low Temperature Plasma Diagnostics, 2013, Rolduc, Kerkrade, The Netherlands.*
- P.O. Kochkin, A.P.J. van Deursen and U. Ebert. “On the origin of hard X-rays in the growth of meter long sparks.” *European Geosciences Union General Assembly 2013 (EGU2013), 2013, Vienna, Austria.*
- P.O. Kochkin, A.P.J. van Deursen and U. Ebert. “On the origin of hard X-rays in the growth of meter long sparks.” *25th NNV-Symposium on Plasma Physics and Radiation Technology (25NNV), 2013, Lunteren, The Netherlands.*

- P.O. Kochkin, A.P.J. van Deursen and U. Ebert. “Experimental study on hard radiation from lightning.” *URSI Benelux Forum, 2013, Eindhoven, The Netherlands.*

2012

- P.O. Kochkin, A.P.J. van Deursen and U. Ebert. “Place of hard radiation in discharge evolution.” (invited) *American Geosciences Union Fall Meeting (AGU2012), 2012, San Francisco, USA.*
- P.O. Kochkin, A.P.J. van Deursen. “Study of X-ray emission in long sparks combined with ns-fast photography.” *1st TEA-IS Summer School, 2012, Malaga, Spain.*
- P.O. Kochkin, A.P.J. van Deursen. “High-speed photography of long laboratory sparks.” *24th NNV-Symposium on Plasma Physics and Radiation Technology (24NNV), 2012, Lunteren, The Netherlands.*

2011

- P.O. Kochkin, C.V. Nguyen, A.P.J. van Deursen. “The observation of X-ray bursts along and perpendicular to the streamer path.” *European Geosciences Union General Assembly 2011 (EGU2011), 2011, Vienna, Austria.*
- P.O. Kochkin, A.P.J. van Deursen. “Statistical analysis of X-ray emission from laboratory sparks.” *American Geosciences Union Fall Meeting (AGU2011), 2011, San Francisco, USA.*
- P.O. Kochkin, C.V. Nguyen, A.P.J. van Deursen. “The observation of X-ray bursts along and perpendicular to the streamer path.” *23th NNV-Symposium on Plasma Physics and Radiation Technology (23NNV), 2011, Lunteren, The Netherlands.*

ACKNOWLEDGEMENTS

This work would have not been done without the support and contribution of many people from all over the world. Foremost, my deepest gratitude goes to my supervisor Dr. Lex van Deursen. You gave me the endless freedom on my way through the Ph.D. which I appreciate most. Countless international and local conferences, you encouraged me to attend, allowed me to develop a broad professional and friendly network. Due to your excellent EMC expertise, which you kindly shared with me, I could perform the precise measurements in extreme electro-magnetic environment. Your persistence in achieving the goals will serve as an example for me for many years.

All the work has been done in a warm atmosphere that prevails at Electrical Engineering Department at Eindhoven University of Technology. Many thanks to Professor Wil Kling - my first promoter and chair of the Electrical Energy Systems group. It was a great pleasure to be a part of the group participating in many wonderful team-building activities organized by fellow Ph.D. students.

My grateful respect goes to Prof. Dr. Ute Ebert. Except of your excellent scientific knowledge of the topic, you possess at least one superpower - to catch tiny details of my chaotically written manuscripts during your way from Amsterdam to Eindhoven. Thank you very much for your help and ceaseless advertising of our research worldwide. Besides that, you collected many talented people at CWI, Amsterdam. Chris, as you mentioned in your thesis, there were indeed enjoyable walks in San Francisco and Vienna. My dear friend with a good sense of humour Aram Markosyan. I hope you are doing well in US now. I still have to teach you how to drive karting, keep this in mind.

We spent unforgettable time with the group of highly skilled Norwegian students together with their supervisor and spiritual leader Nikolai Østgaard. They visited our lab twice in 2012 and 2013 with their own hand-made x-ray detectors to hunt on elusive high-energetic electrons. Meeting you guys on conferences always cheers me up.

Besides there are many appreciated colleagues from the TU/e. My gratitude goes to Guus Pemen, Peter Wouters and Bert van Heesch. They gathered many professionals around, such as Tom, Jin, Lei, Helder, Anna, Wilfred, René, Frank and many bright

fellow students. Working and discussing with them was a great pleasure for me.

My special thanks go to Sjoerd van Driel. He is the first Dutch person I asked to help with adaptation and he responded warmly. My first impression about Dutch people was created by Sjoerd and still remains highly positive.

Two talented engineers I have met here are Alte de Boer and Michiel Bardet. They made the ILDAS system possible for us, which eventually allowed to perform the most incredible experiment I have ever participated in.

Of course my dear son Viktor and my darling wife Malvina. We have been already going this road shoulder to shoulder for 8 years. You shared with me all my ups and downs. Physics Department, hostel, holidays in Crimea, Pobeda, Solnechniy, Viktor, The Netherlands. Thinking of you was my main motivator all these years.

It would be unfair to forget my dear friends Dmytro Strunin and his wife Olena. The couple of geneticist and neuroscientist will create something cute or supernatural soon. Bro, thanks for explaining me some details of genes and for the long scientific discussions we had. Good luck with your new research on HIV.

My new friends whom I met in Eindhoven - Dmytro Malyna, brilliant Mikhailo and Natalia Semkiv and wonderful family Sergei, Veronika and Vlada. Hours of discussions, tons of barbecue, gallons of beer is only a small part of what we did together. My personal respect goes to Denis Ovchinnikov who explained to me many important aspects of the local life in general and the tax system in particular. You also brought me back from hospital and helped in one personal situation. I appreciate that.

Special Thanks to Professor Viktor Klimenko at National University of Dnipropetrovsk who, in spite of countless obstacles, continues sparking young minds.

Last, but not least are my brother Denis and my parents. Thanks for being around and supporting everything I have ever initiated. I'll payback by thankful grandkids :)

Pavlo Kochkin, 2014

CURRICULUM VITAE

Pavlo Kochkin was born on 31-01-1984 in Feodosiya, Crimea, Ukraine. After finishing pre-university education in 2001 at Lyceum of Arts in Kerch, he studied Applied Physics and Computer Science at Dnipropetrovsk National University in Dnipropetrovsk. In 2006 he graduated within the Optoelectronics group on Applied Physics and within the Radio Physics Department on Information Management Systems and Technologies. From 2006 he worked as a technician at Dnipropetrovsk National University and as a software developer in an industrial company.

From 2010 he started a PhD project at Eindhoven University of Technology at Eindhoven, The Netherlands. In 2014 his work finalized in a PhD dissertation.